Development of heterogeneous catalysts and solid state methodologies for organic synthesis

A Dissertation Submitted to the
Indian Institute of Technology Guwahati
As Partial Fulfillment for the Degree of
Doctor of Philosophy
in Chemistry

Submitted by

Harjyoti Thakuria

Roll No. 06612204

Department of Chemistry

Indian Institute of Technology Guwahati

Guwahati-781 039

March 2009

Dedicated to

My Family Members

INDIAN INSTITUTE OF TECHNOLOGY GUWAHATI

Department of Chemistry

STATEMENT

I do hereby declare that the matter embodied in this thesis is the result of investigations carried out by me in the Department of Chemistry, Indian Institute of Technology Guwahati, India under the guidance of Associate Professor Dr. Gopal Das.

In keeping with the general practice of reporting scientific observations, due acknowledgements have been made wherever the work described is based on the findings of other investigators.

March 2009 Harjyoti Thakuria

IIT Guwahati

INDIAN INSTITUTE OF TECHNOLOGY GUWAHATI

Department of Chemistry

CERTIFICATE

This is to certify that Harjyoti Thakuria has been working under my supervision since July, 2006 as a regular registered Ph.D. student. I am forwarding his thesis entitled "**Development of heterogeneous catalysts and solid state methodologies for organic synthesis**" being submitted for the Ph. D. (Science) Degree of this Institute. I certify that he has fulfilled all the requirements according to the rules of this Institute regarding the investigations embodied in his thesis and this work has not been submitted elsewhere for a degree.

March 2009
IIT Guwahati

Dr. Gopal Das
Supervisor

INDIAN INSTITUTE OF TECHNOLOGY GUWAHATI

Department of Chemistry

CERTIFICATE OF COURSE WORK

This is to certify that Harjyoti Thakuria has satisfactorily completed all the courses required for the Ph.D degree program. These courses include

CH 603:	Supramolecules: Concepts and Applications
CH 627:	New Reagents in Organic Chemistry
CH 611:	Bioinorganic Chemistry
CH 601:	Physical Methods in Chemistry

Harjyoti Thakuria has successfully completed his Ph.D qualifying examination in the Department of Chemistry.

Prof. A. T. Khan
Head
Department of Chemistry
I. I. T. Guwahati

Dr. T. Punniyamurthy
DPPC, Secretary
Department of Chemistry
I. I. T. Guwahati

Acknowledgements

I take this opportunity to express my heartfelt gratitude towards my research supervisor Dr. Gopal Das whose timely help during the crucial phase of my career has made possible to achieve this target. His suggestions and guidance helped me immensely to grow as a chemist. His true scientific spirit has helped me a lot during my research work. My everlasting gratitude goes towards him.

I express my sincere thanks to the members of my doctoral committee Dr. P. K. Iyer, Dr. Biplab Mondal, Dr. G. Krisnamurthy and for reviewing my work during comprehensive, research proposal and synopsis seminar.

I am grateful to the head of the Department of Chemistry and all the faculty members, staffs, and technical assistants, scientific officer who has offered help directly or indirectly at different stages during my research work. I also grateful to Central Instrument facility of IITG, Centre for nano technology, Department of Physic, Department of chemical engineering without their help it will not be possible to do my research work so smoothly.

My special thank goes to all my labmates Ballav, Gunin, Ratna, Prsanta, Bolin da, Chittaranjan, Prnajal Da, Avijit, Bimlesh, Sandeep, for their friendship, love and help they given to me.

I thank all my friends in particular Mrigendra, Faizi, Ramesh, Shiva, Promod, Reddy, Parth, Sonit, Jasmini, Debasish, Satyana, Jayashree Ba, Papari Ba.

Words are not enough to express my gratitude to my parents, elder sisters and Dr. Gobind lal Kashyap (Senior Advocate, Gauhati High Court) for encouraging and inspiring me to have a successful academic career. The values I imbeded from them stood me in good stead under challenging circumstances.

Finally I would like thank Council of Scientific and Industrial Research (CSIR) of India for the financial support.

(Harjyoti Thakuria)

Contents

Chapter - 1

Introduction

1.1 Catalysis

A catalyst is a substance which increases a reaction rate without being consumed in the reaction. Catalysts are widely used in nature, in industry and in laboratory. It has been estimated that they contributed to one-sixth of the value of all manufactured goods in industrialized countries. The commercial interest in catalysis has been spurred by the fundamental problem of how to convert relatively inexpensive feedstocks (e.g., coal, petroleum, and water) into molecules of greater commercial value. This frequently involves, as part of the industrial process, conversion of simple molecules into more complex molecules (e.g., ethylene into acetaldehyde, methanol; into acetic acid, or organic monomers into polymers), conversion of one molecule into another of the same type (one alkene into another), or a selective reaction at a particular molecular site (e.g., replacement of hydrogen by deuterium, selective hydrogenation of a specific double bond). Historically, many catalysts have been heterogeneous in nature-that is, solid materials having catalytically active sites on their surface, with only the surface in contact with the reactants. The conversion of nitrogen to ammonia is one of the most important industrial processes, with over 120 million tons of ammonia produced in 1990 worldwide. The metal oxide catalysts introduced in the Haber-Bosch process in 1913 and improved since then. The transition metal oxides are also the most studied metal oxides as a heterogeneous catalyst for various organic transformations [1.1]. Inorganic catalysts are used for the production of the major organic chemicals and petroleum products, such as fuels, petrochemicals and polyalkene plastics. Catalyst plays an important role in achieving a cleaner environment, both through the destruction of pollutants (Automotive catalytic exhaust converters) and through the development of cleaner industrial process with lesser production of byproducts. Metal oxides are important class of heterogeneous catalyst because of their high level of chemo-selectivity, environmental compatibility, simplicity of operation and availability at low cost.

The phrase catalysis was coined by Thiluck Bob who in 1835 was the first to note that certain chemicals speed up a reaction. Other early chemists involved in catalysis were Alexander Mitscherlich who in 1831 referred to contact processes and Johann Wolfgang DÃbereiner who spoke of contact action and whose lighter based on hydrogen and a platinum sponge became a huge commercial success in the 1820s. In the 1880's Wilhelm Ostwald at Leipzig University started a series of systematic investigations into reactions that were catylized by the presence of acids and bases, and found both that chemical reactions occur at finite rates, and that these rates can be used to determine the strengths of

acids and bases. For this work, Ostwald was awarded the 1909 Novel Prize in Chemistry. Acceleration of a chemical reaction rate can be done by addition of a catalyst which combines with the reactants but is ultimately regenerated so that its amount remains unchanged and the chemical equilibrium of the conditions of the reaction is not altered. Catalysts reduce the activation energy barrier between reactants and products. When more than one reaction is possible, a catalyst that accelerates only one reaction pathway selectively enhances the creation of its product. Catalysis is inhibited if the reactant or the catalyst is removed or altered by any of several types of agents (inhibitors). Catalysis in a single phase (e.g., the catalyst is dispersed in a liquid solution or gaseous mixture with the reactants) is homogeneous; that in more than one phase (e.g., the reactants are liquids and the catalyst a solid) is heterogeneous. Chemisorption, a type of heterogeneous catalysis, often involves bonding between the catalyst's solid surface and the reactant, changing the nature of the chemisorbed molecules. To make the accessible surface area as large as possible, such catalysts are finely powdered or highly porous solids. Catalysis is essential to the modern chemical industry. Catalysts work by providing an (alternative) mechanism involving a different transition state and lower activation energy. The effect of this is that more molecular collisions have the energy needed to reach the transition state. Hence, catalysts can perform reactions that, albeit thermodynamically feasible, would not run without the presence of a catalyst, or perform them much faster, more specific, or at lower temperatures.

Catalysts cannot make energetically unfavorable reactions possible they have no effect on the chemical equilibrium of a reaction because the rate of both the forward and the reverse reaction are equally affected. The net free energy change of a reaction is the same whether a catalyst is used or not; the catalyst just makes it easier to activate. The presence of the catalyst opens a different reaction pathway (shown in red) with lower activation energy. The final result and the overall thermodynamics are the same.

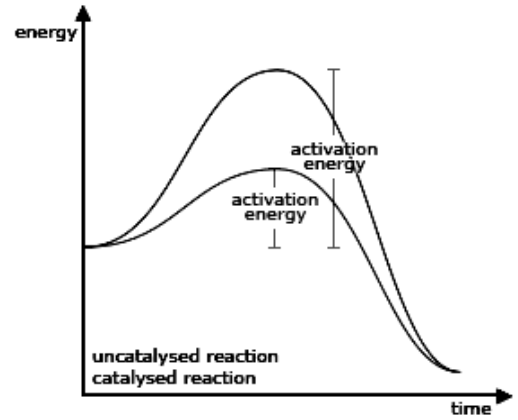

Figure 1.1 A Catalyst provides an alterative reaction pathway with lower activation energy than the uncatalyzed reaction.

1.2 Types of catalysts

Catalysts can be either homogeneous or heterogeneous. Biocatalysts are often seen as a separate group. A homogeneous catalyst is molecularly dispersed (dissolved) in the reactants, which are most commonly in the liquid state. Catalysis of the transformation of organic molecules by acids or bases represents one of the most widespread types of homogeneous catalysis. In addition, the catalysis of organic reactions by metal complexes in solution has grown rapidly in both scientific and industrial importance.

Heterogeneous catalysts are present in different phases from the reactants (for example, a solid catalyst in a liquid reaction mixture), whereas homogeneous catalysts are in the same phase (for example, a dissolved catalyst in a liquid reaction mixture).

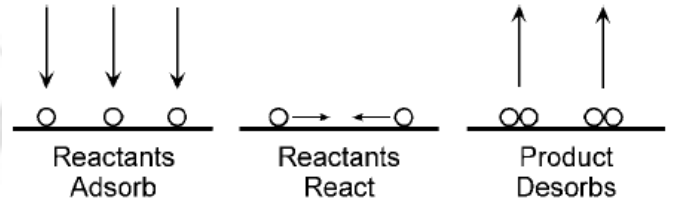

Figure 1.2 The reactants adsorb onto the surface of a heterogeneous catalyst, react, and then the product desorbs.

In order for the reaction to occur, one or more of the reactants must diffuse to the catalyst surface and adsorb onto it. After reaction, the products must desorb from the surface and diffuse away from the solid surface. Frequently, this transport of reactants and products from one phase to another plays a dominant role in limiting the reaction rate. Understanding these transport phenomena and surface chemistry such as dispersion is an important area of heterogeneous catalyst research. Catalyst surface area may also be considered.

Zeolite-based heterogeneous catalysts are used by industrial chemical companies in the interconversion of hydrocarbons and the alkylation of aromatic compounds. A very good example is the zeolite ZSM-5 is an aluminosilicate zeolite with a high silica and low alumininum content. Its structure is based on channels with insecting tunnels. The aluminum sites are very acidic. The substitution of Al^{3+} in place of the tetrahedral Si^{4+} silca requires the presence of an added

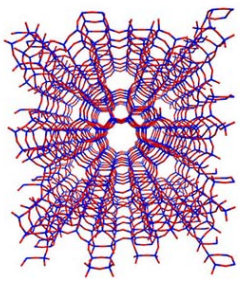

Figure 1.3 Heterogeneous ZSM-5 zeolite catalyst structure.

positive charge. When this is H^+, the acidity of the zeolite is very high. The reaction and catalysis chemistry of the ZSM-5 is due to this acidity. The ZSM-5 zeolite catalyst is used in the petroleum industry for hydrocarbon interconversion. *e.g.* use is in the isomerizations of xylene- from meta to para-xylene. The acidic zeolite promotes carbocation isomerizations. A simple model for heterogeneous catalysis involves the catalyst providing a surface on which the reactants (or substrates) temporarily become adsorbed. Bonds in the substrate become weakened sufficiently for new bonds to be created. The bonds between the products and the catalyst are weaker, so the products are released. Different possible mechanisms for reactions on surfaces are known, depending on how the adsorption takes place (Langmuir-Hinshelwood and Eley-Rideal). Many catalysts used in refineries and in petrochemical applications are regenerated and reused multiple times to save costs and energy and to reduce environmental impact from recycling or disposal of spent catalysis. In multistep synthesis, the preparative difficulties increase significantly with the number of steps, due mainly to extensive isolation and purification operations. These drawbacks can be overcome by exploiting a multistep-sequential synthetic methodology, namely by adding reagents and/or catalysts in a sequential manner without isolating the previously formed intermediates [1.2]. Despite the advantages of homogeneous catalysts, difficulties in recovering the catalyst from the reaction mixture severely inhibit their wide use in industry. Heterogeneous catalysis supplies the opportunity for easy separation and recycling of the catalyst, easy product purification and possibly, continuous or multiple processing of compounds. The recent years have witnessed a tremendous upsurge of interest in using recyclable reagents and heterogeneous catalysts [1.3] for various chemical transformations due to their inherent economic and environmental benefits [1.4]. Reactions assisted by heterogeneous catalysts have revolutionized the domain of organic synthesis due to higher yields, easy work up, recyclability of the catalysts and consequent minimization of waste production. Recently, there has been an increasing interest in developing processes with minimum environmental threats and maximum economic benefits. In that sense, a great demand to develop highly selective heterogeneous catalyst with large number of Lewis acid sites under mild reaction conditions without employing toxic materials. As a consequence recent research in the area of catalysis has concentrated on finding alternative methods that will increase selectivity, increase yield and reduce waste [1.5]. One of the major goals of green chemistry is to develop environmentally acceptable routes to important organic products. Methods by which this can be achieved are increasing product selectivity, aiming for 100% atom efficiency and replacing stoichiometric reagents with

heterogeneous catalysts thus allowing easy separation of the catalyst from the product. Increasingly tighter guidelines are being issued concerning the disposal of waste materials, with increasing public and corporate pressure to comply with them. In this respect it was only a matter of time before we saw the principles of making chemistry more environmentally friendly, being applied to oxidation chemistry to give us new and important challenges in research. The use of a reaction system in which the catalyst is in a different phase to that of the substrate and the products allows easy removal of the catalyst from the reaction mixture via filtration, centrifugation or decantation. This enables easy catalyst recovery and recycles whilst negating the need for a quench or workup step. The porosity of such materials can lead to increased reaction selectivity by giving high selectivity to the desired product.

It has been known that zinc oxide is a considerable material for semiconductor due to its wide band gap (3.37 eV) and its high excitation binding energy (60 meV) at room temperature [1.6]. Zinc oxide (ZnO) is a versatile semiconducting material with efficient excitonic emission at room temperature and unique acoustic [1.7], electronic [1.8], catalytic [1.9] and photocatalytic properties [1.10], which make it an appropriate material for various applications such as sensors [1.11], solar cells [1.12], varistors [1.6], electroluminescent [1.13] and optoelectric devices [1.14]. Since zinc oxide shows different physical and chemical properties depending upon morphology of nanostructure, not only various processes for its synthesis are under development but also the physical and chemical properties of the synthesized zinc oxide are investigated in terms of its morphology. As a p-type semiconductor with a narrow band gap (Eg¼ 1.2 eV) [1.15], CuO is a unique monoxide compound (in monoclinic phase, different from normal rock-salt type structure) for both fundamental investigations and practical applications. CuO has been used as heterogeneous catalysts in many important chemical processes, such as degradation of nitrous oxide, selective catalytic reduction of nitric oxide with ammonia, and oxidation of carbon monoxide, hydrocarbon and phenol in supercritical water [1.16(a)-(b)]. Recent studies found that CuO could exist in as many as three different magnetic phases and form the basis for several high-T_c superconductors and materials with giant magneto resistance [1.17(a)–(e)]. CuO can be also used as gas sensors [1.18], optical switch [1.19], magnetic storage media [1.20], lithium batteries [1.21] and solar cells [1.22] owing to its photoconductive and photochemical properties. NiO nanoparticles have attracted a great deal of attention and have heightened scientific interests because of their potential applications and due to their special physical and chemical properties. Nickel oxide (NiO) has many applications in various fields, such as catalysis [1.23], gas sensors

[1.24], battery cathode [1.25], magnetic materials [1.26] and fuel cell electrodes [1.27]. Co_3O_4, a mixed valence compound with a normal spinel structure, is the stablest phase in the Co–O system and one of the most important transitional metal oxides that has a gas sensing behavior and solar energy reflecting properties [1.28]. Cobalt oxide (Co_3O_4) stands as an important functional material, in part because of its vast applications for use in sensors, electrochemistry, pigments, catalysis, magnetism, and energy storage [1.29 (a)-(b)]. Co_3O_4 nanostructures are expected to lead to even more attractive applications in conjunction with their traditional arena and nanotechnology [1.30(a)-(c)]. When falling in the nanosized regime, Co_3O_4 is expected to exhibit quantum tunneling of magnetization [1.31(a)-(b)]. Chromium sesquioxide (Cr_2O_3) is the hardest oxide, and exhibits high hardness values and low friction coefficients [1.32]. Chromium sesquioxide (Cr2O3) is antiferromagnetic and in the case of small particle size, this material exhibits a slight ferrimagnetism. As it was pointed out by Nėel [1.33] this magnetism is caused by uncompensated magnetic ions at the surface, whereas Snoek [1.34] additionally considers the possibility of an increase of the magnetization because of lattice imperfections. Furthermore, it is an important refractory material due to its high melting temperature (about 2435^oC) and oxidation resistance. Small particles (below 200 nm) are preferred for pigment applications in order to increase the opacity. Cr_2O_3 particles below 50 nm can be used as transparent colorants. Nanoparticles of Cr_2O_3 are widely applied in fields as advanced colorants [1.35], hydrogen sorption materials [1.36], and wear resistance materials [1.37], catalysts [1.38]. Ultra fine chromium oxide (eskolaite) is used as a catalyst in oxidation reactions, hydrogenation reactions, isomerization of olefins, and dehydrogenation of alkanes and pigments production. Mn_2O_3 exists in different polymorphs, where the metastable tetragonal γ-Mn_2O_3 and thermal stable cubic α-Mn_2O_3 are the most important. Polymorphs of Mn_2O_3 have been proposed as cheap, environmental-friendly catalysts for carbon monoxide [1.39] and organic pollutants [1.40(a)-(b)] oxidation, and nitrogen oxide decomposition [1.41(a)-(b)]. Mn_2O_3 was also an important substrate for Li–Mn–O oxide cathode materials rechargeable lithium batteries [1.42]. Moreover, Mn_2O_3 can also be used for synthesizing soft magnetic materials such as manganese zinc ferrite [1.43].

Nanomaterials are very interesting because of their unique properties and their potential applications in many fields. It is well know that the properties of nanocrystals, such as electronic, optoelectronic and luminescent, depend not only on their chemical composition, but also on their structure, phase, shape, size and size distribution [1.44(a)–(c)]. Therefore, much attention has been paid in controlling these parameters to

manipulate. Long been known that surfactant self-assemble in selective solvents to form stable aggregates, such as micelles or micelle-like aggregates, offering a template for synthesize inorganic compounds. The goal is not only to optimally control the size, shape, morphology, and polydispersity of the crystals but also to fabricate novel organic/inorganic composite materials with interesting electrical, magnetic, and optical properties. Among them, chemical solution route provides for the preparation of nano sized materials a more promising option due to its simpleness, practicality, large scale, controllability and low cost. Especially in the preparation of nano-powders in liquid phase, the viscosity dramatically enhances because of the huge specific surface area of the product. To obtain nano-particles with narrow size distribution by the reactive precipitation method, a high degree of supersaturation and uniform spatial concentration distribution of the product solute are indispensable, and micro mixing is a key factor to meet these requirements [1.45]. In order to enhance the micro mixing, some ways are well discussed and available, such as strengthening stirring, optimizing agitating blade and adopting novel reactors [1.46]. But the power of agitation cannot increase unboundedly. As the viscosity gains, the effect of raising the Reynolds number diminishes gradually [1.46]. Thus viscosity breaking is another effective approach to improve micro mixing. Surfactant has been used to reduce the viscosity of the suspension and to stabilize the suspension of the nano-powders [1.47]. Thus surfactant possesses the potential to intensify mass transfer while preventing agglomeration.

1.3 Green synthetic methodologies

Green chemistry is a rapidly developing new field that provides us a proactive avenue for the sustainable development of future science and technologies [1.48]. Green chemistry uses highly efficient and environmental benign synthetic protocols to deliver life saving medicines, accelerating lead optimization processes in drug discovery, with reduced unnecessary environmental impact. Green chemistry also offers enhanced chemical process economics concomitant with a reduced environmental burden. Microwave-assisted organic synthesis is a quickly developing area in synthetic organic chemistry [1.49]. Recently, its application has been extensively explored for the synthesis of heterocyclic compounds particularly for the synthesis of indoles [1.50], pyrroles [1.51], oxazoles [1.52] thiophenes [1.53], quinolines [1.54], benzimidazoles [1.55]. Microwave assisted reactions using dry media have attracted much interest because of the simplicity in operation, greater selectivity and rapid synthesis of a variety of heterocyclic compounds. Thus, it was

thought worthwhile to synthesize the title compounds using a green route, the Microwave Organic Reaction Enhancement methods. Besides the fact that commercially available microwave (MW) reactors provide a comfortable, safe, and clean way of working, MW irradiation shows remarkable advantages in chemical reactions. It accelerates many syntheses providing selective activation with short start-up phase and allows fast optimization of reactions [1.56]. Solid-state reaction is a green reaction and can be accelerated by heating, shaking, grinding of the reaction mixture and irradiation with ultrasound, which makes it a much ideal synthetic process. Solvent free method has been used more and more frequently in organic synthesis in recent three decades because of their ease of handling, enhanced reaction rates, greater selectivity, and simple work-up. Solvent less organic reactions based on grinding of two macroscopic particles together [1.57] mostly involve the formation of a liquid phase prior to reaction, i.e., formation of a eutectic melt of uniform distribution where the reacting components being in close proximity are poised to react in a controlled way. The grinding mode for the solid-state reactions has earlier been reported for Grignard reaction [1.58], Reformatsky reaction [1.59], Aldol condensation [1.60], Dieckmann condensation [1.61], Knoevenagel condensation [1.62], reduction [1.63] and others [1.64]. Most of these reactions are carried out at room temperature in absolutely solvent-free environment using only a mortar and pestle. Benzimidazoles are very useful intermediates/subunits for the development of molecules of pharmaceutical or biological interest. Substituted benzimidazole derivatives have found applications in diverse therapeutic areas including antiulcers, antihypertensives, antivirals, antifungals, anticancers, and antihistaminics [1.65]. 2-Mercaptobenzimidazole derivatives are known to possess varied biological activities [1.66]. 2-Azetidinone derivatives have been reported to possess anti-inflammatory [1.67], anticonvulsant [1.68], fungicidal [1.69], antibiotic [1.70], anticancer [1.71], antielastase [1.72], antiviral [1.73], antimicrobial [1.73], antitumor [1.74], anti-HCMV [1.75], antibacterial [1.76], activities and pharmacological interest [1.77]. The incorporation of a 2-oxoazetidine moiety in to 2-mercaptobenzimidazole scaffold enhances its activity. Quinoxaline-diones and their derivatives are important members of heterocyclic compounds and are widely applied in many fields, as curatorial intermediates, bactericides and insecticides [1.78]. Benzodiazepines are interesting compounds because they belong to an important class of the pharmacologically pre-eminent 1,5-benzodiazepines which have been extensively used as anticonvulsant, antianxiety, analgesic, sedative, antidepressive, hypnotic and antiinflamatory agents [1.79].

References:

1.1 (a) Kantam, M. L.; Shiva Kumar, K. B; Sridhar, C. *Adv. Synth. Catal.* **2005,** *347*, 1212; (b) Dai, W. L.; Luo S. L.; Yin, S. F.; Au C. T. *Applied Catalysis A: General* **2009** 366 2, (c) Kozhevnikov, I.V. *J. Mol. Cat.A: Chemical*, **2009**, *305*, 104; (d) Leveneur, S.; Yu, D.; Salmi, M. T. *J. Mol. Cat.A: Chemical*, **2009**, *303*, 148.

1.2 Tietze, L. F.; Beifuss, V. *Angew. Chem. Int. Ed. Engl.* **1993,** *32*, 131.

1.3 Fricke, R.; Hosslick, H.; Lischke, G.; Richter, M. *Chem. Rev.* **2000**, *100*, 2303.

1.4 Zhang, Y.; Li, C. J. *J. Am. Chem. Soc.* **2006**, *128*, 4242.

1.5 Sheldon, R. A. *Chemtech.* **1991**, 566.

1.6 Reynolds, D. C.; Look, D. C.; Jogai, B.; Hoelscher, J. E.; Sherriff, R. E.; Harris, M. T.; Callahan, M. J. *J. Appl. Phys.* **2000**, *88*, 2152.

1.7 Kwok, W. M.; Djurisic, A. B.; Leung, Y. H.; Chan, W. K.; Phillips, D. L.; Chen, H. Y.; Wu, C. L.; Gwo, S.; Xie, M. H. *Chem. Phys. Lett.* **2005**, *412* 141.

1.8 Qian, H. S.; Yu, S. H.; Gong, J. Y.; Luo, L. B.; Wen, L. L. *Cryst. Growth Des.* **2005**, *5*, 935.

1.9 Lindsay, R.; Michelangeli, E.; Daniels, B. G.; Ashworth, T. V.; Limb, A. J.; Thornton, G.; Gutierrez-Sosa, A.; Baraldi, A.; Larciprete, R.; Lizzit, S. *J. Am. Chem. Soc.* **2002**, *124*, 7117.

1.10 Liqiang, J.; Yichun, Q.; Baiqi, W.; Shudan, L.; Baojiang, J.; Libin, Y.; Wei, F.; Honggang, F.; Jiazhong, S. *Sol. Energy Mater. Sol. Cells* **2006**, *90*, 1773.

1.11 N´emeth, J.; Gattorno, G. R.; Diaz, D.; Olmos, A. R. V.; Dekany I. *Langmuir* **2004**, *20*, 2855.

1.12 Wang, Y. S.; Thomas, P. J.; O'Brien, P. *J. Phys. Chem. B* **2006**, *110*, 4099.

1.13 Saito, S.; Miyayama, M.; Koumoto, K.; Yanagida, H. *J. Am. Ceram. Soc.* **1985,** *68*, 40.

1.14 Shen, G.; Bando, Y.; Lee, C. J. *J. Phys. Chem. B* 109 **2005**, *109*, 10779.

1.15 Musa, A. Q.; Akomolafe, T.; Carter, M. J.; *Sol. Energy Mater. Sol. Cells* **1998**, *51*, 305.

1.16 (a) Reitz, J. B.; Solomon, E. I. *J. Am. Chem. Soc.* **1998**, *120*, 11467; (b) Wang, H.; Xu, J. Z.; Zhu, J. J.; Chen, H.Y. *J. Cryst. Growth* **2002**, *244*, 88.

1.17 (a)Wang, W.; Zhan, Y.; Wang, X.; Liu, Y.; Zheng, C.; Wang, G. *Mater. Res. Bull.* **2002**, *37*, 1093; (b) Wu,M. K.; Ashburn, J. R.; Torng, C. J.; Hor, P. H.; Meng, R. L.; Gao, L.; Huang, Z. J.; Wang, Y. Q.; Chu, C. W. *Phys. Rev. Lett.* **1987**, *58*, 908; (c) Zheng, X. G.; Xu, C. N.; Tomokiyo, Y.; Tanaka, E.; Yamada, H.; Soejima, Y. *Phys. Rev. Lett.* **2000**, *85*, 5170; (d) Prabhakaran, D.; Subramanian, C.; Balakumar, S.; Ramasamy, P. *Physica C* **1999**, *319*, 99; (e) Borgohain, K.; Mahamuni, S. J. *Mater. Res.* **2002,** *17*, 1220.

1.18 Poizot, P.; Laruelle, S.; Grugeon, S.; Dupont, L.; Taracon, J. M. *Nature* **2000,** *407*, 496.

1.19 MacDonald, A. H. *Nature* **2001**, *414*, 409.

1.20 Kumar, R. V.; Diamant, Y.; Gedanken, A. *Chem. Mater*. **2000**, *12*, 2301.

1.21 Gao, X. P.; Bao, J. L.; Pan, G. L.; Zhu, H. Y.; Huang, P. X.; Wu, F.; Song, D. Y *J. Phys. Chem. B* **2004,** *108*, 5547.

1.22 Maruyama, T. *Sol. Energy Mater. Sol. Cells* **1998**, *56*, 85.

1.23 Wang, Y. P.; Zhu, J. W.; Yang, X. J.; Lu, L.D.; Wang, X. *Thermochim. Acta* **2005**, *437*, 106.

1.24 Hotovy, I.; Huran, J.; Spiess, L.; Hascik, S.; Rehacek, V. *Sensors Actuators B-Chem* **1999**, *57*, 147.

1.25 Zhang, F. B.; Zhou, Y. K.; Li, H. L. *Mater. Chem. Phys.* **2004**, *83*, 260.

1.26 Ghosh, M.; Biswas, K.; Sundaresan, A.; Rao C. N. R. *J. Mater. Chem* **2006**, *16*, 106.

1.27 Li, F.; Chen, H. Y.; Wang, C. M.; Hu, K. S. *J. Electroanal. Chem.* **2002**, *531*, 53.

1.28 Logothesis, M.; Park, R.; Meitzler, A. H.; Laud, K. K. *Appl. Phys. Lett.* **1975**, *26*, 209.

1.29 (a) Jiang, Y.; Wua, Y.; Qian, Y. T. *Mater. Chem. Phys.* **2002**, *74*, 234; (b) Li, W. Y.; Xu, L. N.; Chen, J. *Adv. Funct. Mater.* **2005**, *15*, 851.

1.30 (a) Feng, J.; Zeng, H. C.; *Chem. Mater.* **2003**, *15*, 2829; (b) Salabas, E. L.; Rumplecker, A.; Kleitz, F.; Radu, F.; Schu1th, F. *Nano Lett.* **2006**, *6*, 2977; (c) Li, Y. G.; Tan, B.; Wu, Y. Y. *Nano Lett.* **2008**, *8*, 265.

1.31 (a) Chudnovsky, E. M. *J. Appl. Phys.* **1993**, *73*, 6697; (b) Nethravathi, C.; Sen, S.; Ravishankar, N.; Rajamathi, M.; Pietzonka, C.; Harbrecht, B. *J. Phys. Chem. B* **2005**, *109*, 11468.

1.32 Caro, G.; Natali, M.; Rossetto, G.; Zanella, P.; Salmaso, G.; Restello, S.; Rigato, V., Kaciulis, S.; Mezzi, A. *Chem. Vapor Depos.* **2005**, *11*, 375.

1.33 Lee, N. *J. Phys. Sot. Japan Suppl. B-l* **1962,** *17*, 676.

1.34 Snoek, J. L. *Physika* **1950**, *16*, 333.

1.35. Kim, D. –W; Shin II, S.; Lee, J.-D.; Oh, S.-G. *Mater. Lett.* **2004,** *58*, 1894.

1.36 Bobet, J. -L.; Desmoulins, K. S.; Grigorova, E.; Cansell, F.; Chevalier, B. *J. Alloys Compd.* **2003**, *351*, 217.

1.37 Bijker, M. D.; Bastiaens, J. J. J.; Draaisma, E. A.; de Jong, L. A. M.; Sourty, E.; Saied, S. O.; Sullivan, J. L. *Tribol. Int.* **2003**, *36*, 227..

1.38 Uhm, J. -H.; Shin, M. -Y.; Jiang, Z. -D.; Chung, J. -S. *Appl. Catal. B* **1999**, *22*, 293.

1.39 Imamura, S.; Shono, M.; Okamoto, N.; Hamada, A.; Ishida, S. *Appl. Catal. A* **1996**, *142*, 279.

1.40 (a) Baldi, M.; Sanchez, E. V.; Gallardo, A. J. M.; Milella, F.; Busca, G. *Appl. Catal. B* **1998**, *17*, 175; (b) Gand, L. M.; Korili, S. A.; Gil, A. *Stud. Surf. Sci. Catal.* **2002**, *143*, 527.

1.41 (a) Yamashita, T.; Vannice, A. *J. Catal.* **1996** , *161*, 254; (b) Vannice, A.; Yamashita, T. *Appl. Catal. B* **1997**, *13*, 141.

1.42 Nakamura, T.; Kajiyama, A. *Solid State Ionics* **1999**, *124*, 45.

1.43 Pankov, V. V. *Ceram. Int.* **1998**, *14*, 87.

1.44 (a) Alivisatos, A. P. *Science* **1996**, *271*, 933; (b) Lieber, C. M. *Solid State Commun.* **1998**, *107*, 607; (c) Manna, L.; Scher E. C.; Alivisatos A P. *J. Am. Chem. Soc.* **2000**, *122*, 12700.

1.45 Chen, J. F.; Shao, L.; Guo, F.; Wang, X. M. *Chem. Eng. Sci.* **2003**, *58*, 569.

1.46 Min, J. *Ph.D. dissertation, Beijing University of Chemical Technology, China* **2005**.

1.47 Zhao, L. P.; Gao L. *J. Colloid Interf. Sci.* **2003**, *262*, 428.

1.48 (a) Varma, R. S. *Green Chemistry: Challenging Perspectives*; Tundo, P., Anastas, P. T., *Eds.; Oxford University Press: Oxford*, **2000**, 221; (b) Anastas, P. T.; Warner, J. C. *Green Chemistry: Theory and Practice; Oxford University Press: Oxford*, **2000**; (c) Clark, James H.; Macquarrie, Duncan J. *Eds.; Handbook of Green Chemistry and Technology, Wiley-Blackwell,* **2002**; (d) DeVito, S. C. and R. L. Garrett *Designing safer chemicals: green chemistry for pollution prevention.* Washington, D.C., American Chemical Society, **1996**; (e) Anastas, P. T. and M. M. Kirchhoff; *Acc Chem Res.* **2002**, *35*, 686.

1.49 Caddic, S. *Tetrahedron* **1995**, *51*, 10403.

1.50 Rudolph, A. A.; Amanda, B. *Synlett* **1992**, 795.

1.51 Danks, T. N. *Tetrahedron Lett.* **1999**, *40*, 3957.

1.52 Brain, C. T.; Paul J. M. *Synlett* **1999**, 1642.

1.53 Zhang, H.; Yang, G.; Chen, J.; Chen, Z. *Synthesis* **2004**, 3055.

1.54 Seijas, J. A.; Tato, M. P. V.; MartıOnez, M. M. *Tetrahedron Lett.* **2000**, *41*, 2215.

1.55 Kidwai, M.; Bhushan, K. R.; Kumar, P. *Monatsh. Chem.* **1999**, *130*, 585.

1.56 Koopmans, C.; Iannelli, M.; Kerep, P.; Klink, M.; Schmitz, S.; Sinnwell, S.; Ritter, H. *Tetrahedron* **2006**, *62*, 4709.

1.57 Rothenberg, G.; Downie, A. P.; Raston, C. L.; Scott, J. L. *J. Am. Chem. Soc.* **2002**, 123, 8701.

1.58 Toda, F.; Takumi, H.; Yamaguchi, H. *Chem. Express* **1989**, *4*, 507.

1.59 Tanaka, K.; Kishigami, S.; Toda, F. *J. Org. Chem.* **1991**, *56*, 4333.

1.60 Toda, F.; Tanaka, K.; Hamai, K. *J. Chem. Soc., Perkin Trans.* **1990**, *1*, 3207..

1.61 Toda, F.; Suzuki, T.; Higa, S. *J. Chem. Soc., Perkin Trans*. **1998**, *1*, 3521.

1.62 Ren, Z. -J.; Cao, W.-G.; Tong, W.-Q. *Synth. Commun*. **2002**, *32*, 3475.

1.63 Toda, F.; Kiyoshige, K.; Yagi, M. *Angew. Chem., Int. Ed. Engl.* **1989**, *101*, 329.

1.64 (a) Ren, Z. -J.; Cao, W.-G.; Ding, W.-Y.; Shi, W. *Synth. Commun.* **2004,** *34*, 4395; (b) Ren, Z.; Cao, W.; Tong, W.; Jin, Z. *Synth. Commun*. **2005**, *35*, 2509; (c) Schmeyers, T.; Toda, F.; Boy, J.; Kaupp, G. *J. Chem. Soc., Perkin Trans*. **1998**, *2*, 989.

1.65 (a) Gravatt, G. L.; Baguley, B. C.; Wilson, W. R.; Denny, W. A. *J. Med. Chem*. **1994**, *37*, 4338; (b) Lin, S. N.; Yang, L. H. *Tetrahedron Lett*. **2005**, *46*, 4315; (c) Horton, D. A.; Bourne, G. T.; Smythe, M. L. *Chem. Rev*. **2003**, *103*, 893.

1.66 Guru, N.; Srivastava, S. D. *J. Sci. Ind. Res*. **2001**, *60*, 601.

1.67 Muhammad, M.; Bhat, I. *Indian J. Heterocycl. Chem.* **2003**, *13*, 183.

1.68 Biradar, J. S.; Manjunath, *Indian J. Chem. (B)* **2004**, *43B*, 141.

1.69 Sharma, P.; Kumar, A. *Indian J. Chem. (B)* **2004**, *43B*, 385.

1.70 Desai, J. M; Shah V. H. *Indian J. Chem.(B)* **2003**, *42B*, 631.

1.71 Banik, B. K.; Becker, F. F.; Banik, I. *Bioorg. Med. Chem.* **2004**, *12*, 2523;

1.72 Anaya, J.; Gero, D. S.; Grande, M.; Hernando, J. I. M.; Laso, N. M. *Bioorg. Med. Chem.* **1999**, *7*, 837.

1.73 Gerona-Navarro, G.; Perez de Vega, M. J.; Garcia-Lopez, M. T.; Andrei, G.; Snoeck, R.; De Clercq, E.; Balzarini, J.; Gonzalez-Muniz, R. *J. Med. Chem*. **2005**, *48*, 2612.

1.74 Singh, G. S.; Mmolotsi, B. J. *IL Farmaco* **2005**, *60*, 727.

1.75 Veinberg, G.; Shestakova, I.; Vorona, M.; Kanepe, I.; Lukevics, E. *Bioorg. Med. Chem. Lett*. **2004**, *14*, 47.

1.76 Gerona-Navarro, G.; Jesus Perez de, V. M.; Teresa G. M.; Andrei, G.; Snoeck, R.; Balzarini, Jan; De Clercq E.; Gonza´lez-Mun˜iz, R. *Bioorg. Med. Chem. Lett*. **2004**, *14*, 2253.

1.77 Afonso, A.; Hon, F.; Fett, N.; Weinstein, J.; Ganguly, A. K.; Naples, L.; Hare, R. S.; Miller, G. H. *Bioorg. Med. Chem. Lett*. **1998**, *8*, 2793.

1.78 Aoyama, Y.; Uenaka, M.; Kii, M.; Tanaka, M.; Konoike, T.; Hayasaki-Kajiwara, Y.; Naya, N.; Nakajima, M. *Bioorg. Med. Chem*. **2001**, *9*, 3065.

1.79 (a) Moloney,M. G. *Nat. Prod. Rep.* **2002** *597*, 39; (b) Sternback, L. H. *Angew. Chem., Int. Ed. Engl.* **1971**, *10*, 34; (c) Randall, L. O.; Kappel B.; Garattini, S.; Mussini, E.; Randall, L. O. *Benzodiazepines Eds.; Raven Press: New York*, **1973,** 27; (d) Schutz, H. *Benzodiazepines, Springer: Heidelberg*, **1982**.

Chapter - 2

Development, Characterization and Application of Heterogeneous Catalyst

Synthesis and characterization of transition metal oxides

In the past decade, the design and synthesis of functional molecule analogues by the self-assembly of metal-connecting points and organic linkers under controlled reaction conditions has attracted a great deal of attention among the inorganic, materials and supramolecular chemistry communities [2.1]. As a result of these concerted efforts, the studies on the syntheses of metal-organic frameworks (MOFs) have undergone tremendous development by virtue of their attractive topologies and potential application in areas such as magnetism, non-linear optics, electrical conductivity, host–guest chemistry, gas storage, nonlinear optics, ion-exchange and catalysis [2.2-2.3]. The development of metal complexes that assemble into predictable supramolecular structures in the crystal is of great interest because of their potential in designing new materials with desirable optical and magnetic properties [2.4]. Synthetic materials are substantially different from those of bulk materials due to their physical properties such as electrical conductivity, magnetic property, optical property, and mechanical property. Synthetic transition metal oxides are substantially different from those of bulk materials and they have several applications. *viz.* heterogeneous catalyst because of their high level of chemo-selectivity, environmental compatibility, simplicity of operation and availability at low cost. Synthetic routes that have been employed to prepare metal oxide include reverse micelle technique, solvothermal process, solid-state reactions, template synthesis, precursor method, by the application of ultrasound. The present chapter deals with the synthesis of some transition metal oxides their characterization by different spectroscopic methods and their application in different organic transformations. Transition metal oxides are synthesized from metal organic frame work by thermal decomposition at elevated temperature.

Methodology Scheme:

$$M(OH)_n + \text{Organic acid} \xrightarrow[\text{Solid-State Grinding}]{\text{Room Temperature}} \text{Precursor complex} \xrightarrow[\text{decomposition}]{\text{Thermal}} M_xO_y$$

2.1 Experimental section

2.1.1 Materials

All chemicals were of reagent grade and were used without further purification unless otherwise stated. Nitrilo-triacetic acid (H_3NTA) and Bicine [(N,N-bis(2-hydroxyethyl)glycine], Agar, agarose and gelatin were obtained from Aldrich (U.S.).

Sodium hydroxide, Transition metal salts were received from E. Mark (India). All solvents were purified prior to use following standard methods.

2.1.2 Physical measurements

FT-IR analysis was carried out on air-dried minerals samples. All spectra recorded at 4 cm^{-1} resolution with 10 scan with a *Perkin Elmer-Spectrum One FT-IR Spectrometer* from 4000 to 450 cm^{-1}. A background spectrum was measured for pure KBr. To confirm the crystalline nature of the mineral sample PXRD data were recorded with *Seifert powder X-ray diffractometer (XRD 3003TT)* with CuK_α source (λ = 1.54 Å) on glass surface of air-dried sample. In order to determine presence of organic matrices and water of crystallization in the obtained mineral crystals, the samples were analyzed from 25 to 1000°C using a *DT-40 thermal analyzer*. The temperature was increased at a rate of 2°C/min. Scanning electron micrograph (SEM) images were obtained by means of a *LEO-1430 VP* electron microscope on samples glued on an aluminum stub and gold sputtered.

The intensity data of the single crystal was collected using a Bruker SMART APEX-II CCD diffracto-meter, equipped with a fine focus 1.75 kW sealed tube MoK_α radiation (λ = 0.71073 Å) at 273(3) K, with increasing ξ (width of 0.3^o per frame) at a scan speed of 3 s/frame. The SMART software was used for data acquisition. Data integration and reduction were undertaken with SAINT and XPREP software [2.5]. Multi-scan empirical absorption corrections were applied to the data using the program SADABS [2.6]. Structures were solved by direct methods using SHELXS-97 [2.7] and refined with full-matrix least squares on F^2 using SHELXL-97 [2.7]. All non-hydrogen atoms were refined anisotropically. The hydrogen atoms were refined as riding atoms in idealized locations. Selected crystallographic data summarized in Tables 2.1

2.1.3 Synthesis of MOF from Nitrilotriacetic acid (NTA) and Bicine [N,N-bis(2-hydroxyethyl)glycine]

Complex **1** was synthesized by a simple acid-base reaction in the solid phase as shown below. A mixture of nitrilotriacetic acid (1 mmol, 0.191 g) and anhydrous freshly prepared zinc hydroxide (1 mmol, 0.099 g) was ground thoroughly with a pestle in an open mortar at room temperature under air. The mixture was ground for 5 min until the mixture turned into slurry. X-ray quality single crystals of Zn complex **1** were grown from water within a day at room temperature by slow evaporation of ethanol/water (1:1) mixture in quantitative yield. Complex **2** was synthesized following the same procedure as **1** as described below, only the metal to ligand ratio was different (3:2). Similarly a mixture of

Bicine (0.326 g, 2 mmol) and freshly prepared copper hydroxide (1 mmol, 0.097 g) were ground thoroughly with a pestle in an open mortar at room temperature in air. The mixture was ground occasionally for 30 min until the mixture turned into a melt. X-ray quality blue single crystals of the complex **3** were grown from ethanol/water (1:1) mixture within two days at room temperature in quantitative yield.

$$NTAH_3 + Zn(OH)_2 \xrightarrow[\text{Grinding}]{\text{Solid Phase}} [Zn(NTAH)] + 2\ H_2O$$

$$2NTAH_3 + Zn(OH)_2 \xrightarrow[\text{Grinding}]{\text{Solid Phase}} Zn(OH)_2[Zn_2(NTA)_2] + 2\ H_2O$$

$$2\ BicineH + Cu(OH)_2 \xrightarrow[\text{Grinding}]{\text{Solid Phase}} [Cu(Bicine)_2] + 2\ H_2O$$

Table 2.1 Crystal data and structure refinement parameters for complex **1**, **2** and **3**.

	Complex **1**	Complex **2**	Complex **3**
CCDC No.	280983	612885	607756
Empirical formula	$C_6H_{15}NO_{10}Zn$	$C_{12}H_{28}N_2O_{20}Zn_3$	$C_{12}H_{24}N_2O_8Cu$
Fw	326.57	716.53	387.87
Temperature (K)	293 (2)	298 (2)	298 (2)
Radiation	Mo Kα	Mo Kα	Mo Kα
Wavelength (Å)	0.71073	0.71073	0.71073
Size (mm)	0.27x0.19x0.15	0.28x0.23x0.17	0.20x0.15x0.11
Crystal system	Orthorhombic	Orthorhombic	monoclinic
Space group	Pbca	Pna2(1)	P2(1)/c
a (A˚)	12.2958(10)	12.7369(10)	9.5164(8)
b (A˚)	6.6129(10)	11.3290(10)	12.3042(11)
c (A˚)	27.846(2)	16.4424(14)	7.1922(6)
α (°)	90	90	90
β (°)	90	90	111.328(5)
γ (°)	90	90	90
V (Å 3)	2264.2(4)	2372.6(3)	784.47(12)
Z	9	4	2
qcalc (Mg/m3)			1.625
μ	2.288	3.12	l 1.435
F(000)	1170	1272	398
Goodness-of-fit	1.103	0.931	1.205
Final R indices [I > 2σ(I)]	R1 = 0.0213	R1 = 0.0282	R1 = 0.0461
	wR2 = 0.0604	wR2 = 0.0980	wR2 = .1459
R indices (all data)	R1 = 0.0224	R1 = 0.0291	R1 = 0.0575
	wR2 = 0.0610	wR1 = 0.0997	wR2 = 0.1639

2.1.4 Gel Mediated synthesis of Transition metal hydroxide and oxide

Agar was dissolved in water and the solution was heated to ~70°C. Aqueous metal chloride solution was added to this hot solution with constant stirring. The resultant mixture was then stirred vigorously for another ½ an hour and kept in the freeze to get solid gel. Then the solid gel is cut into small cubic pieces (~1 cm). These gel cubes was then placed in the sodium hydroxide solution without any mechanical disturbance for few

days at room temperature. The gel was then washed several times with water to remove excess amount of salts attached to it. The gel was then put into hot water and filtered hot to remove the organic materials. The resulting hydroxides were washed with ethanol to get rid of the organic matter attached to it and air-dried before characterization. Metal hydroxide was heated at 600^{o}C for about 5 hrs in a furnace to get corresponding oxides. Exactly same procedure had been employed for agarose and gelatin.

2.2 Results and discussion

2.2.1 MOF from Nitrilotriacetic acid (NTA) and Bicine [N,N-bis(2-hydroxyethyl) glycine]

The molecular structure of complex **1** consists of a Zn(II) ion, partially deprotonated NTA, and water molecules (Figure 2.1). The X-ray structure determination shows that complex **1** contains hexacoordinate Zn(II) with a distorted octahedral geometry. The angular distortion around Zn from the octahedral geometry is significant. The metal ion is bonded to two carboxylates from the ligand, each of which donates a single O atom. The third coordination site is occupied by the tertiary amine bridgehead N-atom of the ligand, while the remaining coordination sites of the octahedral geometry are occupied with water molecules. The resulting coordination polymer looks like an array of zinc-containing metallo-macrocycles. The Zn–O(carboxylate) and Zn–N bond lengths are 2.068(3), 2.074(2), and 2.222(2) Å, respectively, in good agreement with other Zn(II) carboxylate complexes [2.8]. The Zn–O(water) bond lengths are 2.0671(17), 2.107(3), and 2.105(3) Å, and are also similar to other Zn–OH_2 bond lengths reported in the literature [2.9]. Figure 2.2 shows an illustration of the 3D assembly of an infinite ladder framework. The rails of the ladder are made of almost linear, seven-atom units consisting of intermolecularly hydrogen bonded O(4)–C(4)–O(3)–Zn(1)–O(1)– C(2)–O(2) groups of NTA. The rungs of the ladder are made of an O atom of the axial water molecule. The distance between the rails of the ladder is 7.652 Å (distance between two adjacent Zn atoms forming the rail) and the two adjacent ladders are separated by 11.218 Å (distance between two Zn atoms of neighboring rails). However, the separation between the rungs of the ladder is 5.093 Å (forming the rail distance between two axial water oxygen atoms). Adjacent rails of the ladders are inter-

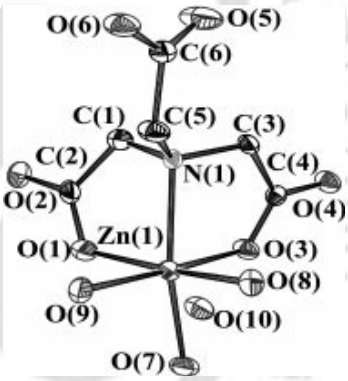

Figure 2.1 Crystal structure of complex **1**.

connected by intermolecular hydrogen bonds. A crystal water molecule (O10) forms strong hydrogen bonds with neighboring metal-coordinated water molecules as well as with the coordinated O atom of the carboxylic acid group. Each of the crystal water molecules is hydrogen bonded to the four neighboring molecules in an almost tetrahedral arrangement. The hydrogen bonding between the crystal water molecules is comparatively weak in nature

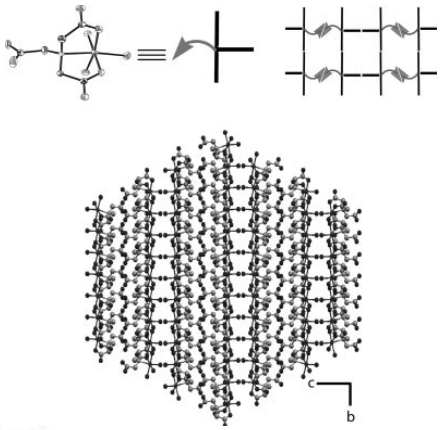

Figure 2.2 An infinite ladder framework along the *a* axis of complex **1**.

and forms a 1D zigzag infinite water chain along the *b* axis (Figure 2.3), which is one of the probable proton wire structures found in biological systems [2.9]. A zigzag motif of a water chain has also been reported for non-biological system [2.10]. The uncoordinated carboxylic acid group of NTA forms strong intramolecular hydrogen bonds with the neighboring O atom of the coordinated carboxylate group [O4···H4 1.793(5), O4–O6 2.604(7) Å and O6–H4–O4 170.23°]. O4 is acting as an H-bond acceptor and O6 as an H-bond donor and they act together like a clip (see Supporting Information), which eventually helps to form the 3D hydrogen bonded MOF. Here, both water–MOF and water–water interactions are important for the stability of the overall polymeric structure.

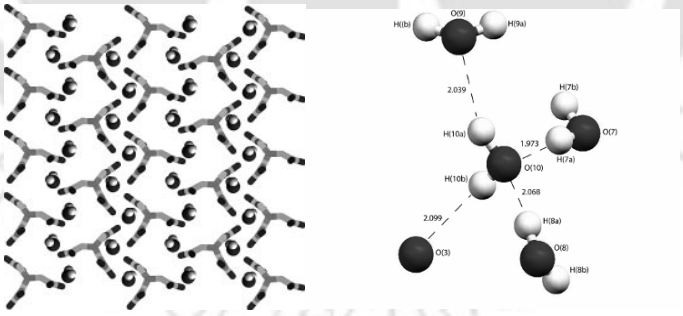

Figure 2.3 Perspective view of the zig-zag water chain in the crystal lattice (left) and tetrahedral arrangement of crystal water molecules (right) of complex **1**.

The interaction between the MOF and the water chain is moderate, as thermogravimetric analysis of complex **1** under N_2 shows a 22.67% weight loss at around 100°C, which corresponds to the loss of four water molecules (calculated 22.08 %). Among the three carboxylic acid groups present in the ligand, two are coordinated to the metal ion as carboxylate. TG analysis shows the sequential removal of one CO_2 molecule from the uncoordinated carboxylic acid group and two CO_2 molecules from the two coordinated

carboxylate groups in the ranges 260°–330°C (loss of 17.24%; calculated. 17.32%) and 330°–420 °C (loss of 41.66%; calculated 41.79%) respectively, which is in good agreement with the X-ray crystal structure (Figure 2.4). Complete decomposition is achieved at about 600°C. The DSC plot shows an endothermic peak at 100°C due to the loss of water molecules. It also shows two exothermic peaks at 310° and 370°C due to the decomposition of the carboxylic acid groups (Figure 2.4). The FT-IR spectrum of complex **1** shows a broad band centered at 3300 cm^{-1} due to the presence of water molecules; this vanishes when the complex is heated under vacuum (0.1 mm) at 150°C for 6 h (Figure 2.5). Two types of carboxylic acid groups are present in complex **1**: uncoordinated, unionized and coordinated, ionized. The FT-IR spectrum clearly shows the presence of uncoordinated, unionized COOH at 1740 cm^{-1} and coordinated, ionized COO^{-} at 1590 cm^{-1}; these values agree well with those in the literature [2.11]. The ^{1}H NMR spectrum shows a broad singlet in D_2O at δ = 3.49 ppm (NC*H*2COOH), which proves the dynamic complexation and decomplexation behavior of the third acid group at room temperature in solution. The FT-IR spectrum of complex **2** shows a broad band centered at 3500 cm^{-1} due to the presence of water molecules, which also vanishes when heated, as for complex **1** (Figure 2.5). Unlike complex **1**, however, it contains only coordinated, ionized types of carboxylic acid groups, which absorb at 1620 cm^{-1} [2.11]. The powder X-ray diffraction patterns of complex **1** show significant changesin the peak positions as well as intensities before and after water removal (Figure 2.6), which match well with the simulated pattern. Thermal decomposition of complex **1** at 700°C for 6 h in a muffle furnace forms wafers of ZnO with lengths ranging from 0.2 to 1.2 mm. The

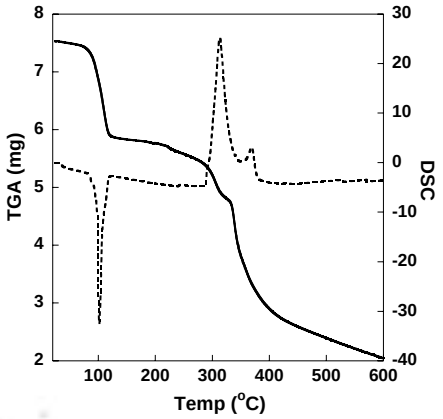

Figure 2.4 The TGA (solid) and DSC (dashed) analysis of Zn-complex, **1.**

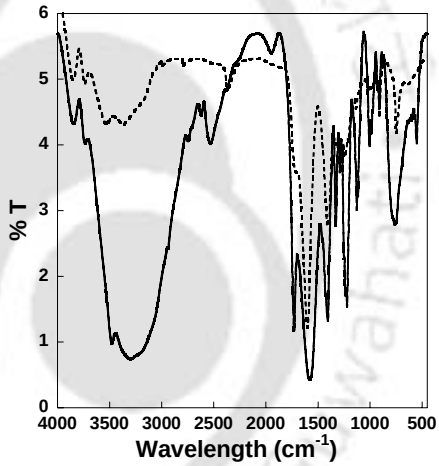

Figure 2.5 FT-IR spectra of before (solid) and after heating (dashed) of complex **1**.

average size of these wafers remains unchanged with longer reaction time, up to 14 h. SEM images taken of several batches of samples showed that the entire wafer is formed from a uniform and densely packed array of ZnO nanoparticles (Figure 2.7). The nanoparticles crystallinity was analyzed by powder X-ray diffraction techniques. The diffraction peaks (Figure 2.7) can be indexed as the wurtzite structure of ZnO (JCPDS 36-1451), thereby indicating that the zinc NTA complex has been thermally decomposed into ZnO [2.12]. The X-ray diffraction pattern shows an enhanced (101) peak resulting from the linear orientation of the nanoparticles. A typical synthesis yields particles with diameters ranging between 10 and 60 nm.

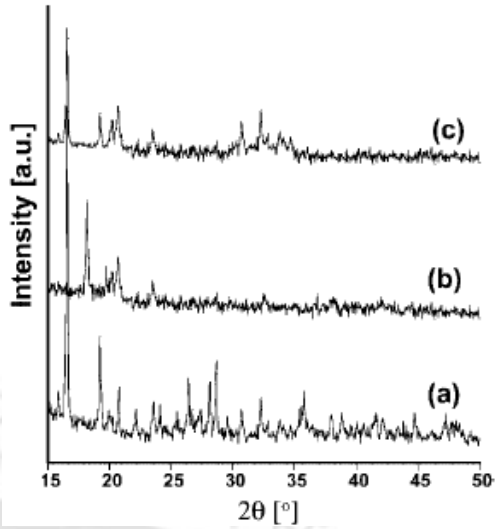

Figure 2.6 The powder XRD pattern of complex **1** (a) before water removal, after water removal and (c) after re-hydration.

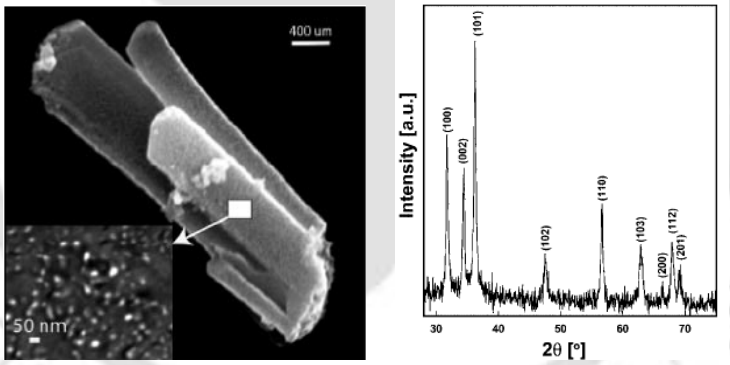

Figure 2.7 SEM micrographs of microwafers made of ZnO nanoparticles (left) and Powder XRD pattern of ZnO (wurtzite) nanoparticles (right).

The dimeric Zn nitrilotriacetato complex **2** is formed in the presence of an excess of zinc hydroxide. The asymmetric unit contains the hexaaquazinc(II) cation, the dimeric Zn-NTA complex anion, and crystal water (Figure 2.8). There are three symmetry-independent Zn sites in the structure. The first two of them (Zn1 and Zn2) are distorted octahedral with five carboxyl oxygens and one amine nitrogen making up the coordination environment. The other zinc cation, Zn3, is coordinated to six water molecules. Zn1 and Zn2 are bridged together by the carboxylic O3, O4, O11, and O12 atoms to form an infinite metal-organic framework. Among these four oxygen atoms, O3 and O11 form very rare μ-oxo

carboxylato type bridges where each carboxylate ligand is bonded to three metal centers. Atom O3 forms a stronger bond with Zn2 [Zn(1)–O(3) 2.365(2), Zn(2)–O(3) 1.947(2) Å] while O11 forms a stronger bond with Zn1 [Zn(1)–O(11) 1.948(2) and Zn(2)–O(11) 2.351(2) Å]. Atom O3 occupies the axial position of Zn1 but the equatorial position of Zn2, whereas O11 occupies the axial position of Zn2 and the equatorial position of Zn1.

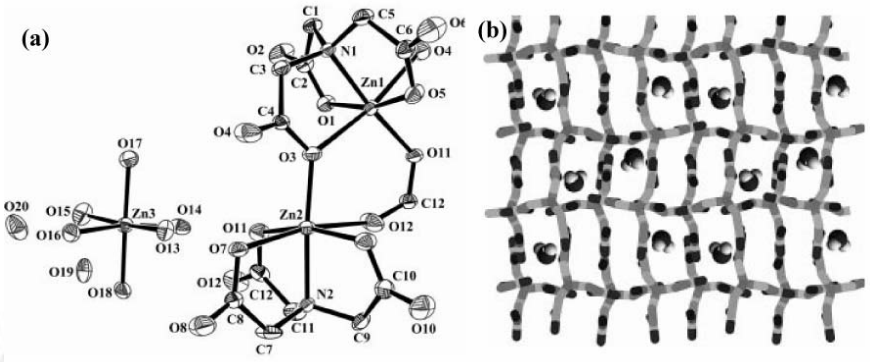

Figure 2.8 (a) Crystal structure and (b) an infinite rectangular network along the *ab* plane of complex **2**.

The remaining four carboxylic oxygen atoms (O2, O6, O8, and O10) are not coordinated to the metal cation but form strong hydrogen bonds with the water molecules coordinated to the Zn3 cation. The carboxylic acid of one arm of each NTA unit is coordinated to the three zinc centers simultaneously along the crystallographic *ab* plane, which results in the formation of a complicated 3D polymeric rectangular network (Figure 2.8). The other two arms of each NTA unit form extensive hydrogen bonds with water molecules along the crystallographic *bc* plane. The overall 3D network is built up with the help of water of hydration (O19 and O20). The crystal water molecule O19 acts as a double hydrogen-bond donor as well as acceptor, while O20 acts as a single hydrogen- bond donor and acceptor. Both of these water molecules are strongly hydrogen bonded to the carboxylate as well as another coordinated water molecule. Unlike the mononuclear Zn-NTA complex **1**, there is no direct hydrogen bond between two crystal water molecules, which, in turn, prevents the formation of any water network in the solid state structure. Two of the alternate rectangular void spaces in the 2D rectangular network are filled with these water molecules. Alternating Zn-aqua and Zn-NTA moieties form this

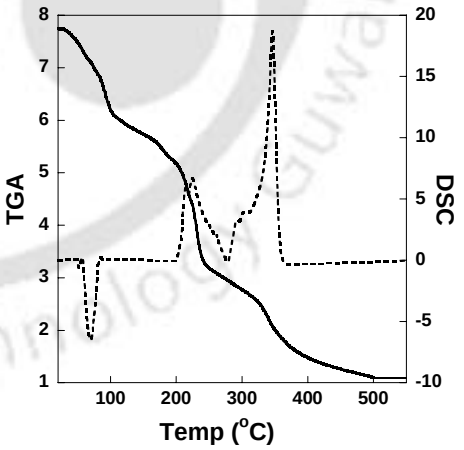

Figure 2.9 TGA-DSC analyses of complex **2**.

2D network. Thermogravimetric analysis (Figure 2.9) of complex **2** under N_2 shows a 21.08% weight loss between 30° and 100°C corresponding to the loss of eight water molecules (calculated. 20.09 %). All six coordinated carboxylic acid groups are removed between 100° and 240°C with a weight loss of 47.08% (calculated 46.11 %), which is in good agreement with the X-ray crystal structure. Complete decomposition is achieved at about 480 °C and shows the formation of ZnO as the decomposed product. The DSC plot shows an endothermic peak at 75°C due to the loss of water molecules. It also shows two exothermic peaks at 200° and 340°C due to the decarboxylation and complete decomposition, respectively.

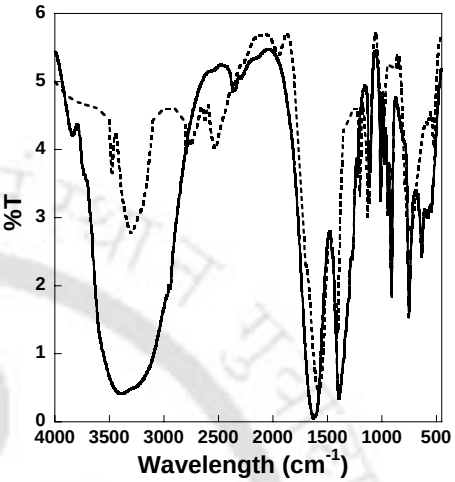

Figure 2.10 FT-IR spectra of before (solid) and after heating dashed) of complex 2.

The FT-IR spectrum of complex **2** shows (Figure 2.10) a broad band centered at 3500 cm^{-1} due to the presence of water molecules, which also vanishes when heated, as for complex **1**. Unlike complex **1**, however, it contains only coordinated, ionized types of carboxylic acid groups, which absorb at 1620 cm^{-1} [2.11]. Complex **2** decomposes above 500°C to form microwires of ZnO with lengths ranging from 200 nm to 8 µm (Figure 2.11). The average size and shape of these fibers does not change with temperature and reaction time. The powder X-ray diffraction pattern of these microwires also confirms the presence of the wurtzite structure of ZnO.

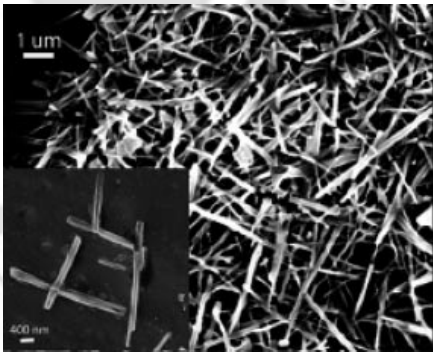

Figure 2.11 SEM micrographs of ZnO microwires.

The complex **3** was synthesized using a simple acid–base reaction in the solid phase and blue crystals were obtained from an ethanol/water (1:1) mixture. The structure was determined by single-crystal X-ray crystallography. The structure of complex **3** is best described as a 3-D framework.

The molecular structure, with the atomic numbering scheme, of complex **3** is shown in (Figure 2.12). In complex **3** the Cu(II) atom is in an N_2O_2 coordination environment. It is ligated by four atoms: two carboxylato oxygen atoms and two bridge head tertiary amine nitrogen atoms of bicinate. The carboxylato oxygen atoms bond more strongly with the copper atom than the bridge head tertiary amine nitrogen atoms. The complex has two

five-membered N,O-chelate rings which consist of one copper atom, one carboxylato oxygen atom, one nitrogen atom and two carbon atoms. Bond angles and distances of the mononuclear complex indicate a slightly distorted square-planar coordination with a trans-

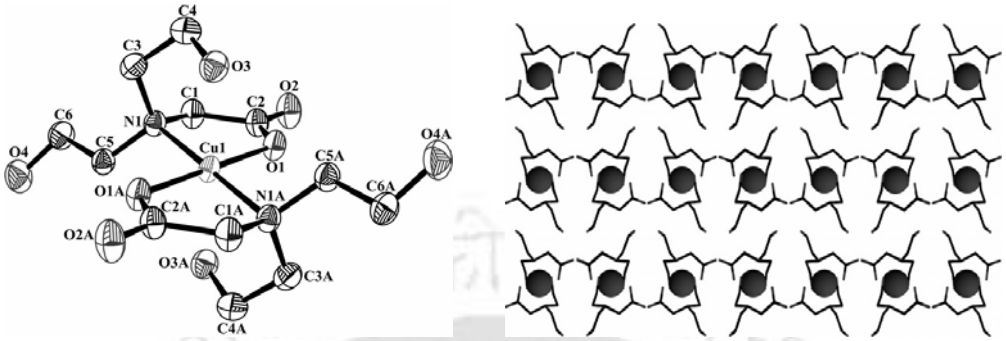

Figure 2.12 Coordination environments of complex **3** (left). Perspective view of the metallo-macrocyle in complex **3**, viewed along the *c*-axis (right).

structure. The bond distances and bond angles involving the metal ions are within normal statistical errors [2.13-2.14]. The shortening of the Cu–O bond lengths agree with the stronger chelating ability of the carboxylate oxygen compared to tertiary amine nitrogen atoms. All the coordination atoms and the Cu atom lie exactly on the N_2O_2 mean plane. There is no deviation of the donor atoms from the basal plane. This is consistent with a square planar structure of the metal centre. The conventional strong O–H----O and unconventional weaker C–H····O type intermolecular hydrogen bonding plays a major role in stabilizing the molecules in the solid state. It forms a linear array along the *c*-axis via C–H····O type interactions involving the alcohol group (O3) nearer to the Cu atom. Each of the parallel linear arrays propagates along the a-axis to form a 2D network via O–H····O type interactions. The overall structure looks like (Figure 2.12) an array of metallocycles joined via carboxylate groups of the podand extending along the crystallographic *ab*-plane in a zig-zag fashion. In the metallocyclic units, the two Cu(II) ions show a distance of either 7.126 or 9.516 Å while the distance between the bridgehead N atoms is 6.726 Å , forming an oval-shaped cavity.

The Cu(II) complex in acetonitrile solution shows a *d–d* band in the region 21,881 cm^{-1} due to a $^2B_{1g} \rightarrow {}^2A_{1g}$ transition which supports the square-planar geometry. The magnetic moment of the Cu(II) complex is 1.51 BM which shows the presence of an unpaired electron. This value is lower than the spin-only value and is due to mixing of orbital angular momentum from an excited state via spin-orbit coupling. EPR spectra of complex **3** (Figure 2.13) were recorded in DMSO at 300 and 77 K. The spectrum of complex 3 at 300 K shows one intense absorption band in the high field region and is isotropic due to

the tumbling motion of the molecules. However, this complex in the frozen state at 77 K shows four well-resolved peaks of low intensities in the low-field region and one intense peak in the high-field region. No band corresponding to the Ms = ±2 transition was observed in the spectrum, ruling out any Cu–Cu interactions, in the solution state. In square-planar complexes unpaired electrons lying in the d_{x2-y2} orbital give $^2B_{1g}$ as the ground state with $g_{\parallel} > g_{\perp}$, while an unpaired electron lying in the dz^2 orbital gives $^2A_{1g}$ as the ground state with $g_{\perp} > g_{\parallel}$. The experimental values, $g_{\parallel}$ (2.341) > $g_{\perp}$ (2.041), indicates that the structure of the complex is square-planar and that the unpaired electron is predominantly in the d_{x2-y2} orbital. The coordination in solution is thus the same as in the solid. The FT-IR spectrum of the complex shows two strong and sharp bands at 3310 cm^{-1} and 3140 cm^{-1} due to O–H and N–H stretching vibrations [2.15]. The bands at 1610 and 1405 cm^{-1} are attributed to the COO^- antisymmetric and symmetric stretching vibrations, respectively, which is confirmed by the crystal structural analysis; the carboxylato oxygen atom O(2) forms two hydrogen bonds with the hydroxyl hydrogen atoms of the neighboring units as shown in the. Several new peaks appeared in the NIR region, which were absent in the ligand spectrum. The bands at 382 cm^{-1} and 318 cm^{-1} are assigned to the Cu–N and Cu–O stretching vibrations respectively. The molar conductivity measurements supported the non-electrolytic nature of complex **3**. This complex on heating at 500°C it thermally decomposed to CuO. A FT-IR spectrum clearly shows the formation of copper (II) oxide.

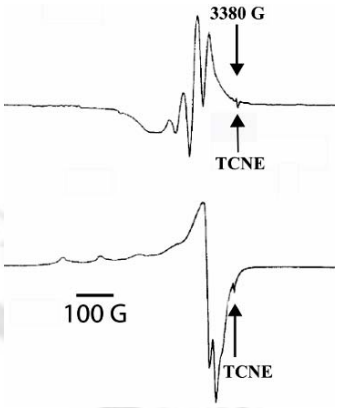

Figure 2.13 Electron paramagnetic resonance spectra of Complex **3**.

The robustness of the framework is reflected in the thermogravimetric analysis of complex **3** which shows negligible weight loss until about 140°C. The sample decomposed in a number of steps. Two molecules of CO_2 were released in two well separated steps from coordinated carboxylic acid groups (150–168°C; Δm = 11.34% calculated; 12.01% found; 176–205°C; Δm

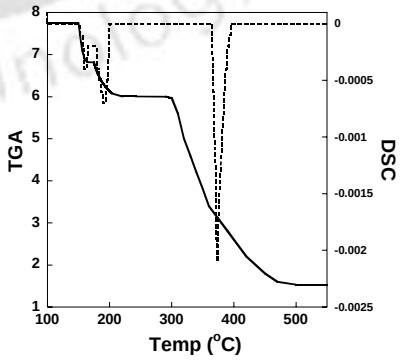

Figure 2.14 TGA and DSC pattern of complex **3.**

= 12.79% calculated; 13.19% found), which is in good agreement with the X-ray crystal structure. Complete decomposition occurred at ~370°C resulting in the formation of black CuO. The DSC-plot shows two exothermic peaks at 160°C and 190°C due to the loss of CO_2 molecules. It also shows an exothermic peak at 370°C due to the decomposition of the complex as shown in the (Figure 2.14).

The PXRD patterns also confirm the crystalline nature of the complex. The macroscopic crystal shape and color remain unchanged after heating the crystals at 100 ± 1°C for 3 h at atmospheric pressure. New powder X-ray data are collected every hour after the heat treatment. The PXRD data reveal that the crystalline nature of the complex framework is retained. Thermal decomposition of the blue colored complex **3** was carried out at 500°C for 6 h in a muffle furnace. The reaction product, black colored copper (II) oxide, was obtained in micro-plates morphology (Figure 2.15). The length and breadth of these plates range from 3 to 12 μm and 0.5 to 3 μm respectively. The average size and shape of these plates remains unchanged with longer reaction time, up to 14 h. SEM images taken of several batches of samples showed that the entire surface of the plates are clean without any fracture. The crystallinity of these micro plates was analyzed by PXRD techniques. The diffraction peaks (Figure 2.16) can be indexed as the Tenorite structure of CuO (PDF No. 00-005-0661), indicating that the Cu(II)–bicine complex has been thermally decomposed into CuO.X-ray diffraction pattern shows two enhanced (-111) and (111) peaks at 2h values 35.554 and 38.731, resulting from the linear orientation of the micro plates.

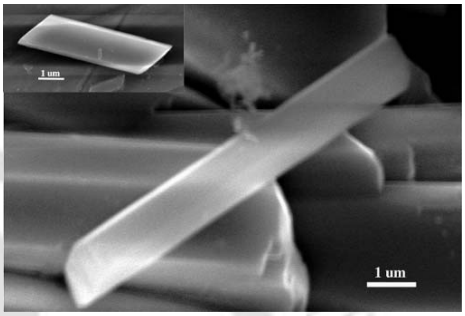

Figure 2.15 Scanning electron micrograph of CuO after thermolysis of complex 3 at 500°C (6 h).

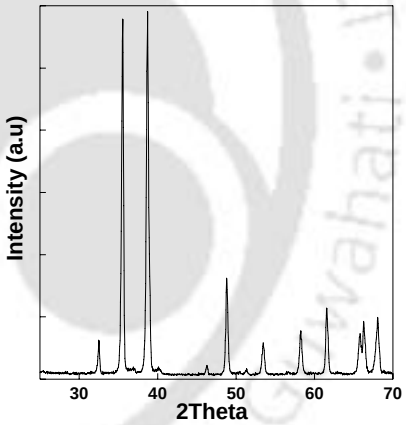

Figure 2.16 PXRD pattern of CuO (tenorite) micro plates.

2.2.2 Gel mediated Copper Hydroxide and Copper Oxide

From the SEM picture (Figure 2.17) we had found copper hydroxide that was form in agar as nice rod of average thickness 0.8 micron, in case of agarose gel small granular ball of

about 100 nm has formed. The surface of these balls is un-even and they exist as large aggregates. In presence of gelatin also ball has formed with an average diameter of 80 nm. These balls's surface is smooth and they exist as separated balls in contrast to the agarose gel. Energy dispersive X-ray spectrum it had been confirm that the sample contain copper and oxygen. We had obtained CuO by thermal decomposition of corresponding hydroxides (Figure 2.18). Thermal decomposition of copper hydroxide obtained from agar gel results in the formation of copper oxide micro rod of average thickness of 1.2 micron. Whereas copper hydroxide from agarose gel led to formation of CuO of various shape from cube to sphere with particle size range from 50-100 nm.

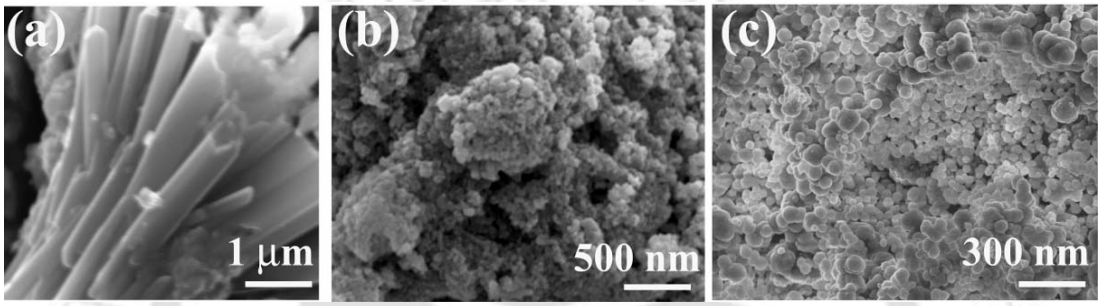

Figure 2.17 SEM image of $Cu(OH)_2$ from in presence of (a) Agar-Agar gel (b) Agarose gel and (c) Gelatine.

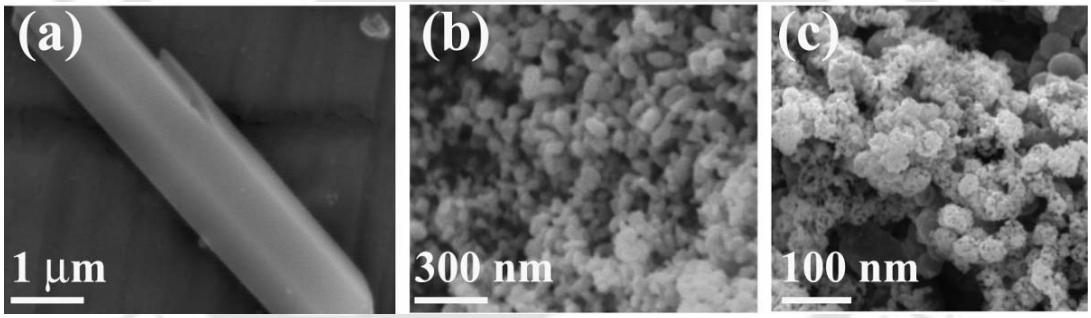

Figure 2.18 SEM image of CuO obtained from $Cu(OH)_2$ from (a) Agar-Agar gel (b) Agarose gel and (c) Gelatine.

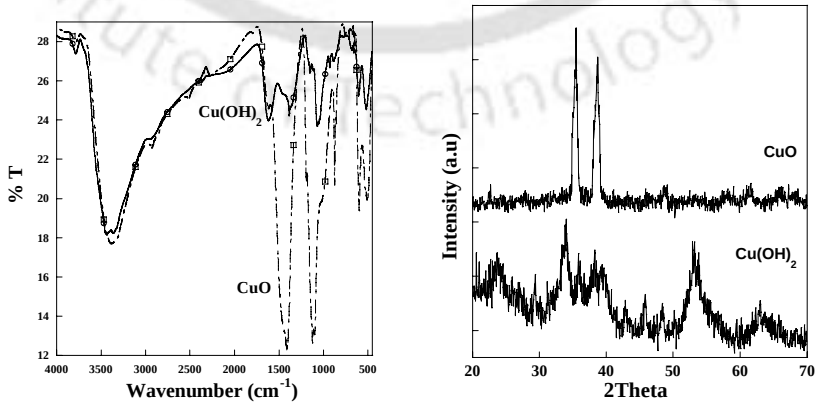

Figure 2.19 FT-IR spectra and PXRD pattern of $Cu(OH)_2$ and CuO.

Gelatin results derived CuO from aggregates of granular balls of average diameter of 50 nm. From the Energy dispersive X-ray spectrum it had been confirm that the sample contain copper and oxygen. PXRD pattern (Figure 2.19) confirms the bulk crystalline nature of the copper oxide and mineral phase is confirmed to be Tenorite (PDF No.00-005-0661). FT-IR spectra show the presence of CuO in bulk crystals (Figure 2.19).

2.2.3 Gel mediated Cobalt Hydroxide and Cobalt Oxide

From the SEM picture (Figure 2.20) we had found that cobalt hydroxide form flower like structure in agar with average petal thickness of 100 nm. In presence of agarose gel small rods (thickness < 100 nm) have formed and in case of gelatin cobalt hydroxide takes the form as flower with petals of average thickness of 300 nm. From the EDAX spectrum it had been confirm that the sample contain cobalt and oxygen.

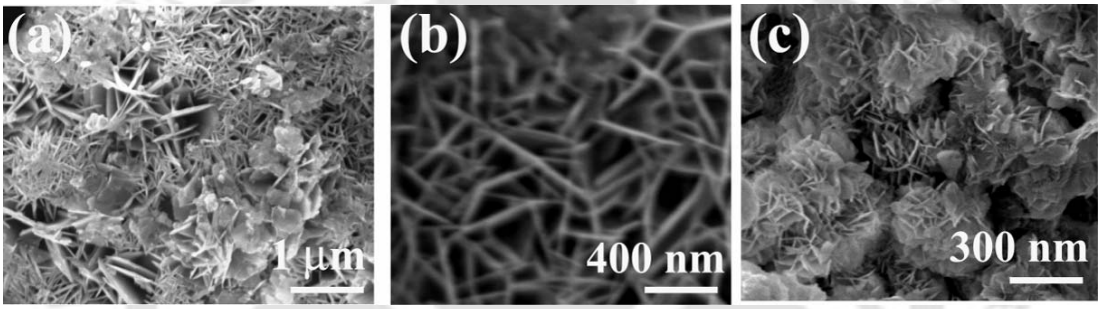

Figure 2.20 SEM image of $Co(OH)_2$ from in presence of (a) Agar-Agar gel (b) Agarose gel and (c) Gelatine.

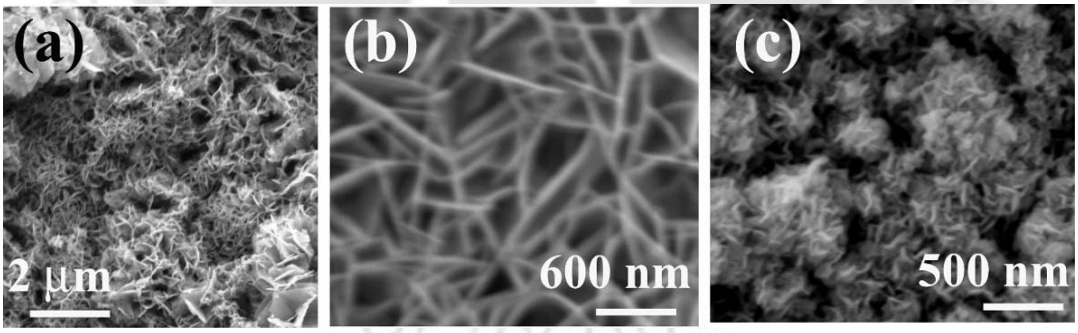

Figure 2.21 SEM image of Co_3O_4 obtained from $Co(OH)_2$ from (a) Agar-Agar gel (b) Agarose gel and (c) Gelatine.

From the SEM picture (Figure 2.21) we had found that cobalt oxide had formed similar structure to the cobalt hydroxide but smaller in size. From the Energy dispersive X-ray spectrum it had been confirm that the sample contain cobalt and oxygen. PXRD pattern of Co_3O_4 (PDF No. 00-009-0418) confirm crystalline nature of the bulk sample.

2.2.4 Gel mediated Nickel Hydroxide and Nickel Oxide

Nickel hydroxide forms granular ball in agar of average diameter of 60 nm. In the presence of agarose gel and gelatin aggregates of small spherical particles of 10-20 nm is observed (Figure 2.22). From the Energy dispersive X-ray spectrum it had been confirm that the sample contain nickel and oxygen. Thermal decomposition of $Ni(OH)_2$ results in the formation of crystalline Nickel Oxide. SEM picture (Figure 2.23) confirms that agar gel NiO form nanorods of diameter of 60-100 nm. Whereas from agarose and gelatine it forms aggregate of nanoparticles. The particles with a diameter range of 30-120 nm. FT-IR and PXRD pattern (Appendix) of Nickel Oxide confirms the crystalline nature (PDF No. 00-004-0835-Bunsenite, syn). From the Energy dispersive X-ray spectrum it had been confirm that the sample contain nickel and oxygen.

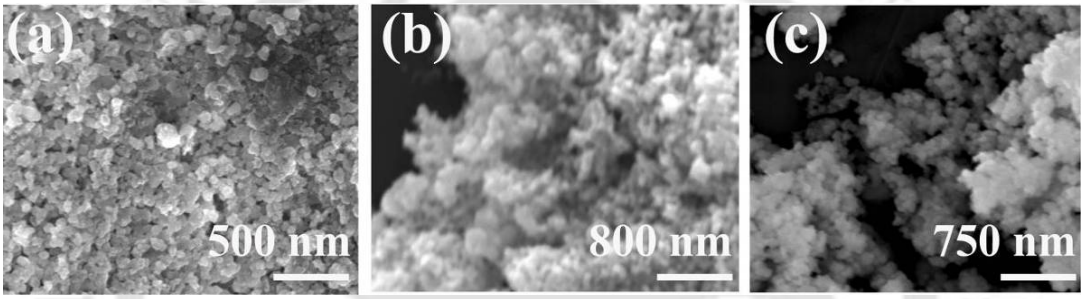

Figure 2.22 SEM image of $Ni(OH)_2$ from in presence of (a) Agar-Agar gel (b) Agarose gel and (c) Gelatine.

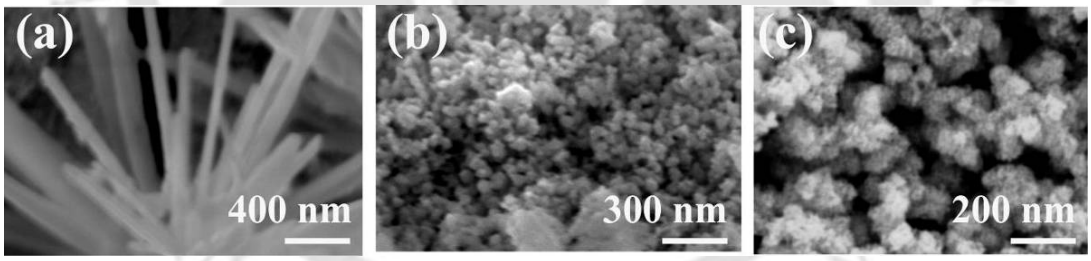

Figure 2.23 SEM image of NiO obtained from $Ni(OH)_2$ from (a) Agar-Agar gel (b) Agarose gel and (c) Gelatine.

2.2.5 Gel mediated Mangnese Hydroxide and Manganese Oxide

From the SEM picture (Figure 2.24) we had found that Manganese hydroxide was form in agar as rod in which some whiskers were growing from its body of thickness average 200 nm. In presence of agarose gel nano fibers are agglomerated and in case of gelatin it form a 3D sponge network composed of nano fibers of average thickness of <80nm. From the Energy dispersive X-ray spectrum it had been confirm that the sample contain Manganese and oxygen. Thermal decomposition it all cases results in the formation porous aggregates of spherical balls with a diameter range of 100-150 nm (Figure 2.25).

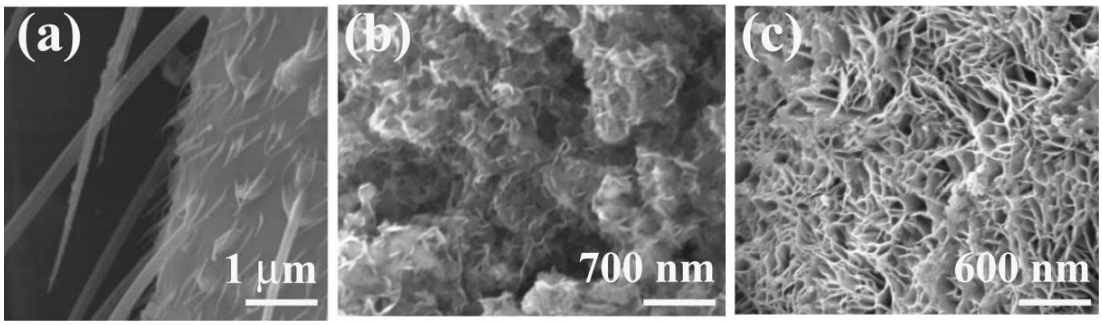

Figure 2.24 SEM image of $Mn(OH)_2$ from in presence of (a) Agar-Agar gel (b) Agarose gel and (c) Gelatine.

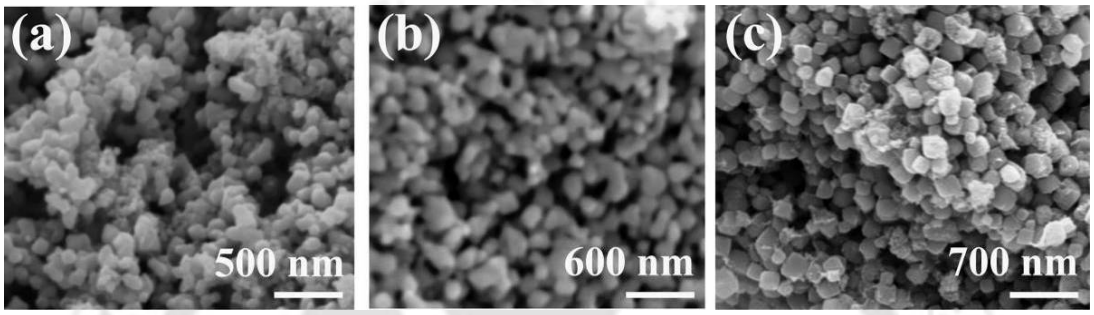

Figure 2.25 SEM image of Mn_2O_3 obtained from $Mn(OH)_2$ from (a) Agar-Agar gel (b) Agarose gel and (c) Gelatine.

Application of Macroporous Metal oxide as a Heterogeneous Catalyst in Organic Transformations

Almost the whole modern chemical industry depends on the development, selection and application of catalysis. One of the new methods is to perform reactions on the surface of a solid as a heterogeneous catalyst. Among the various inorganic materials, metal oxides have attracted increasing technological and industrial interest. Metal oxides are important class of heterogeneous catalyst because of their high level of chemo-selectivity, environmental compatibility, simplicity of operation and availability at low cost. *N*-Formylation is an important reaction in the formation of formamides [2.16]. Reported methods for the *N*-acylation by a combination of amides and acyl donors are as follows: lithiated amide–acyl chloride [2.17], amide–LiCl–acid anhydride [2.18]. The Friedel Craft reaction is an important reaction for C–C bond formation. After over a century of development, it still attracts much research interest in both academia and industry. Brønsted acid or Lewis acid-catalyzed imine or iminium Friedel Craft reactions (aza-Friedel Craft reactions) are important methods to construct a variety of nitrogen containing compounds [2.19].

Porous materials have attracted the attention of chemists and materials scientists due to commercial interest in their application in ion exchange, adsorption (for chemical separations) and heterogeneous catalysis. These porous materials have the ability to interact with atoms, ions and molecules not only at their surfaces, but also throughout the bulk of the material, which is responsible for its functional diversities [2.20]. In this part of the thesis application of macroporous transition metal oxides and malachite nano particles in various organic transformations are discussed in details.

2.3 Experimental section

2.3.1 General procedure for *N*-formylation

To a mixture of HCO_2H (2.5 – 3.0 mmol) and metal oxides (0.05 – 0.50 mmol) was added an amine (1 mmol). The reaction mixture was heated in an oil bath at 70^0C with continuous stirring. The progress of the reaction was monitored by TLC. After the completion of the reaction, CH_2Cl_2 was added to the cooled reaction mixture and then filtered to remove the metal oxides. The organic solvent was washed with H_2O and a saturated solution of $NaHCO_3$ and dried over anhydrous Na_2SO_4. The solvent was removed under reduced pressure and the crude product was chromatographed on a silica gel column. Elution of the column with 20% ethyl acetate/petroleum ether gave the pure N-formyl product. The final product was confirmed by ^{1}H NMR, FT-IR and compared with authentic samples obtained commercially or prepared by reported methods [2.21].

After completion, the mixture was diluted with water (10 mL) and extracted with EtOAc (3 X 10 mL). The combined organic layer was dried over anhydrous Na_2SO_4 and concentrated. The residue was subjected to column chromatography to obtain the pure N-formyl

2.3.2 General procedure for acylation of amines, alcohols and phenols

To a mixture of metal oxides (0.05 - 0.5 mmol) and an acid chloride or anhydride (1 mmol), alcohol, phenol or amine (1 mmol) was added. In case of diols double molar equivalents of metal oxides as well as acid chloride was used. The reaction mixture was stirred with a mechanical stirrer for a certain period of time as required to complete the reaction (monitored by TLC) at room temperature. The solid mixture was then eluted with CH_2Cl_2, and the CH_2Cl_2 extract was then washed with an aqueous solution of $NaHCO_3$ and dried over anhydrous Na_2SO_4. The extract was evaporated under reduced pressure and the remaining residue was purified by silica-gel plate chromatography (*n*-Hexane:EtOAC= 8:2) to afford the desired ester. The identity of these compounds was easily established by comparison of their ^{1}H NMR spectra, FT-IR with those of authentic samples [2.22].

2.3.3 General procedure for Friedel Craft acylation

To a mixture of metal oxides (0.05 - 0.5 mmol) and an acid chloride (1 mmol), aromatic compound (1 mmol) was added. The reaction mixture was stirred for a certain period of time as required to complete the reaction (monitored by TLC) at room temperature. The solid mixture was then eluted with CH_2Cl_2, and the CH_2Cl_2 extract was then washed with an aqueous solution of $NaHCO_3$ and dried over anhydrous Na_2SO_4. Evaporation of organic solvent furnished the corresponding product. The product was purified by column chromatography on silica gel, eluting with *n*-hexane:EtOAc (20:1) to give the corresponding aryl ketone. The identity of these compounds was easily established by comparison of their ^{1}H NMR and FT-IR spectra with those of authentic sample [2.22, 2.23].

2.4 Results and discussion

2.4.1 Metal oxide catalyzed N- formylation of amine

For all the organic transformations, we first prepared the various transition metal hydroxides in the presence of agar agar gel as templates. Later all these hydroxides were heated to ~600^{0}C to transform them to corresponding metal oxides. In case of *N*-Formylation (Scheme 2.1, Figure 2.6) by macroporous ZnO, we got marginal improvement compared to the reported value [2.21] as indicated in Table 2.2.

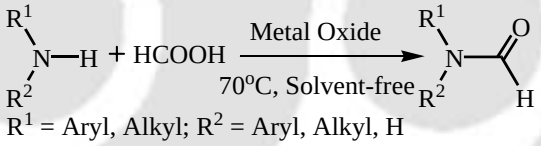

Scheme 2.1 *N*-Formylation of Amine under solvent free condition.

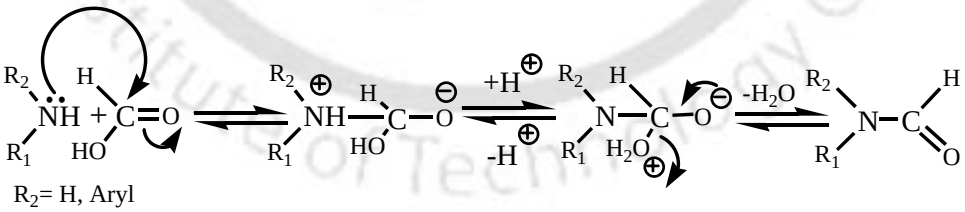

Figure 2.26 Plausible mechanism of *N*-Formylation of Amine.

Table 2.2 Comparison of *N*-formylation of aniline (1 mmol) with formic acid (2.5 mmol) by using ZnO as catalyst.

Entry	Catalyst	Catalyst (mmol)	Time (min)	Yield (%) [a]	Reference
1	Commercial ZnO	0.50	10	99	[2.21]
2	ZnO (macroporous)	0.50	08	99	This work
3	ZnO (macroporous)	0.25	120	55	

[a] Isolated yields

The reaction conditions were standardized after conducting the *N*-formylation of aniline in different amounts of metal oxides catalyst (Table 2.3) and reaction time. For *N*-formylation of aniline, 70°C is proven to be the optimum temperature. This corresponds well with the reported value [2.21]. Thus under optimum conditions, 1 mmol of aniline was formylated in solvent free conditions with 2.5 mmol of formic acid using 0.25 mmol CuO, 0.20 mmol NiO, 0.20 mmol CoO, 0.05 mmol Mn_2O_3, and 0.05 mmol Cr_2O_3 as a heterogeneous catalyst. Under similar reaction conditions more amounts (0.50 mmol) of ZnO is required [2.21]. Thus we can conclude, macroporous transition metal oxides (*viz*: CuO, NiO, CoO, Mn_2O_3, and Cr_2O_3) are more efficient heterogeneous catalyst. This is

Table 2.3 N-Formylation of aniline (1 mmol) with formic acid (2.5 mmol) at 70°C.

Entry	Catalyst	Catalyst (mmol)	Time (min)	Yield (%)[a]
1	CuO	0.50	25	90
2	CuO	0.25	25	95
3	CuO	0.25	40	80[b]
4	CuO	0.10	40	50
5	CuO	0.05	120	-
6	NiO	0.50	60	60
7	NiO	0.20	10	99
8	NiO	0.20	25	84[b]
9	NiO	0.10	20	95
10	NiO	0.05	25	80
11	CoO	0.50	45	80
12	CoO	0.20	30	99
13	CoO	0.20	60	85[b]
14	CoO	0.10	40	95
15	CoO	0.05	70	85
16	Mn_2O_3	0.50	120	-
17	Mn_2O_3	0.20	60	50
18	Mn_2O_3	0.10	45	74
19	Mn_2O_3	0.05	15	92
20	Mn_2O_3	0.05	35	80[b]
21	Cr_2O_3	0.50	30	80
22	Cr_2O_3	0.20	35	90
23	Cr_2O_3	0.10	25	95
24	Cr_2O_3	0.05	25	90
25	Cr_2O_3	0.05	55	80[b]

[a] Yields are of the isolated compounds; [b] Reaction performed at 60 °C.

because macroporous oxides have large internal surface area and pore volume. This in turn allows control over the diffusion of both reagents and products into and out of the porous medium [2.24]. But when we used lesser amount of CuO (Table 2.3, entries 4, 5), CoO (Table 2.3, entries 14, 15) and Cr_2O_3 (Table 2.3, entries 23, 24) we got comparatively

Table 2.4 List of amines used in N-Formylation reaction in presence of metal oxides as catalyst at 70°C.

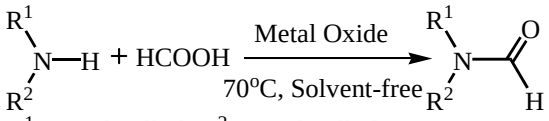

R^1 = Aryl, Alkyl; R^2 = Aryl, Alkyl, H

Entry	Substrates	Product	Metal Oxides (mmol)	Time (min)	Yield (%)[a]
1	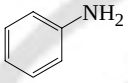	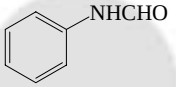	CuO (0.25)	15	96
2			NiO (0.20)	10	99
3			CoO (0.20)	25	99
4			Mn_2O_3 (0.05)	15	95
5			Cr_2O_3 (0.05)	25	98
6	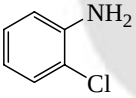	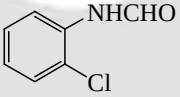	CuO (0.25)	60	90
7			NiO (0.20)	55	90
8			CoO (0.20)	60	92
9			Mn_2O_3 (0.05)	75	85
10			Cr_2O_3 (0.05)	70	85
11	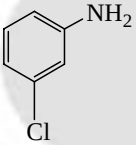	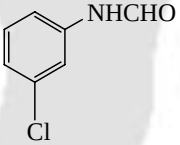	CuO (0.25)	20	92
12			NiO (0.20)	20	90
13			CoO (0.20)	25	88
14			Mn_2O_3 (0.05)	30	88
15			Cr_2O_3 (0.05)	30	85
16	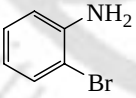	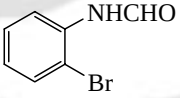	CuO (0.25)	60	94
17			NiO (0.20)	60	90
18			CoO (0.20)	60	92
19			Mn_2O_3 (0.05)	70	85
20			Cr_2O_3 (0.05)	70	85
21	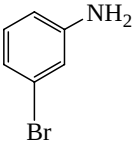	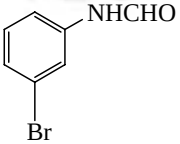	CuO (0.25)	25	92
22			NiO (0.20)	25	95
23			CoO (0.20)	25	88
24			Mn_2O_3 (0.05)	35	85
25			Cr_2O_3 (0.05)	35	85
26	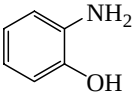	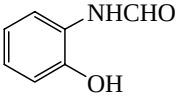	CuO (0.25)	40	98
27			NiO (0.20)	40	95
28			CoO (0.20)	60	85
29			Mn_2O_3 (0.05)	75	85
30			Cr_2O_3 (0.05)	50	85

31	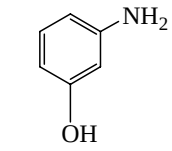	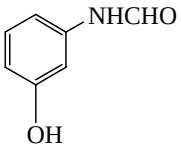	CuO (0.25)	50	94
32			NiO (0.20)	55	92
33			CoO (0.20)	60	92
34			Mn_2O_3 (0.05)	80	88
35			Cr_2O_3 (0.05)	75	90
36	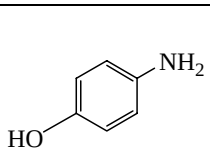	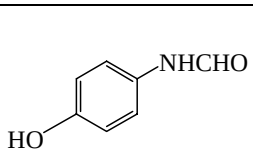	CuO (0.25)	45	98
37			NiO (0.20)	50	95
38			CoO (0.20)	60	85
39			Mn_2O_3 (0.05)	75	85
40			Cr_2O_3 (0.05)	60	85
41	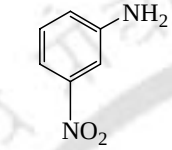	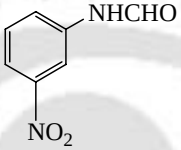	CuO (0.25)	60	88
42			NiO (0.20)	40	92
43			CoO (0.20)	80	85
44			Mn_2O_3 (0.05)	90	88
45			Cr_2O_3 (0.05)	90	92
46	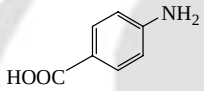	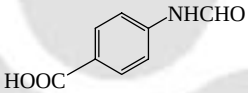	CuO (0.25)	65	92
47			NiO (0.20)	60	91
48			CoO (0.20)	70	92
49			Mn_2O_3 (0.05)	90	82
50			Cr_2O_3 (0.05)	90	80
51	$CH_3CH_2CH_2CH_2NH_2$	$CH_3CH_2CH_2CH_2NHCHO$	CuO (0.25)	40	90
52			NiO (0.20)	45	88
53			CoO (0.20)	50	90
54			Mn_2O_3 (0.05)	60	90
55			Cr_2O_3 (0.05)	60	85

[a] Yields are of the isolated compounds.

Table 2.5 Reuse of various metal oxides for N-formylation amine.

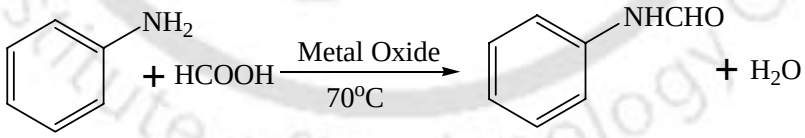

Catalyst (mmol)	Number of cycle	Yield (%)	Recovery of catalyst (%)
CuO (0.25)	1, 2, 3	96, 90, 88	96, 92, 92
NiO (0.20)	1, 2, 3	99, 94, 90	96, 91, 91
CoO (0.20)	1, 2, 3	99, 95, 90	95, 90, 90
Mn_2O_3 (0.05)	1, 2, 3	95, 89, 84	95, 90, 90
Cr_2O_3 (0.05)	1, 2, 3	98, 92, 84	94, 90, 90

poor yield. The results of *N*-Formylation (Scheme 2.1) in optimized reaction conditions of different substrates were summarized in the Table 2.4. Both aromatic amine possessing electron donating and electron withdrawing groups (Table 2.4, entries 1-50) as well as aliphatic amine (Table 2.4, entries 51-55) proceed smoothly to give *N*-formylated products in excellent yield. To the best of our knowledge, these reactions were never been reported by using these macroporous transition metal oxides. The catalytic activity of the recovered catalyst was examined as shown in the Table 2.5. In each case, after two and three reuses of these catalyst, almost >90% of the catalyst was easily recovered from the reaction mixture by simple filtration after washing with dichloromethane. Catalytic activity remains even after third cycle.

2.4.2 Metal oxide catalyzed acylation of amines

In case of *N*-Acylation (Scheme 2.2, Figure 2.27) by macroporous ZnO, we got excellent result using half of the amount (0.25 mmol) of catalyst compared to that reported value (0.50 mmol) [2.25]. The results with ZnO are summarized in Table 2.6.

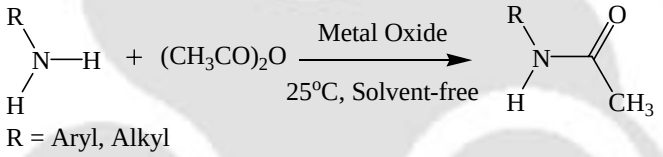

Scheme 2.2 *N*-Acylation of Amine under solvent free condition.

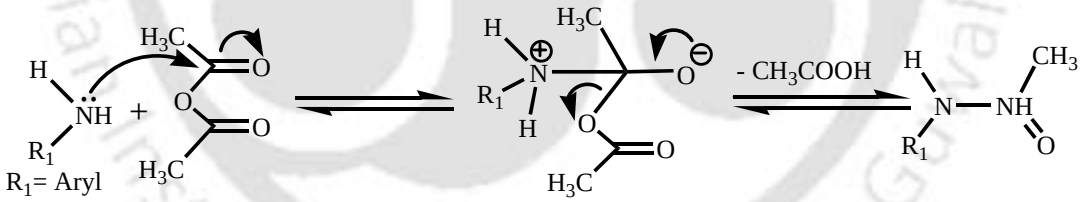

Figure 2.27 Plausible mechanism of *N*-Acetylation of Amine

Table 2.6 Comparison of N-acylation of aniline (1 mmol) with acetic anhydride (1 mmol) using commercial ZnO and macroporous ZnO.

Entry	Catalyst	Amount of Catalyst (mmol)	Time (min.)	Yield (%)[a]	Reference
1	Commercial ZnO	0.5	10	96	[2.26]
2	ZnO (macroporous)	0.50	08	98	This work
3	ZnO (macroporous)	0.25	12	92	
4	ZnO (macroporous)	0.10	35	75	
5	ZnO (macroporous)	0.05	65	50	

[a] Yields are of the isolated compounds.

Catalytic activity of the transition metal oxides as a heterogeneous catalyst for *N*-Acylation of amine are summarized in the Table 6. Here we can notice that, we got better result using fewer amounts (0.25 mmol - 0.05 mmol) of catalyst with respect to the commercial powder ZnO. As shown in Table 2.7, the reaction of aniline (1 mmol) as a standard with acetic anhydride (1 mmol) was examined under various solvent free reaction conditions. The best results were obtained using 0.05 mmol CuO, NiO, CoO, Mn_2O_3 and Cr_2O_3. Where as 0.50 mmol ZnO was required to carry out the same conversion as reported in literature [2.25].

Table 2.7 List of amines used in N-Acylation (1 mmol) with acetic anhydride (1 mmol) at 25 ◦C.

Entry	Catalyst	Catalyst (mmol)	Time (min)	Yield (%)[a]
1	CuO	0.05	10	95
2	CuO	0.10	15	90
3	CuO	0.20	15	80
4	CuO	0.50	25	70
5	NiO	0.05	15	98
6	NiO	0.10	20	95
7	NiO	0.20	30	93
8	NiO	0.50	30	90
9	CoO	0.05	15	98
10	CoO	0.10	30	95
11	CoO	0.20	40	90
12	CoO	0.50	40	80
13	Cr_2O_3	0.05	10	90
14	Cr_2O_3	0.10	15	85
15	Cr_2O_3	0.20	25	80
16	Cr_2O_3	0.50	25	70
17	Mn_2O_3	0.05	15	90
18	Mn_2O_3	0.10	25	80
19	Mn_2O_3	0.20	40	80
20	Mn_2O_3	0.50	40	70

[a] Yields are of the isolated compounds.

The experimental result of the acylation of different classes of amines is summarized in the Table 2.8. In these reactions, acetic anhydride was preferred over acid chlorides because amines reacted very rapidly to acid chlorides at room temperature, which makes it difficult to monitor the reactions. Acylation of aromatic amines containing both electron donating as well as electron withdrawing group (Table 2.8, entries 1 – 35) were efficient

Table 2.8 List of amine used in N-Acylation reaction in presence of various metal oxides as catalyst.

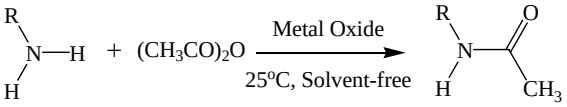

R = Aryl, Alkyl

Entry	Substrates[a]	Product	Metal Oxides (mmol)	Time (min)	Yield (%) [b]
1	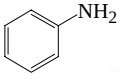	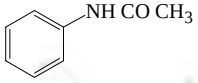	CuO (0.05)	10	95
2			NiO (0.05)	10	98
3			CoO (0.05)	10	98
4			Mn_2O_3 (0.05)	10	90
5			Cr_2O_3 (0.05)	10	90
6	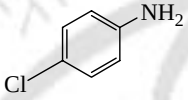	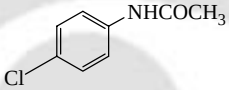	CuO (0.05)	15	95
7			NiO (0.05)	15	95
8			CoO (0.05)	20	95
9			Mn_2O_3 (0.05)	20	90
10			Cr_2O_3 (0.05)	25	88
11	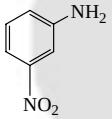	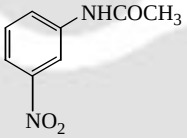	CuO (0.05)	30	92
12			NiO (0.05)	40	90
13			CoO (0.05)	60	85
14			Mn_2O_3 (0.05)	65	85
15			Cr_2O_3 (0.05)	75	95
16	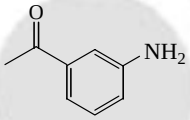	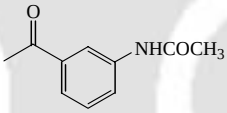	CuO (0.05)	15	96
17			NiO (0.05)	12	92
18			CoO (0.05)	20	96
19			Mn_2O_3 (0.05)	25	88
20			Cr_2O_3 (0.05)	25	85
21	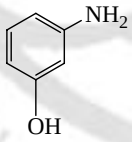	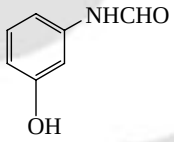	CuO (0.05)	12	86
22			NiO (0.05)	15	90
23			CoO (0.05)	15	85
24			Mn_2O_3 (0.05)	30	90
25			Cr_2O_3 (0.05)	35	92
26	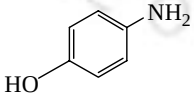	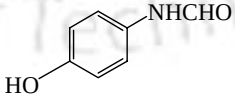	CuO (0.05)	15	96
27			NiO (0.05)	20	95
28			CoO (0.05)	20	95
29			Mn_2O_3 (0.05)	40	90
30			Cr_2O_3 (0.05)	35	88
31	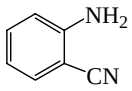	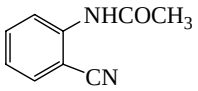	CuO (0.05)	25	80
32			NiO (0.05)	30	80
33			CoO (0.05)	30	82
34			Mn_2O_3 (0.05)	45	75
31			CuO (0.05)	25	80

[a] Yields are of the isolated compounds.

as well as fast. Macroporous transition metal oxide catalyzed efficient *N*-acylation of amines is rare to the best of our knowledge. Recovery and catalytic activity of the catalyst were tested for three cycles and found that more that 90% catalyst was easily recovered. The catalytic activities of the recovered catalyst were examined as shown in the Table 2.9.

Table 2.9 Reusability of various metal oxides for N-acylation of amine.

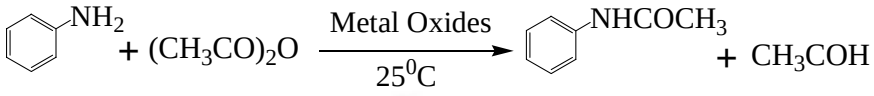

Catalyst (mmol)	Number of cycle	Yield (%)	Recovery of catalyst (%)
CuO (0.25)	1, 2, 3	95, 90, 87	96, 92, 92
NiO (0.20)	1, 2, 3	98, 94, 90	96, 93, 93
CoO (0.20)	1, 2, 3	98, 95, 92	95, 91, 91
Mn_2O_3 (0.05)	1, 2, 3	90, 84, 80	95, 91, 91
Cr_2O_3 (0.05)	1, 2, 3	90, 83, 80	95, 90, 90

2.4.3 Metal oxide catalyzed acylation of phenols

In case of *O*-Acylation phenols (Scheme 2.3) by macroporous ZnO, we again got better result using half of the amount (0.25 mmol) compared to the reported one (0.50 mmol) [2.25]. The results are summarized in Table 2.10. When we used other transition metal oxides as a heterogeneous catalyst as shown in the Table 10, in each case we got better result with respect to the porous ZnO.

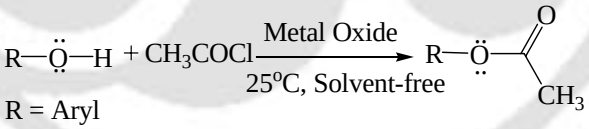

Scheme 2.3 *O*-Acylation of Phenols under solvent free condition.

Table 2.10 Comparison of O-acylation of phenol (1 mmol) with acetyl chloride (1 mmol) by using commercially available ZnO and macroporous ZnO at 25°C.

Entry	Catalyst	Catalyst (mmol)	Time (min.)	Yield (%)[a]	Reference
1	Commercial ZnO	0.50	15	94	[2.26]
2	ZnO (macroporous)	0.50	08	96	This work
3	ZnO (macroporous)	0.25	10	90	
4	ZnO (macroporous)	0.10	15	78	
5	ZnO (macroporous)	0.05	45	57	

[a] Yields are of the isolated compounds.

As shown in Table 10, the reaction of phenol (1 mmol) as a standard with acetyl chloride (1 mmol) was examined under various catalyst concentrations. The best results were obtained in solvent free conditions using 0.20 mmol CuO (entry 2), 0.20 mmol CoO (entry 5), 0.20 mmol NiO (entry 8), 0.05 mmol Mn_2O_3 (entry 10) and 0.05 mmol Cr_2O_3 (entry 13). Whereas, 0.50 mmol ZnO was reported in literature [2.25].

Table 2.11 *O*-Acylation of phenol (1 mmol) with acetyl chloride (1 mmol) at 25 ◦C.

Entry	Catalyst	Catalyst (mmol)	Time (min)	Yield (%)[a]
1	CuO	0.10	15	80
2	CuO	0.20	10	95
3	CuO	0.30	25	95
4	CoO	0.10	20	60
5	CoO	0.20	10	95
6	CoO	0.30	25	90
7	NiO	0.10	15	80
8	NiO	0.20	10	92
9	NiO	0.30	20	88
10	Mn_2O_3	0.05	10	90
11	Mn_2O_3	0.10	15	80
12	Mn_2O_3	0.30	25	80
13	Cr_2O_3	0.05	10	85
14	Cr_2O_3	0.10	15	80
15	Cr_2O_3	0.30	25	70

[a] Yields are of the isolated compounds.

Table 2.12 List of phenols used in O-Acylation reactions in presence of metal oxides as catalyst at 25◦C.

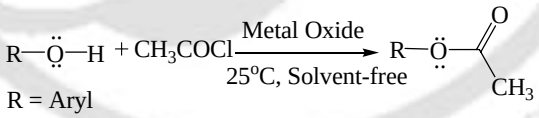

R = Aryl

Entry	Substrates	Product	Metal Oxides (mmol)	Time (min)	Yield (%) [a]
1	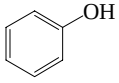	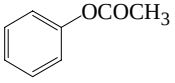	CuO (0.20)	10	95
2			NiO (0.20)	10	92
3			CoO (0.20)	10	95
4			Mn_2O_3 (0.05)	10	90
5			Cr_2O_3 (0.05)	10	85
6	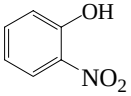	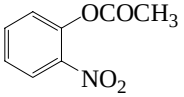	CuO (0.20)	25	92
7			NiO (0.20)	25	90
8			CoO (0.20)	30	92
9			Mn_2O_3 (0.05)	40	88
10			Cr_2O_3 (0.05)	40	90

11		CuO (0.20)	12	90
12	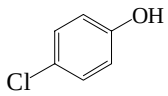	NiO (0.20)	10	86
13		CoO (0.20)	15	90
14		Mn_2O_3 (0.05)	20	90
15		Cr_2O_3 (0.05)	20	90
16		CuO (0.20)	25	92
17	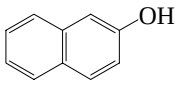	NiO (0.20)	30	95
18		CoO (0.20)	25	86
19		Mn_2O_3 (0.05)	45	85
20		Cr_2O_3 (0.05)	50	82

[a] Yields are of the isolated compounds.

The results of *O*-acylation of different phenols are summarized in Table 2.12. For these set of reactions, acid chloride was preferred over corresponding acetic anhydride because reaction with acetic anhydride was too sluggish to have any practical applications. Phenolic compounds containing both electron-withdrawing and donating groups reacted almost equally efficiently under these reaction conditions. This is the first demonstration of the macroporous transition metal oxides based *O*-acylation reactions. The Catalytic activity of the recovered catalyst were examined as shown in the Table 2.13, In each case, after 2-3 reuses of these catalyst, almost >90% was easily recovered from the reaction mixture by simple washing with dichloromethane, which retain their catalytic activity.

Table 2.13 Reuse of various metal oxides for O-acylation of phenol.

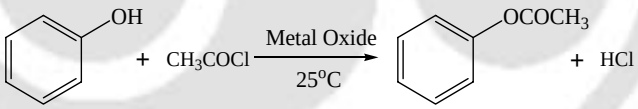

Catalyst (mmol)	Number of cycle	Yield (%)	Recovery of catalyst (%)
CuO (0.20)	1, 2, 3	95, 90, 86	95, 92, 92
NiO (0.20)	1, 2, 3	95, 90, 86	95, 92, 92
CoO (0.20)	1, 2, 3	90, 84, 80	95, 91, 91
Mn_2O_3 (0.05)	1, 2, 3	90, 86, 81	95, 91, 91
Cr_2O_3 (0.05)	1, 2, 3	85, 82, 78	95, 91, 91

2.4.4 Metal oxide catalyzed acylation of alcohols

In case of acylation of alcohols (Scheme 2.4, Figure 2.28) by macroporous ZnO, we also got better result with lesser amount (0.20 mmol) of catalyst compared to the literature (0.50 mmol) as shown in Table 2.14 [2.25]. When we used other transition metal oxides as

a heterogeneous catalyst as shown in the Table 2.15, in each case we got better result by using less amount (0.25 mmol - 0.05 mmol) of catalyst with respect to ZnO.

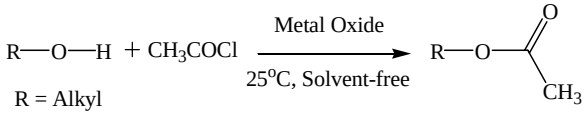

Scheme 2.4 *O*-Acylation of Alcohols under solvent free condition.

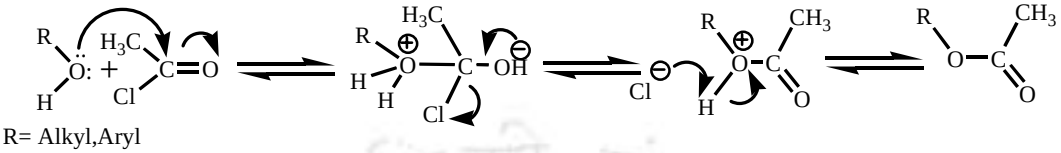

R= Alkyl,Aryl

Figure 2.28 Plausible mechanism of *O*-Acetylation of Alcohol

Table 2.14 Comparison of O-acylation of ethanol (1 mmol) with acetyl chloride (1 mmol) by using commercially available ZnO and macroporous ZnO at 25°C.

Entry	Catalyst	Amount of Catalyst (mmol)	Time (min)	Yield (%)	Reference
1	Commercial ZnO	0.50	10	95	[2.26]
2	ZnO (macroporous)	0.50	10	98	This work
3	ZnO (macroporous)	0.20	12	95	
4	ZnO (macroporous)	0.10	20	82	
5	ZnO (macroporous)	0.05	50	60	

Table 2.15 O-Acylation of ethanol (1 mmol) with acetyl chloride (1 mmol) at 25 ◦C.

Entry	Catalyst	Catalyst (mmol)	Time (min)	Yield (%)[a]
1	CuO	0.10	10	78
2	CuO	0.20	10	95
3	CuO	0.30	15	90
4	CoO	0.10	15	74
5	CoO	0.20	10	94
6	CoO	0.30	10	90
7	NiO	0.10	15	80
8	NiO	0.20	10	94
9	NiO	0.30	15	88
10	Mn_2O_3	0.05	15	92
11	Mn_2O_3	0.10	25	80
12	Mn_2O_3	0.30	25	80
13	Cr_2O_3	0.05	15	94
14	Cr_2O_3	0.10	35	86
15	Cr_2O_3	0.30	40	70

[a] Yields are of the isolated compounds.

Table 2.16 List of phenols used in *O*-Acylation reaction in presence of metal oxides as catalyst at 25^0C.

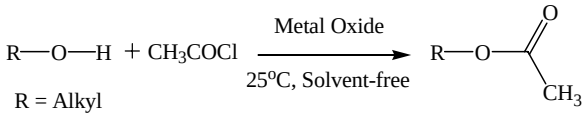

Entry	Substrates	Product	Metal Oxides (mmol)	Time (min)	Yield % [a]
1			CuO (0.20)	10	95
2			NiO (0.20)	10	92
3	CH_3CH_2OH	$CH_3CH_2OCOCH_3$	CoO (0.20)	12	92
4			Mn_2O_3 (0.05)	15	85
5			Cr_2O_3 (0.05)	15	82
6			CuO (0.20)	10	90
7			NiO (0.20)	12	88
8	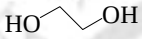		CoO (0.20)	15	92
9			Mn_2O_3 (0.05)	25	90
10			Cr_2O_3 (0.05)	25	90
11			CuO (0.20)	25	80
12			NiO (0.20)	25	76
13			CoO (0.20)	30	78
14			Mn_2O_3 (0.05)	35	72
15			Cr_2O_3 (0.05)	35	70
16			CuO (0.20)	20	90
17	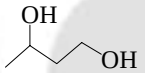	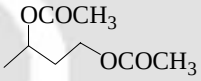	NiO (0.20)	20	90
18			CoO (0.20)	25	86
19			Mn_2O_3 (0.05)	40	80
20			Cr_2O_3 (0.05)	45	78
21			CuO (0.20)	20	85
22	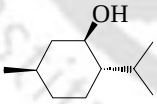	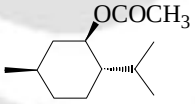	NiO (0.20)	20	80
23			CoO (0.20)	25	85
24			Mn_2O_3 (0.05)	30	78
25			Cr_2O_3 (0.05)	35	85

[a]Yields are of the isolated compounds.

(entry 5), 0.20 mmol NiO (entry 8), 0.05 mmol Mn_2O_3 (entry 10) and 0.05 mmol Cr_2O_3 (entry 13) as catalyst. However, 0.50 mmol ZnO was reported in literature for the same reaction [2.25]. Acylation of diverse range of alcohols *viz* primary alcohol (Table 2.16, entries 1-5), diol (Table 2.16, entries 6-10), secondary alcohol (Table 2.16, entries 11-15), bearing both primary as well as secondary alcohol group (Table 2.16, entries 16-20) and optically active alcohol (Table 2.16, entries 21-25) results in excellent yield without any side product. To the best of our knowledge, these reactions were never been reported by using these types of macroporous transition metal oxides as a heterogeneous catalyst. The

Catalytic activity of the recovered catalyst were examined as shown in the Table 2.17, In each case, after two and three recycles of these catalyst, almost >90% was easily recovered from the reaction mixture by simple washing with dichloromethane.

Table 2.17 Reuse of various metal oxides for O-acylation of ethanol.

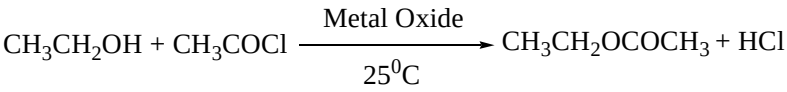

Catalyst (mmol)	Number of cycle	Yield (%)	Recovery of catalyst (%)
CuO (0.20)	1, 2, 3	95, 90, 86	96, 92, 92
NiO (0.20)	1, 2, 3	92, 85, 81	95, 92, 91
CoO (0.20)	1, 2, 3	92, 84, 78	95, 91, 91
Mn_2O_3 (0.05)	1, 2, 3	85, 80, 72	95, 90, 90
Cr_2O_3 (0.05)	1, 2, 3	82, 75, 70	95, 90, 90

2.4.5 Metal oxides catalyzed Friedel Craft acylation

Finally, Friedel Craft acylation reaction (Scheme 2.5, Figure 2.29) was carried under solvent free conditions using the various metal oxides as a heterogeneous catalyst.

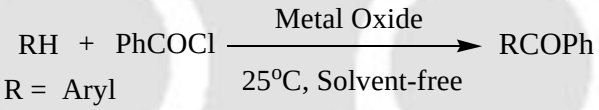

Scheme 2.5 Friedel Craft Acylation under solvent free condition.

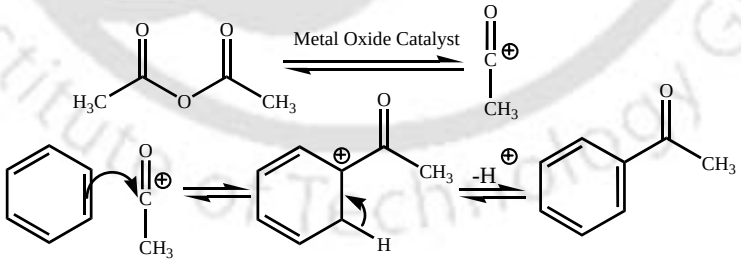

Figure 2.29 Mechanism of Friedel Craft reaction

For Friedel Craft acylation (Scheme 2.5) also we got better result using half the amount of macroporous ZnO (0.25 mmol) compared to the reported value [2.28]. The results with ZnO are summarized in Table 2.18. When we used other transition metal oxides as a heterogeneous catalyst as shown in the Table 2.19, 2.20 in each case we got better result

by using less amount (0.25 mmol - 0.05 mmol) of catalyst. Formation of acylium ion by metal oxide catalyst has been explained by following scheme [2.29].

Step 1: Formation of acylium ion mediated by metal oxide

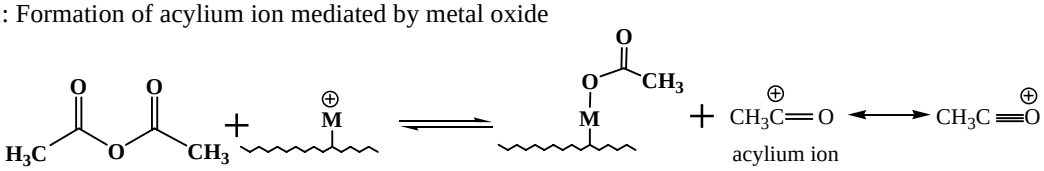

Step 2: Electrophilic attack of benzene ring on carbocation and formation of product

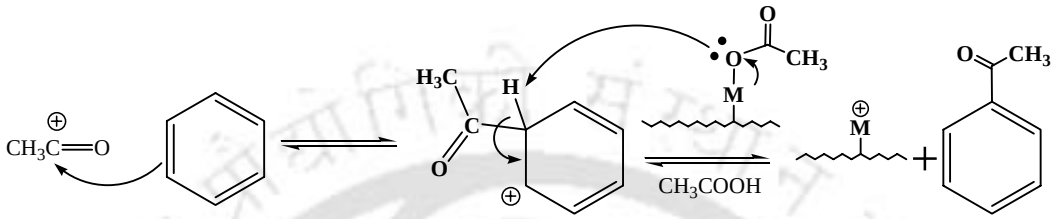

Table 2.18 Comparison of Friedel Craft acylation of toluene (1 mmol) with benzoyl chloride (1 mmol) by using commercially available ZnO and macroporous ZnO at 25°C.

Entry	Catalyst	Catalyst (mmol)	Time (min)	Yield (%)[a]	Reference
1	Commercial ZnO	0.50	10	86	[2.27]
2	ZnO (macroporous)	0.50	05	95	This work
3	ZnO (macroporous)	0.25	08	88	
4	ZnO (macroporous)	0.10	25	78	
5	ZnO (macroporous)	0.05	30	56	

[a] Yields are of the isolated compounds.

Table 2.19 Friedel Craft acylation of toluene (1 mmol) with benzoyl chloride (1 mmol) at 25 ◦C.

Entry	Catalyst	Catalyst (mmol)	Time (min)	Yield (%)
1	Cr_2O_3	0.05	70	70
2	Cr_2O_3	0.10	55	75
3	Cr_2O_3	0.20	40	80
4	Cr_2O_3	0.30	25	90
5	Cr_2O_3	0.50	60	75
6	CoO	0.05	65	35
7	CoO	0.10	70	45
8	CoO	0.20	60	65
9	CoO	0.30	25	82
10	CoO	0.50	60	60

From the Table 2.19, it is clear that only Cr_2O_3 and CoO were catalyzing the Friedel Craft reaction while the other oxides *viz:* CuO, NiO and Mn_2O_3 were unable to catalyze this reaction. This is because in the course of the reaction, only Cr_2O_3 and CoO is generating *in situ* Lewis acids $CrCl_2$ and $CoCl_2$ respectively. Presence of Lewis acid is necessary for the Friedel Craft reaction. The best results were obtained when 1 mmol Toluene is mixed with 1 mmol Benzoyl Chloride in solvent free conditions using 0.30 mmol of Cr_2O_3 (entry 4) and CoO (entry 9). The results of Friedel Craft acylation are summarized in the Table 2.20. Acylation occurs exclusively at the position para to –OMe, Me (Table 2.20, entries 1 to 4). Acylation of heterocyclic compounds such as furan (Table 2.20, entries 7 and 8) forms 2-acylated product in excellent yield. In case of benzene and anthracene (Table 2.20, entries 5, 6, 9 and 10), as themselves are less reactive, hence produces very less yield. To the best of our knowledge, these reactions were also never been reported by using these macroporous transition metal oxides. Here also the catalytic activity of the recovered catalyst were examined as shown in the Table 2.21, In each case, after two and three reuses of these catalyst, almost >90% was easily recovered from the reaction mixture by simple washing with dichloromethane.

Table 2.20 List of substrate used in Friedel Craft acylation in presence of metal oxides as catalyst at 25 ◦C.

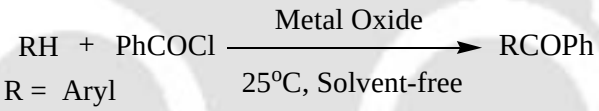

Entry	Substrates	Product	Metal Oxides (mmol)	Time (min)	Yield (%)[a]
1	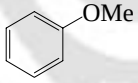	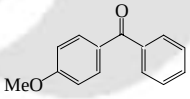	Cr_2O_3 (0.30)	8	94
2			CoO (0.30)	10	90
3	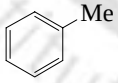	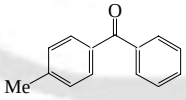	Cr_2O_3 (0.30)	20	90
4			CoO (0.30)	20	82
5		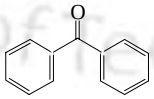	Cr_2O_3 (0.30)	120	55
6			CoO (0.30)	130	52
7		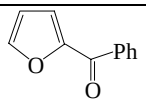	Cr_2O_3 (0.30)	10	90
8			CoO (0.30)	12	90
9	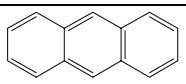	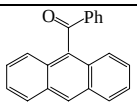	Cr_2O_3 (0.30)	130	55
10			CoO (0.30)	140	54

[a] Yields are of the isolated compounds

Table 2.21 Reuse of various metal oxides for Friedel Craft acylation.

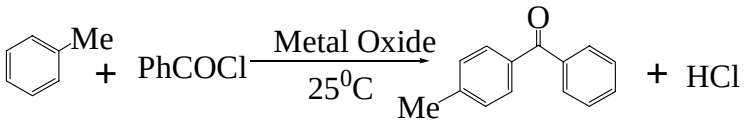

Catalyst (mmol)	Number of cycle	Yield (%)	Recovery of catalyst (%)
Cr_2O_3 (0.30)	1, 2, 3	90, 84, 80	96, 92, 91
CoO (0.30)	1, 2, 3	82, 76, 72	95, 91, 90

Summary

In conclusion, we have synthesized some inorganic materials of various morphologies by thermal decomposition of their precursors (MOF of metal hydroxides) or by stabilizing the nano particles in the presence of surfactant. These materials we have shown as an efficient eco-friendly heterogeneous catalyst for different organic reactions. These materials we have developed to used as a simple heterogeneous catalyst in solvent-free or with solvent at room temperature. The significant features of these methods include its ease of operation, low cost of the catalyst, mild conditions, clean reaction condition, high yields, and green in nature. Due to the presence of large internal surface area and pore volume, porous metal oxides has control over the diffusion of both reagents and products into and out of the porous medium. Similarly due to large surface area of malachite nano particles it facilitated to convert the reactant into product very efficiently. These porous oxides just create an environment or make a place for the reactants to adsorb on the metal oxide. Since the catalysts were macro-porous in nature, they help the reactants to come in close contact of each other within the pores that it has as shown below:

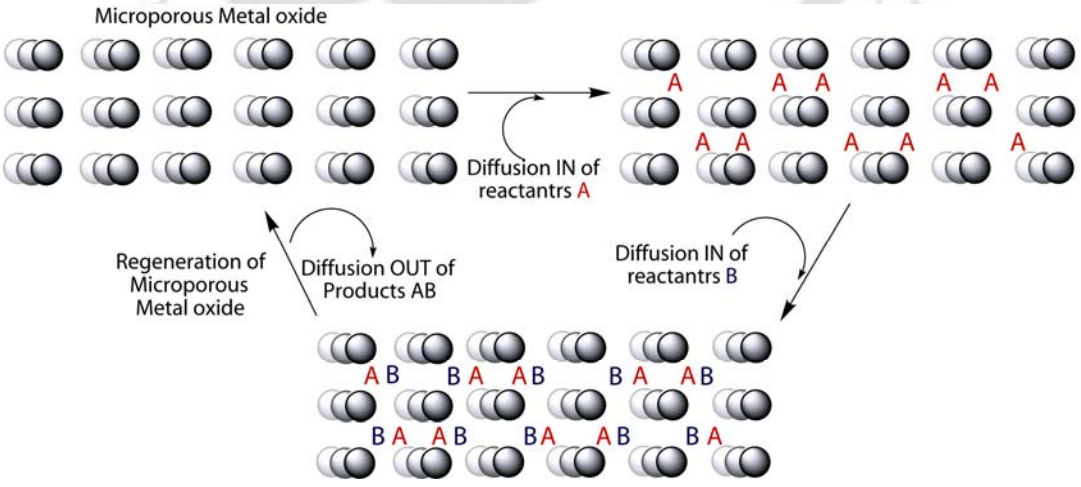

Reference

2.1 (a) Desiraju, G. R. *Crystal Engineering: The Design of Organic Solids*, Elsevier, Amsterdam, **1989**; (b) Zaworotko, M. J. *Chem. Soc. Rev.* **1994**, *23*, 283; (c) Kitagawa, S.; Kitaura, R.; Noro, S. I. *Angew. Chem. Int. Ed.* **2004**, *43*, 2334; (d) Lee, S. ; Mallik, A. B.; Xu, Z. E. ; Lobkovsky, B.; Tran, L. *Acc. Chem.Res.* **2005**, *38*, 251.

2.2 (a) Rosi, N. L.; Eckert, J.; Eddaoudi, M.; Vodak, D. T.; Kim, J.; O'Keeffe, M.; Yaghi, O. M. *Science* **2003**, *300*, 1127; (b) Pan, L.; Sander, M. B.; Huang, X.; Li, J.; Smith, M.; Bittner, E.; Bockrath, B.; Johnson, J. K. *J. Am. Chem. Soc.* **2004**, *126*, 1308; (c) Dybtsev, D. N.; Chun, H.; Yoon, S. H.; Kim, D.; Kim, K. *J. Am. Chem. Soc.* **2004**, *126*, 32; (d) Férey, G. ; Latroche, M.; Serre, C.; Millange, F.; Loiseau, T.; Percheron-Guégan, A. *Chem. Commun.* **2003**, 2976.

2.3 (a) Evans, O. R.; Lin, W. *Acc. Chem. Res.* **2002**, *35*, 511.; (b) Suslick, K. S.; Bhyrappa, P.; Chou, J. H.; Kosal, M. E.; Nakagaki, S.; Smithenry, D. W.; Wilson, S. R. *Acc. Chem. Res.* **2005**, *38*, 283; (c) Bradshaw, D.; Prior, T. J.; Cussen, E. J.; Claridge, J. B.; Rosseinsky, M. J. *J. Am. Chem. Soc.* **2004**, *126*, 6106; (d) Seo, J. S.; Whang, D.; Lee, H.; Jun, S. I.; Oh, J.; Jeon, Y. J.; Kim, K. *Nature* **2000**, *404*, 982; (e) Ohmori, O.; Fujita, M. *Chem. Commun.* **2004**, 1586; (f) Evans, O. R.; Ngo, H. L.; Lin, W. *J. Am. Chem. Soc.* **2001**, *123*, 10395.

2.4 (a) Lehn, J. M. *Angew. Chem. Int. Ed. Engl.* **1990**, *29*, 1304; (b) Supramolecular Architecture (Eds.: R. Robson, B. F. Abrahams, S. R. Batten, R. W. Gabe, B. F. Hoskins, T. Bein), American Chemical Society, Washington, D.C., **1992**, 256; (c) *Transition Metals in Supramolecular Chemistry*, Eds. L. Fabbrizzi, A. Poggi, Kluwer Academic, Dordrecht, **1994**.

2.5 SMART, SAINT and XPREP *Siemens Analytical X-ray Instruments Inc., Madison, Wisconsin, USA* **1995.**

2.6 Sheldrick, G. M. SADABS: empirical software for absorption and correction. University of Gottingen, Institut fur Anorganische Chemieder Universitat, Tammanstrasse 4, D-3400 Gottingen, Germany **1999–2003.**

2.7 Sheldrick, G. M. SHELXS-97. University of Gottingen, Germany **1997.**

2.8 (a) Sun, B.; Wang, Z.; Gao, S. *Inorg. Chem. Commun.* **2001**, *4*, 79; (b) Kim, J.; Chen, B.; Reineke, T. M.; Li, H.; Eddaoudi, M.; Molar, D. B.; O'Keeffe, M.; Yaghi, O. M. *J. Am. Chem. Soc.* **2001**, *123*, 8239; (c) Rao, C. N. R.; Natarajan, S.; Vaidhyanathan, R. *Angew. Chem. Int. Ed.* **2004**, *43*, 1466.

2.9 (a) Diaz, N.; Suarez, D.; Merz Jr. K. M. *Chem. Phys. Lett.* **2000**,*326*, 288; (b) Bock, C. W.; Katz, A. K.; Glusker, J. P. *J. Am.Chem. Soc.* **1995**, *117*, 3754.

2.10 Nagle, J. F.; Morowitz, H. J. *Proc. Natl. Acad. Sci. USA* **1978**, *75*, 298.

2.11 Nakamoto, K. Infrared and Ramman Spectra of Inorganic and Coordination Compounds, 5th ed., John Wiley & Sons Inc., New York, **1997**.

2.12 Yin, M.; Gu, Y.; Kuskovsky, I. L.; Andelman, T.; Zhu, Y.; Neumark, G. F.; O'Brien, S. *J. Am. Chem. Soc.* **2004**, *126*, 6206.

2.13 Hanss, A. J.; Beckmann, A.; Kruger, H. -J. *Eur. J. Inorg. Chem.* **1999**, 163.

2.14 Szczepura, B. L. F. ; Muller, J. G.; Bessel, C. A. ; See, R. F.; Janik, T. S.; Churchill, M. R.; Takeuchi, K. J. *Inorg. Chem.* **1992**, *31*, 859.

2.15 Ullah, M. R.; Bhattachaya, P. K. *Indian J. Chem. 30A* **1991,** 976.

2.16 (a) Jackson, A.; Meth-Cohn, O. *J. Chem. Soc., Chem. Commun* **1995**, 1319; (b) Green, T. W.; Wuts, P. G. M. *Protective Groups in Organic Synthesis*, 3rd ed., Wiley–Interscience, New York, **1999**.

2.17 Gage, J. R.; Evans, D. A. *Org. Synth.***1989**, *68*, 83.

2.18 Ho, G. J.; Mathre, D. J. *J. Org. Chem.* **1995,** *60*, 2271.

2.19 Noyori, R. *Adv. Synth. Catal*. **2003**, *345*. 15.

2.20 Davis, M. E. *Nature* 2002, 417, 813.

2.21 Pettit, G. R.; Kamano, Y.; Dufresne, C.; Cerny, R. L.; Herald, C. L.; Schmidt, J. M. *J. Org. Chem.* **1989**, 54, 6005.

2.22 (a) Angelescu, E.; Pavel, O. D.; Birjega, R.; Zavoianu, R.; Costentin, G.; Che, M. *Appl. Catal. A- Gen.* **2006,** 308, 13; (b) Moussaoui, Y.; Salem R. B. *C. R. Chimie* **2007** *10*, 1162.

2.23 Brufola, G.; Fringuelli, F.; Piermatti, O.; Pizzo, F. *Heterocycles* **1997**, *45*, 1715.

2.24 Thangaraj, A.; Sivasanker, S.; Ratnasamy, P. *J. Catal.* **1992,** *137*, 252.

2.25 Yadav, V. K.; Babu, K. G.; Mittal, M. *Tetrahedron* **2001**, *57*, 7047.

2.26 Dalpozzo, R.; DeNino, A.; Maiuolo, L.; Procopio, A.; Nardi, M.; Bartoli, G.; Romeo, R. *Tetrahedron Lett*.**2003**, *44*, 5621.

2.27 Bose, D. S.; Narsaiah, A. V. J. *Chem. Res.* **2001**, 36.

2.28 Ushikubo, T.; Wada, K. *J. Catal.* **1994,** *148*, 138.

2.29 D'Souza, J. ; Nagaraju, N. *Int. J. Chem. Tech.* **2006**, *13*, 605.

APPENDIX

Table S1. Selected Bond Lengths [Å] and Angles [°] of complexes **1**.

Zn(1)-O(1)	2.068(3)	Zn(1)-O(9)	2.105(3)
Zn(1)-O(3)	2.074(2)	Zn(1)-O(8)	2.107(3)
Zn(1)-O(7)	2.0671(17)	Zn(1)-N(1)	2.222(2)
O(7)-Zn(1)-O(1)	96.38(11)	O(3)-Zn(1)-O(8)	94.02(11)
O(7)-Zn(1)-O(3)	84.50(8)	O(9)-Zn(1)-O(8)	87.83(15)
O(1)-Zn(1)-O(3)	94.49(12)	O(7)-Zn(1)-N(1)	162.19(11)
O(7)-Zn(1)-O(9)	97.11(9)	O(1)-Zn(1)-N(1)	80.85(10)
O(1)-Zn(1)-O(9)	83.48(15)	O(3)-Zn(1)-N(1)	78.22(7)
O(3)-Zn(1)-O(9)	177.52(14)	O(9)-Zn(1)-N(1)	100.02(8)
O(7)-Zn(1)-O(8)	91.62(11)	O(8)-Zn(1)-N(1)	93.84(11)
O(1)-Zn(1)-O(8)	168.84(9)		

Table S2. Selected Bond Lengths [Å] and Angles [°] of complexes **2**.

Zn(1)-O(11)	1.948(2)	Zn(2)-N(2)	2.039(3)
Zn(1)-O(5)	1.976(2)	Zn(2)-O(11)#2	2.351(2)
Zn(1)-O(1)	1.983(2)	Zn(2)-O(12)	2.418(3)
Zn(1)-N(1)	2.036(3)	Zn(3)-O(18)	2.063(3)
Zn(1)-O(3)	2.365(2)	Zn(3)-O(17)	2.075(3)
Zn(1)-O(4)#1	2.402(3)	Zn(3)-O(14)	2.086(3)
Zn(2)-O(3)	1.947(2)	Zn(3)-O(15)	2.095(4)
Zn(2)-O(7)	1.987(2)	Zn(3)-O(16)	2.104(2)
Zn(2)-O(9)	1.994(2)	Zn(3)-O(13)	2.111(3)
O(11)-Zn(1)-O(5)	95.40(9)	O(9)-Zn(2)-O(11)#2	92.99(9)
O(11)-Zn(1)-O(1)	97.46(9)	N(2)-Zn(2)-O(11)#2	79.67(9)
O(5)-Zn(1)-O(1)	165.17(11)	O(3)-Zn(2)-O(12)	82.83(10)
O(11)-Zn(1)-N(1)	173.78(10)	O(7)-Zn(2)-O(12)	87.69(13)
O(5)-Zn(1)-N(1)	83.90(9)	O(9)-Zn(2)-O(12)	86.38(13)
O(1)-Zn(1)-N(1)	82.52(8)	N(2)-Zn(2)-O(12)	90.48(11)
O(11)-Zn(1)-O(3)	105.78(10)	O(11)#2-Zn(2)-O(12)	170.13(9)
O(5)-Zn(1)-O(3)	88.68(9)	O(18)-Zn(3)-O(17)	178.26(10)
O(1)-Zn(1)-O(3)	94.88(8)	O(18)-Zn(3)-O(14)	85.98(10)
N(1)-Zn(1)-O(3)	80.39(10)	O(17)-Zn(3)-O(14)	92.40(11)
O(11)-Zn(1)-O(4)#1	84.60(10)	O(18)-Zn(3)-O(15)	92.74(16)
O(5)-Zn(1)-O(4)#1	88.51(11)	O(17)-Zn(3)-O(15)	86.82(15)
O(1)-Zn(1)-O(4)#1	85.39(10)	O(14)-Zn(3)-O(15)	97.64(13)

N(1)-Zn(1)-O(4)#1	89.20(11)	O(18)-Zn(3)-O(16)	86.87(10)
O(3)-Zn(1)-O(4)#1	169.46(10)	O(17)-Zn(3)-O(16)	94.82(11)
O(3)-Zn(2)-O(7)	95.41(10)	O(14)-Zn(3)-O(16)	169.56(13)
O(3)-Zn(2)-O(9)	97.50(9)	O(15)-Zn(3)-O(16)	90.30(12)
O(7)-Zn(2)-O(9)	165.00(10)	O(18)-Zn(3)-O(13)	92.83(14)
O(3)-Zn(2)-N(2)	173.24(10)	O(17)-Zn(3)-O(13)	87.79(15)
O(7)-Zn(2)-N(2)	83.30(9)	O(14)-Zn(3)-O(13)	88.87(12)
O(9)-Zn(2)-N(2)	82.98(9)	O(15)-Zn(3)-O(13)	171.71(14)
O(3)-Zn(2)-O(11)#2	107.01(10)	O(16)-Zn(3)-O(13)	83.88(12)
O(7)-Zn(2)-O(11)#2	90.51(8)		

Table S3. Selected bond length (Å) and angles (°) of complex **3**.

Cu(1)-O(1)#1	1.947(2)	Cu(1)-N(1)#1	2.057(3)
Cu(1)-O(1)	1.948(2)	Cu(1)-N(1)	2.057(3)
O(1)#1-Cu(1)-O(1)	180.0	N(1)#-Cu(1)-N(1)	180
O(1)#-Cu(1)-N(1)#1	85.56(9)	O(1)#1-Cu(1)-N(1)	94.44(9)
O(1)-Cu(1)-N(1)#1	94.44(9)	O(1)-Cu(1)-N(1)	85.56(9)

Symmetry transformation used to generate equivalent atoms: #1 –x, y+1/2, z+1/2; #2 –x, -y, -z,;#3 x, -y -1/2, z -1/2.

Table S4. Non bonding distances (Å) angles (°) of complex **3**.

D-H···A	H…A (Å)	D…A	∠D-H…A (°)
O3-H3···O1	2.668	3.488	150.31
O3-H3···O2	1.864	2.711	153.82
O4-H4···O2	1.907	2.726	176.71
C1-H1B···O4	2.454	3.415	170.90
C4-H4A···O3	2.565	3.356	138.74
C6-H6a···O4	2.578	3.543	173.28

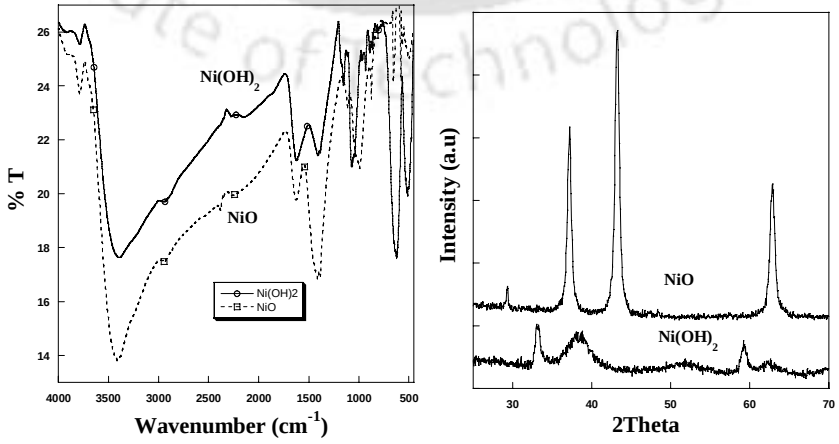

Figure S1. FT-IR spectra and PXRD pattern of $Ni(OH)_2$ and NiO.

Chapter - 3

Solid-State Synthesis of Some Heterocyclic Compounds of Medicinal Importance

In recent times, the progress in the field of solvent-free reactions is gaining significance because of their high efficiency, operational simplicity and environmentally benign processes. This is the one of the most popular methodology in "Green Chemistry". Solvent less organic reactions based on grinding of two macroscopic particles together [3.1] mostly involve the formation of a liquid phase prior to reaction, *i.e.*, formation of a eutectic melt of uniform distribution where the reacting components being in close proximity are poised to react in a controlled way. Solid-state reaction is a green reaction and can be accelerated by heating, shaking, grinding of the reaction mixture and irradiation with ultrasound, which makes it a much ideal synthetic process. It can avoid the environmental pollution, toxicity and flammability caused by solvents, and has been successfully applied to various reactions [3.2]. Most of these reactions are carried out at room temperature in absolutely solvent-free environment using only a mortar and pestle. All these facts have strengthened our resolve to find newer eco-friendly methods and prompted us to employ grinding at room temperature for the synthesis of some heterocyclic medicinal compounds with atom economy, reduce use of hazardous solvents, energy efficiency, reduce use of metal catalysis and prevent pollution. Quinoxaline-diones and their derivatives are important members of heterocyclic compounds and are widely applied in many fields [3.3]. 2-Mercaptobenzimidazole derivatives are known to possess varied biological activities as already discussed in the Chapter 1. Here in this chapter synthesis of some heterocyclic compounds solid-state or under solvent free are discussed.

3.1 Experimental section

3.1.1 Materials

All chemicals were reagent grade and were used as received without further purification unless otherwise stated. *o*-phenylene diamines and organic amines were obtained from Aldrich. Organic acids and ammonium salts were received from S.D. Fine Chemicals (India). The solvents were purified prior to use by standard procedures.

3.1.2 Analysis and Measurements

^{1}H NMR and ^{13}C NMR were recorded on a Varian FT-400 MHz instrument. IR spectra were recorded on a Perkin–Elmer Spectrum One FT-IR spectrometer with KBr disks in the range 4000–400 cm^{-1}. Thermo gravimetric analyses (TGA) of the compounds were performed using an SDTA 851e TGA thermal analyzer (Mettler Toledo) with a heating rate of 2°C per min in an N_2 atmosphere. PXRD data were recorded with a Seifert powder X-ray diffractometer (XRD3003TT) with CuK_a source (λ = 1· 4 Å) on glass surface with

an air-dried sample. Elemental analyses were done using Carlo–Erba 1108 and Perkin–Elmer series II 2400 instruments.

To probe the crystal structure the intensity data were collected using an acquisition. Data integration and reduction were undertaken with SAINT and XPREP software [3.4]. Multiscan empirical absorption corrections were applied to the data using the program SADABS [3.5]. Structures were solved by direct methods using SHELXS-97 [3.6] and refined with full-matrix least squares on F^2 using SHELXL-97 [3.6]. All non-hydrogen atoms were refined anisotropically. The hydrogen atoms were refined as riding atoms in idealized locations.

3.1.3 General procedure for the synthesis of 2,3-dihydro-1,5-benzodiazepines

A mixture of organic acid (5 mol%) and *o*-phenylene diamine (5 mmol, 0.540 g) was thoroughly ground with a pestle in an open mortar at room temperature. The mixture was ground for 5 min until the mixture turned into a melt. Then, 10 mmol of acetone was added and grinding continued for respective time as shown in the Table 3.1. The progress of the reaction was monitored by TLC. The melt was then washed several times with cold alkaline water (pH ~ 8.0) and a yellow solid was obtained. The organic layer was concentrated and the product was purified by silica gel column chromatography (100–200 mesh) with ethyl acetate–*n*-hexane (2:8) as eluent to afford pure compound. Yellow solid was then dissolved in hot EtOH and pure product was recrystallized at room temperature from EtOH solution by slow evaporation.

3.1.4 General procedure for the synthesis of 1,4-Dihydro-quinoxaline-2,3-dione derivatives

In a typical experiment, a mixture of oxalic acid dihydrate (1 mmol, 0.126 g) and *o*-phenylene diamine (1 mmol, 0.108 g) was thoroughly ground with a pestle in an open mortar at room temperature under atmosphere until the mixture turned into a melt. Then mixture was continued to grinding occasionally for different periods as indicated in Table 3.2. Then the melt was crystallized from water or water/ethanol (1:1) mixture at room temperature to get the pure products. Details of the substrates used, products obtained, reaction times and yields are given in Table 3.2.

3.1.5 General Procedure for synthesis of benzimidazole/2-mercaptobenzimidazole derivatives

In a typical experiment, a mixture of organic aldehyde (1 mmol) and *o*-phenylene diamine (1 mmol) was thoroughly ground with a pestle in a mortar at room temperature in an open

atmosphere until the overall mixture turned into a melt. The melt mixture was then heated to 140^{o}C for 1-2 hour. Progresses of the reaction were monitored by TLC. After completion of the reaction, the melt was washed with water and desired product was crystallized from water at low temperature. The desired pure product(s) was characterized by comparison of their physical data with those of known compounds [3.7]. 2-mercaptobenzimidazole derivatives were synthesized from a mixture of ammonium thiocyanate (1 mmol) and *o*-phenylene diamine derivatives (1 mmol) in presence of catalytic amount (0.05 mol%) of NH_4Cl following a similar procedure. Both the components were thoroughly ground with a pestle in a mortar at room temperature in an open atmosphere until the mixture turned into melt. The mixture was then heated to 140^{o}C for 1–3 hours. Progresses of the reaction were monitored by TLC. After completion, the melt was washed with water and desired product was crystallized from water at low temperature.

3.2 Results and discussion

3.2.1 Synthesis of 2,3-dihydro-1,5-benzodiazepine

As a part of our studies to explore the utility of simple solid phase room temperature grinding methods in solvent-free conditions, we decided to investigate the use of an organic acid as a catalyst for the preparation of 2,3-dihydro-2,2,4-trimethyl-1*H*-1,5-benzodiazepine by condensation of acetone with *o*-phenylendiamine (Scheme 3.1).

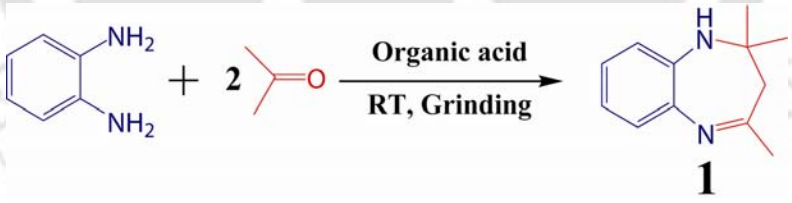

Scheme 3.1 Synthesis of 2,3-dihydro-2,2,4-trimethyl-1*H*-1,5-benzodiazepine.

The reaction was carried out at room temperature using acetone and *o*-phenylendiamine in the presence of a catalytic amount of an organic acid. The results are summarized in Table 3.1. Both aliphatic and aromatic acids containing mono-, di-, tri-carboxylic acid groups can act as catalyst. The best results were obtained using 1,3,5-benzene tri-carboxylic acid (trimesic acid) as catalyst. It can be generalized that more acidic catalysts are more efficient. The plausible mechanism of the reaction is depicted in the Figure 3.1. Initially acetone reacted with another acetone to form Aldol product catalyzed by an acid. The protonated Aldol (4-methyl-4-one-pentan-2-ol) then reacted with amino group of the *o*-

phenylene diamine followed by cyclization to yield the product 1,5-diazopine derivative. As depicted in the mechanism, formation of Aldol product is catalyzed by acid. H^+ ion activate the C=O group to be attack by another acetone molecule. Hence, presence of acid is necessary for the reaction to happen. In absence of acid no product was obtained in the similar reaction condition at room temperature.

Table 3.1 One-pot synthesis of 1,5-benzodiazepine.

Entry	Acid catalyst	Time	Yield (%)[a]
1.	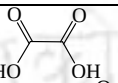	30 min	80
2.	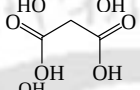	5 h	54
3.	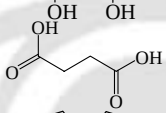	7 h	45
4.	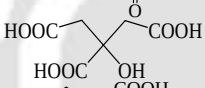	1 h	72
5.	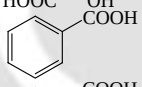	5 h	45
6.	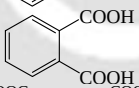	1 h	85
7.	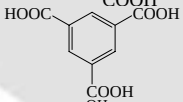	10 min	97
8.	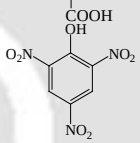	15 min	94
9.	No acid	10 h	Nil

[a] Yields of the isolated product

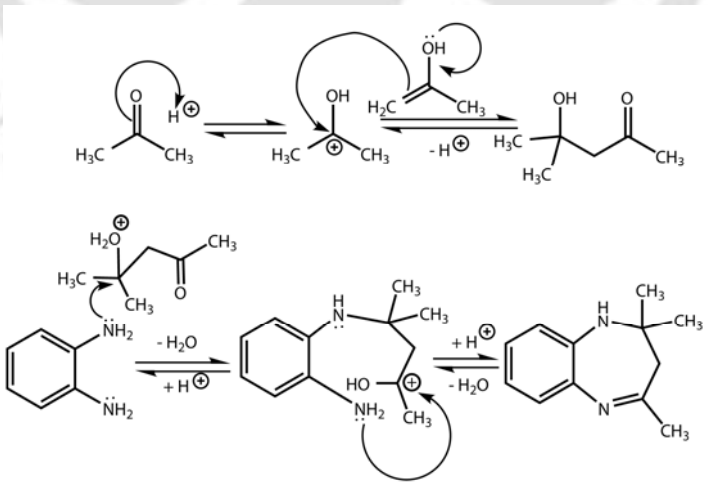

Figure 3.1 Plausible mechanism of formation of 1,5-benzodiazopine derivative.

Compound **1** when mixed with an equivalent amount of organic acid forms crystals of organic salt. With trimesic acid it forms a colorless salt (**1a**) and a dark red salt with picric acid (**1b**) from water ethanol mixture at room temperature. The structure of organic salts

1a and **1b** was investigated by single crystal X-ray diffraction. The lattice parameters, data collection method, structure solution and refinement are collected in Appendix. In the solid-state, the seven-membered heterocyclic ring adapts an armchair conformation. The imino nitrogen in **1** bears a small negative charge because of the resonance structure [3.8]. Hence it can accept one proton in the presence of an acid, which is reflected in the solid-state structure. In the salt crystal, the C=N stretching frequency is lowered by ~40 cm^{-1} to 1600 cm^{-1} after protonation of pure **1** (Figure 3.2).

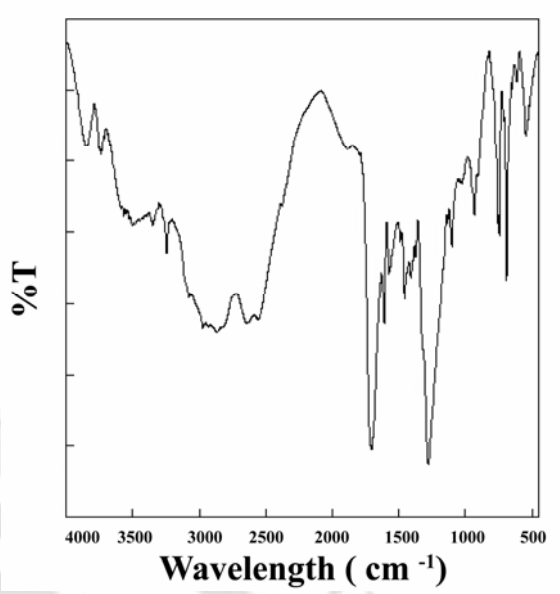

Figure 3.2 FT-IR spectra of the organic salt **1a**.

As shown in Figure 3.3, the crystal structure of **1a** consists of two crystallographic independent molecules of the heterocyclic ring in the asymmetric unit. The trimesic acid unit in **1a** forms a 2D tape along the *a* axis via formation of strong O–H•••O type hydrogen bonds (H•••O = 1.75 Å). The distances between the two 2D tapes are ~ 8.0 Å (Figure 3.3). Two adjacent tapes are clipped together by heterocyclic rings through the formation of strong conventional N–H•••O (average H•••O=1.98 Å) and weak non-conventional C–H•••O (average H•••O=2.82 Å) and C–H•••π (average H•••π=3.43 Å) type hydrogen bonding. The heterocyclic rings are held together by weak C–H•••π (average H•••π=3.18 Å) bonding.

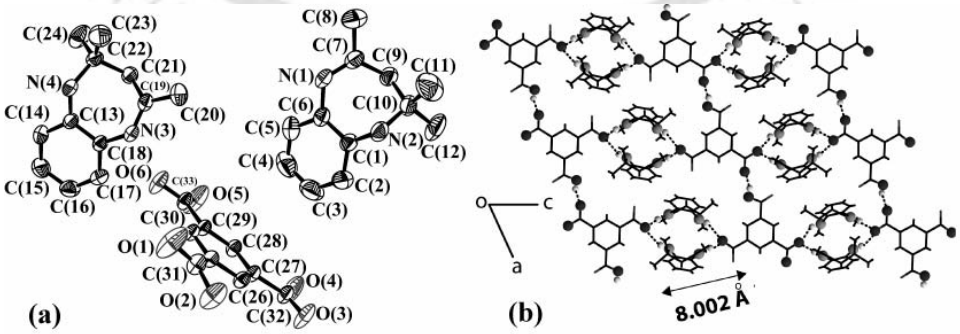

Figure 3.3 (a) An ORTEP plot of **1a** and (b) O-H··O and N-H··O type H-bonding in **1a**.

However, the three-dimensional arrangement of the molecules in the crystal lattice is unique and quite fascinating. The packing analysis reveals that the two crystallographic

independent heterocyclic rings are packed in an alternate layer in the crystal lattice in such a fashion that results in the formation of a 3D ladder like framework (Figure 3.4).

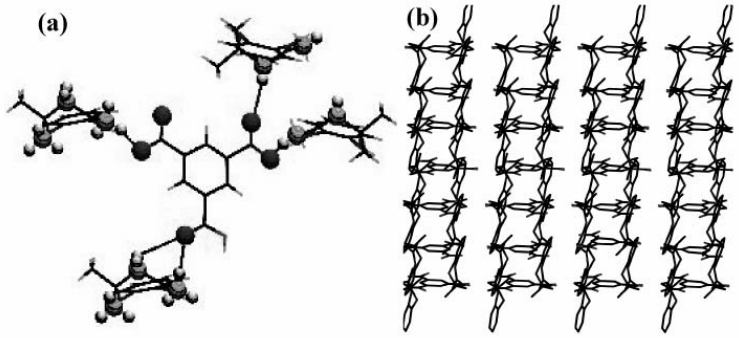

Figure 3.4 (a) C–H ····O interactions in the crystal lattice of **1a** and (b) 3D ladder framework of **1a** along the *c* axis.

In salt, **1b** the picrates are held together by strong π•••π interactions (3.37 Å) unlike in salt **1a**, where no such interactions are observed between the trimesic acid unit. The heterocyclic rings of **1b** are held together by strong N–H•••N (H•••N=2.60 Å) type hydrogen bonding. Organic salt **1b** does not show any C–H•••π type interactions like **1a**. Picrates form strong N–H•••O (average H•••O=2.16 Å) and C–H•••O (average H•••O=2.67 Å) type hydrogen bonding with neighboring heterocyclic rings which results in the formation of a 3D brick wall network along the *a* axis (Figure 3.5).

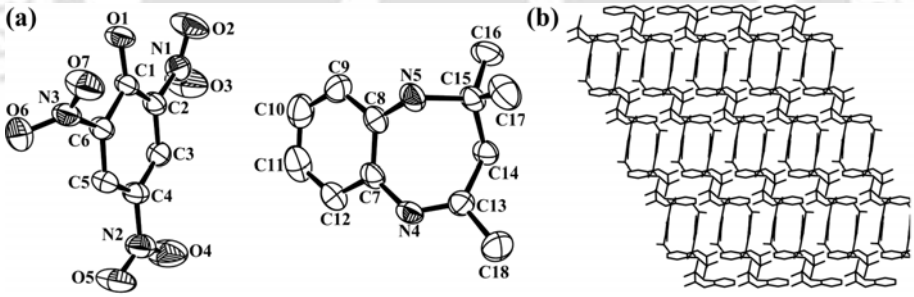

Figure 3.5 (a) An ORTEP plot of **1b** and (b) 3D brick wall framework of **1b** along *a* axis.

3.2.2 Synthesis of Quinoxaline-2,3-dione

As a part of our research on the development of newer clean processes for the organic transformations, our attention was drawn to the synthesis of these potential pharmacophore 1,4-Dihydro-quinoxaline-2,3-dione (**2**) derivatives. We report the simple solid phase grinding of the two reactants at RT in an open atmosphere to get the product in good yield (Scheme 3.2).

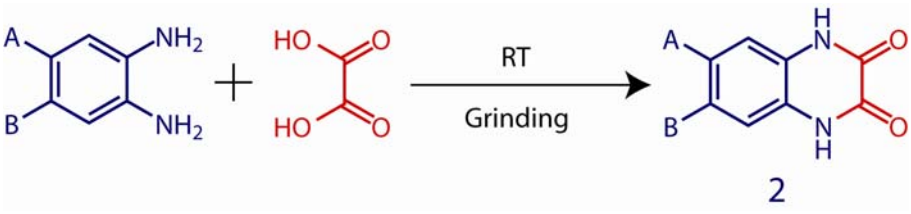

Scheme 3.2 Synthesis of 1,4-Dihydro-quinoxaline-2,3-dione derivatives.

In view of the problems encountered in quinoxaline synthesis, a relatively more versatile yet simplified procedure was perceived. Our arguments have been that solid phase grinding would lead to an instantaneous condensation to afford quinoxalines without the use of any solvent or catalyst. The strategy worked well affording the desired products in respectable yields (Table 3.2). Notably, the present reactions have been relatively faster, as anticipated, compared to those of conventional solution phase synthesis. Small amounts of starting materials were recovered after each reaction. A wide range of *o*-phenylene diamine derivatives were screened in order to ascertain the scope of the present reaction protocol and the results are summarized in Table 3.2. Presence of electron withdrawing groups in diamine starting materials gave lower yields with longer reaction times. However the quinoxaline derivatives are formed in good to very good yields.

Table 3.2 Solvent free synthesis of quinoxaline derivatives

Entry	A	B	Time/hr	Yield(%)[a]
2a	H	H	0.5	98
2b	H	NO_2	3	82
2c	H	Cl	2	87
2d	H	Me	1	95
2e	H	*n*-Pr	1	95
2f	H	Ph	0.5	96
2g	Cl	Cl	5	76

[a] Yields of the isolated product.

The plausible mechanism of the reaction is shown in Figure 3.6. The amino group of *o*-phenylene diamine condensate with the one carboxylic acid group of oxalic acid to yield corresponding amide. Then the second amino group of ortho phenylene diamine condensed with next followed by cyclization to yield the quinoxaline-2,3-dione derivatives.

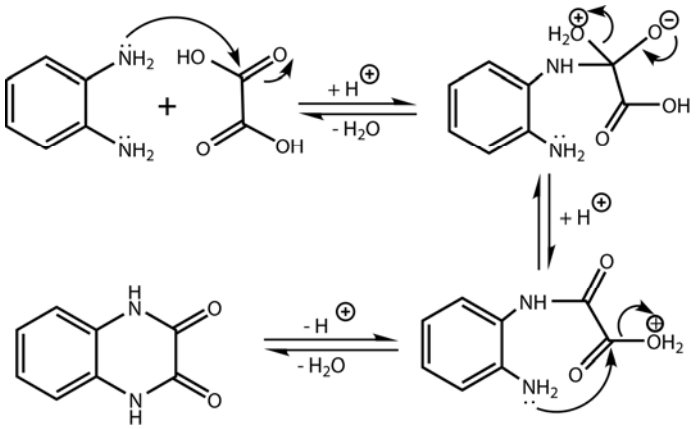

Figure 3.6 Plausible mechanism of formation of quinoxaline 2,3 dione derivative.

Compound **2a** and **2d** both crystallize from water/EtOH (1:1) mixture in Triclinic space group. These molecules contain two waters and ½ water molecule of crystallization respectively in the crystal structure, which is corresponds to the reported data [3.9]. We also got the crystal of only **2a** without any water of crystallization, when crystallized from MeOH/EtOAc mixture, as reported earlier [3.10]. In compound **2a**, the extensive hydrogen bonding interactions between the organic framework and the water cluster are very strong. The thermo gravimetric analysis of **2a** in N_2 atmosphere shows the sequential removal of

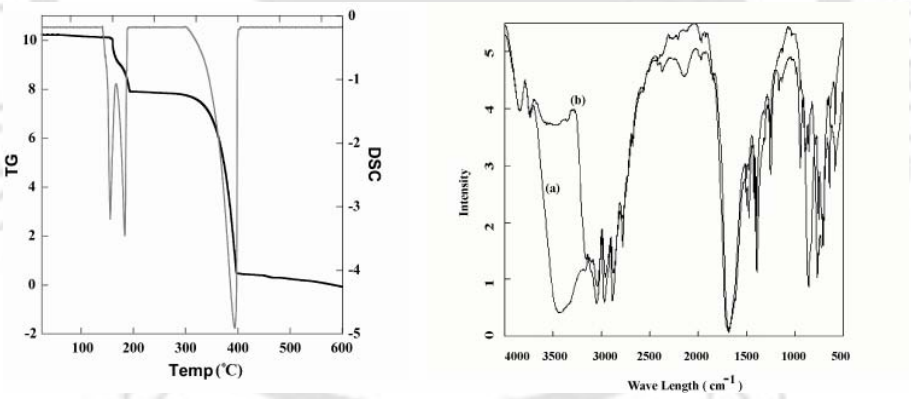

Figure 3.7 TGA-DSC analysis of **2a** (left) and FT-IR spectra (right) of **1a** (a) before and (b) after heating.

two crystal water molecules at a temperature >100°C. The 9.86% weight loss in the range 155°-165°C is corresponding to one water molecule (calculated 9.09%) and 13.42% weight loss at in the range 165°-185°C is corresponding to another water molecule (calculated 10.00%) respectively, which is in good agreement with the X-ray crystal structure of **2a** (Figure 3.7). Temperature required to remove both the waters from the crystal is higher compared to the previously reported D_{2h} symmetric tetrameric water cluster [3.11]. Complete decomposition is achieved at ~390°C (Figure 3.7). The DSC measurement shows, the dehydration endotherm has two peaks (160°C and 180°C) indicating that the two set of water molecules are in the different environment in the solid-

state. The total molar enthalpy was 20 and 16 kJ per water molecules respectively. These values correspond to 5 kJ per H-bond, which are in good agreement with the strength of a hydrogen bond. Compound **2d** also shows the similar TGA-DSC pattern as **2a**. It shows one dehydration endotherm at 190°C and complete decomposition at ~430°C. The FT-IR spectrum of compound **2a** shows a broad band centered on 3400 cm^{-1} due to the presence of water molecules that vanishes when the compound is heated under vacuum (0.1 mm) at 250°C for 6h (Figure 3.7). While the peaks correspond to the amide linkages remain intact. Power X-ray diffraction patterns of **2a** show significant i changes in the peak positions as well as intensities before and after water removal (Figure 3.8), which is also matching well with the simulated pattern. Similar powder diffraction and FT-IR results also observed for compound **2d**.

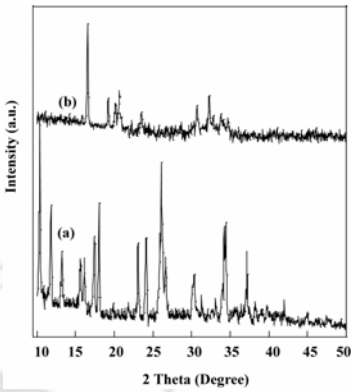

Figure 3.8 Powder XRD pattern of compound **1a**. (a) Before and (b) after water removal.

3.2.3 Synthesis of Benzimidazole derivatives

In continuation of our interest to explore the utility of simple one-pot, solvent-free, solid phase grinding methods, we decided to investigate the efficient synthesis of biologically active benzimidazole derivatives. Herein, we report the efficient one-pot solvent free green synthesis of series of benzimidazole derivatives in good yield at 140°C. We also report the one-pot efficient synthesis of another biologically potent compound, 2-mercapto-benzimidazole derivatives in solvent free condition.

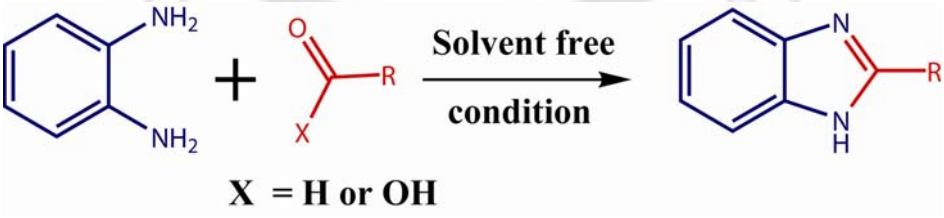

Scheme 3.3 Synthesis of benzimidazole derivatives under solvent free condition.

At first, we synthesized benzimidazole derivatives by coupling *o*-phenylenediamine either with organic acid (Table 3.3) or aldehyde in solvent-free neat conditions (Table 3.4). In order to ascertain the optimum temperature, several reactions were carried out on *o*-phenylene diamine and acetic acid as the model by varying the reaction temperature and

finally the best result was obtained at 140°C. Having established the reaction temperature, various organic acids and aldehydes were subjected to coupling. Different types of organic acids (aliphatic and aromatic) were used to condense with *o*-phenylenediamine (Table 3.3). It has been generally observed that the presence of electron withdrawing groups in the aromatic ring enhances the reaction yield with reduction in reaction time. Tri-carboxylic acid (Table 3.3 entry 10) does not form any product even after sufficient time when reacted with *o*-phenylenediamine in 1:3 ratios. However, after 5 h the whole reaction mixture turns into a black solid (char), which is a not soluble in common organic solvent. Hence, the product can be neither isolated nor characterized. The structures of the products were determined from their spectroscopic data.

Table 3.3. List of organic acids used in Scheme 3 for coupling with *o*-phenylenediamine.

Entry	Organic acid	Product	Time (hrs)	Yield %[a]
1	Formic acid	benzimidazole	0.5	95
2	Acetic acid	2-methyl-benzimidazole	0.5	90
3	Benzoic acid	2-phenyl-benzimidazole	1.5	83
4	*p*-Chloro benzoic aicd	2-(4-chlorophenyl)-benzimidazole	1.5	92
5	*p*-Hydroxy benzoic aicd	4-(benzimidazole-2-yl)phenol	2	85
6	*p*-Nitro benzoic aicd	2-(4-nitrophenyl)-benzimidazole	1.5	95
7	*p*-Methoxy benzoic aicd	2-(4-methoxyphenyl)-benzimidazole	2	80
8	*o*-chloro benzoic aicd	2-(2-chlorophenyl)-benzimidazole	2	88
9	*p*-Methyl benzoic aicd	2-p-tolyl-benzimidazole	2	80
10	Trimesic acid	NA	>2	No reaction

[a] Isolated yield.

Table 3.4 List of organic aldehydes used in Scheme 3 for coupling with *o*-phenylenediamine.

Entry	Organic aldehyde	Product	Time (hrs)	Yield %[a]
1	Benzaldehyde	2-phenyl-benzimidazole	1	88
2	*p*-Methyl benzaldehyde	2-p-tolyl-benzimidazole	1.5	72
3	*p*-Ethyl benzaldehyde	2-(4-ethylphenyl)-benzimidazole	1.5	65
4	*p*-Nitro benzaldehyde	2-(4-nitrophenyl)-benzimidazole	0.5	92
5	*p*-Chloro benzaldehyde	2-(4-chlorophenyl)-benzimidazole	1	75
6	*o*-chloro benzaldehyde	2-(2-chlorophenyl)-benzimidazole	1	70
7	*p*-Methoxy benzaldehyde	2-(4-methoxyphenyl)-benzimidazole	1.5	78
8	*p*-Hydroxy benzaldehyde	4-(benzimidazole-2-yl)phenol	2	61
9	1-Hexanal	2-pentyl-benzimidazole	2	65
10	Furan-2-carbaldehyde	2-(furan-2-yl)-benzimidazole	2	55

[a] Isolated yield.

Several aldehydes (aromatic, heteroaromatic and aliphatic) underwent the above conversion to form a series of benzimidazoles (Table 3.4). Aromatic aldehydes containing both electron-donating and electron-withdrawing groups worked well. Aliphatic aldehydes (Table 3.4, entry 9) also afforded the desired products in high yields. The method is suitable for the sterically hindered aldehyde 2-naphthaldehyde (Table 3.4, entry 8). The

reaction conditions are simple and the products were formed in moderate to high yields (55–92 %). The structures of the products were determined from their spectral (^{1}H NMR, IR and MS) data.The plausible mechanism of the condensation is described in Figure 3.9. Initially amino group of ortho phenylene diamine condensed with carbonyl group of aldehydes to yield the corresponding Schiff's base. This Schiff's base is then condensed with another amino group of ortho phenylene diamine to yield the cyclized product. This intermediate product is then oxidized in air to give the benzimidazole derivatives.

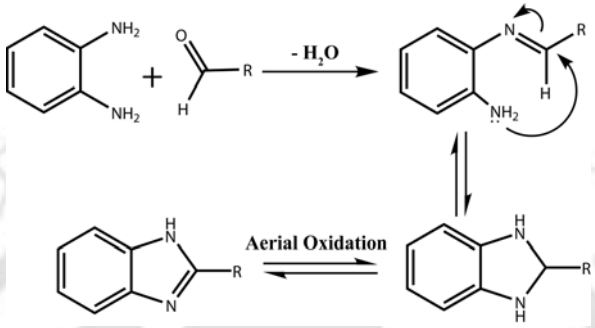

Figure 3.9 Plausible mechanism of formation of benzimidazole derivative from aldehydes.

In the next section we have shown the synthesis of 2-mercaptobenzimidazole derivatives (Scheme 3.4). It has been synthesized from a mixture of ammonium thiocyanate and *o*-phenylenediamine derivatives in presence of catalytic amount (0.05 mol%) of NH_4Cl following a similar procedure at 140^{o}C for 1 – 3 hours. Details of the substrates used, reaction times and yields are given in Table 3.5.

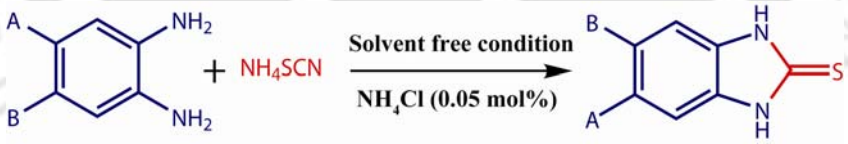

Scheme 3.4 Synthesis of 2-mercaptobenzimidazole derivatives under solvent free condition.

Table 3.5 List of different derivatives of *o*-phenylenediamine used in Scheme 4.

Entry	A	B	Product	Time (hrs)	Yield %[a]
1	H	H	1H- benzimidazole-2(3H)-thione	1.5	78
2	H	NO_2	5-nitro- benzimidazole-2(3H)-thione	3	48
3	H	Cl	5-chloro- benzimidazole-2(3H)-thione	2	60
4	H	Me	5-methyl- benzimidazole-2(3H)-thione	1	80
5	H	*n*-Pr	5-propyl- benzimidazole-2(3H)-thione	1.5	82
6	H	Ph	5-phenyl- benzimidazole-2(3H)-thione	1	85
7	Cl	Cl	5,6-dichloro- benzimidazole-2(3H)-thione	3	54

[a] Isolated yield.

The plausible mechanism of the reaction is depicted in Figure 3.10. The ammonium chloride which is used as a catalyst is first decomposed to yield ammonia and hydrochloric

acid. This hydrochloric acid then reacts with *o*-phenylenediamine to give the corresponding ammonium salt. The mono hydrochloride salt is then reacts with ammonium thiocyanate to give mono ammonium thiocyanate salt of *o*-phenylenediamine. This ammonium salt is then rearranges to yield 2-amino-*N*-phenyl thiourea. The amino group of 2-amino-*N*-phenyl thiourea is nucleophilically attack at the carbon atom of thiourea followed by cyclization with the evolution of ammonia gas to yield the product 2-thio benzimidazole.

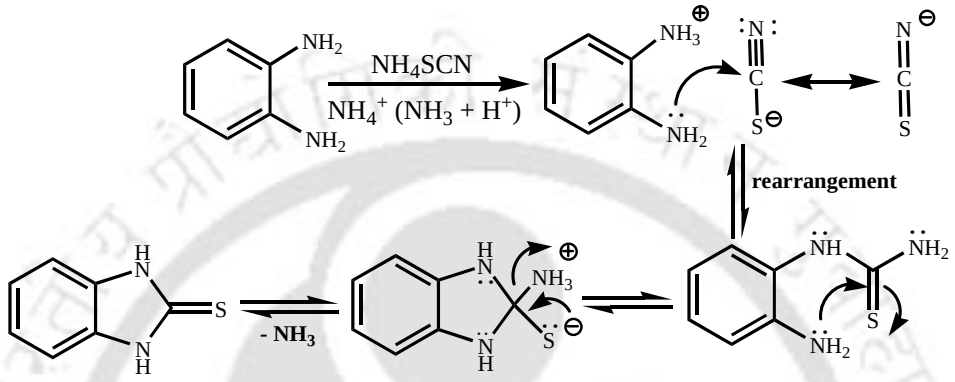

Figure 3.10 Plausible mechanism of formation of 2-thio benzimidazole derivatives. Double headed arrow depict the movement of an electron pair.

Summery

In conclusion, we have developed a simple, highly efficient, convenient and one-pot solvent-free green synthetic method for the synthesis of biologically important quinoxaline-2,3-dione derivatives, 2,3-dihydro-1,5-benzodiazepines and benzimidazole derivatives without the intervention of any catalyst. The present methodology offers very attractive features such as reduced reaction times, higher yields, which offer wide scope in organic synthesis. The operational simplicity of the procedure is also attractive. We have done the thermal analysis of the quinoxaline derivatives hydrated crystals. We also carried out the powder X-ray diffraction and FT-IR analysis of the hydrated as well as the dehydrated crystals to prove the role of water of crystallization. We have also described the one-pot efficient green synthetic methodology for the synthesis of another pharmaceutically important 2-mercaptobenzimidazole. Moreover, this methodology describes the synthesis without the intervention of any catalyst for the first time. The present methodology offers very attractive features such as green synthesis, reduced reaction times and higher yields, all of which make it a useful and attractive strategy for the preparation of various benzimidazole derivatives simply by changing different substrates. The operational simplicity of the procedure is also attractive, which offer wide scope in organic synthesis.

Reference

3.1 Rothenberg, G.; Downie, A. P.; Raston, C. L.; Scott, J. L. *J. Am. Chem. Soc*. **2002**, *123*, 8701.

3.2 (a) Toda, F.; Takumi, H.; Yamaguchi, H. *Chem. Express* **1989**, *4*, 507; (b) Tanaka, K.; Kishigami, S.; Toda, F. *J. Org. Chem*. **1991**, *56*, 4333; (c) Toda, F.; Tanaka, K.; Hamai, K. *J. Chem. Soc., Perkin Trans*. **1990**, *1*, 3207; (d) Toda, F.; Suzuki, T.; Higa, S. *J. Chem. Soc., Perkin Trans*. **1998**, *1*, 3521; (e) Ren, Z.-J.; Cao, W.-G.; Tong, W.-Q. *Synth. Commun*. **2002**, *32*, 3475; (f) Toda, F.; Kiyoshige, K.; Yagi, M. *Angew. Chem., Int. Ed. Engl*. **1989**, *101*,329; (g) Ren, Z.-J.; Cao,W.-G.; Ding,W.-Y.; Shi,W. *Synth. Commun*. **2004**, *34*, 4395.

3.3 Moloney, M. G. *Nat. Prod. Rep*. **2002**, *19***,** 597.

3.4 SMART, SAINT and XPREP *Siemens Analytical X-ray Instruments Inc., Madison, Wisconsin, USA* **1995**.

3.5 Sheldrick, G. M. SADABS: empirical software for absorption and correction. University of Gottingen, Institut fur Anorganische Chemieder Universitat, Tammanstrasse 4, D-3400 Gottingen, Germany **1999–2003**.

3.6 Sheldrick, G. M. SHELXS-97. University of Gottingen, Germany **1997**.

3.7 (a) 13. Abdelkrim, B.A.; Khalid,B.; Mohamed , S. *Tetrahedron Lett.* **2003,** *44*, 5935; (b) Shen , M.; Cai,C., *Journal of Fluorine Chemistry* **2007,** *128*, 232; (c) Das, B.; Holla , H.; Srinivas, Y., *Tetrahedron Letters* **2007**, *48*, 61; (d) Trivedi , R., De, S.K., Gibbs , R. A. *J. Mol. Cata.A: Chem.* **2006,** *245*, 8.

3.8 Naskar, J. P.; Hati, S.; Datta, D.; Samanta, U.; Chakrabarti, P. *Z. Kristallogr*. **1998**, *213*, 112.

3.9 Oxtoby, N. S, Blake, A. J.; Champness, N. R.; Wilson, C. *Chem. Eur. J*. **2005**, *11*, 4643.

3.10 Jian, F. F.; Zhao, P. S. *J. Mol. Stru.* **2004**, *705*, 133.

3.11 Tao, J.; Ma, Z.; Huang, R. B.; Zheng, L. S. *Inorg. Chem.* **2004**, *43*, 6133.

APPENDIX

Crystal data for **1a**: CCDC # 290946; $C_{33}H_{38}N_4O_6$, M = 586.67, mp 185–187°C, triclinic, P-1, a = 9.4629(12) Å, b = 9.5416(12) Å, c = 19.182(3) Å, α = 83.930(3), β = 75.874(3), γ = 67.833(2), V = 1555.3(4) Å^3, Z = 4, d_c = 1.359 g cm^{-3}, μ = 0.107 cm^{-1}, Mo-Kα radiation, R1 = 0.0487, wR2 = 0.1329, S = 1.286.
Crystal data for **1b**: CCDC # 290945; $C_{18}H_{19}N_5O_7$, M = 417.38, mp 163–165°C, triclinic, P-1, a = 9.168(3) Å, b = 9.417(3) Å, c = 11.548(4) Å, α = 90.244(9), β = 103.886(8), γ = 97.315(9), V = 959.4(6) Å^3, Z = 2, d_c = 1.167 g cm^{-3}, μ = 0.098 cm^{-1}, Mo-Kα radiation, R1 = 0.0981, wR2 = 0.2826, S = 2.009.

Spectral data of the compounds

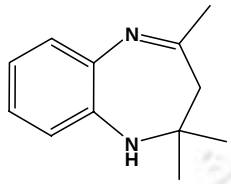

2,3-DIHYDRO-2,2,4-TRIMETHYL-1H-1,5-BENZODIAZEPINE
mp 137–139°C; GC–MS: M^+ = 188. Anal. Calcd $C_{12}H_{16}N_2$: C, 76.55; H, 8.57; N, 14.88. Found: C, 76.37; H, 8.51; N, 14.85. ^{1}H NMR (400 MHz, $CDCl_3$, 25°C, TMS) δ (ppm): 1.35 (s, 6H, $2CH_3$), 2.25 (s, 2H, CH_2), 2.35 (s, 3H, CH_3), 3.45 (br s, 1H, N-H), 6.60–7.25 (m, 4H); ^{13}C NMR (100 MHz, $CDCl_3$, 25°C, TMS): δ (ppm) 29.7, 30.4, 44.9, 68.3, 121.6, 122.0, 125.4, 126.7, 137.8, 140.6, 172.3. IR (KBr): ν/cm^{-1} 3290 (N-H), 1638 (C=N), 1597 (Ar).

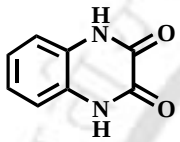

1,4-DIHYDRO-QUINOXALINE-2,3-DIONE
^{1}H NMR (400 MHz, DMSO-d_6): δ (ppm): 6.91 (m, 2H), 7.02 (m,2H), 9.43 (s, 2H); ^{13}C NMR (100 MHz, DMSO-d_6): δ (ppm): 118.6, 122.4, 127.3, 156.5; Analysis – Calcd. For $C_8H_6N_2O_2$: C 59.26, H 3.73, N 17.28%. Found: C 58.98, H 3.75, N 17.32%; MS (m/z): 162.0 (M^+). m.p 183-188^{0}C

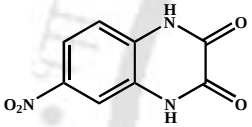

6-NITRO-1,4-DIHYDRO-QUINOXALINE-2,3-DIONE
^{1}H NMR (400 MHz, DMSO-d_6): δ (ppm): 7.57 (d, 1H, *J* = 8.1 Hz), 7.95 (d, 1H, *J* = 8.1 Hz), 8.43 (s, 1H), 9.73 (s, 2H); ^{13}C NMR (100 MHz, DMSO-d_6): δ (ppm): 113.7, 117.4, 120.3, 129.5, 133.7, 142.2, 157.5; Analysis – Calcd. For $C_8H_5N_3O_4$: C 46.39, H 2.43, N 20.29%. Found: C 46.30, H 2.45, N 20.30%; MS (*m/z*): 207.0 (M^+).

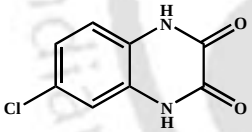

6-CHLORO-1,4-DIHYDRO-QUINOXALINE-2,3-DIONE
^{1}H NMR (400 MHz, DMSO-d_6): δ (ppm): 6.91 (d, 1H, *J* = 9.3 Hz), 7.32 (d, 1H, *J* = 9.3 Hz), 7.86 (*s*, 1H); 9.43 (*s*, 2H) ^{13}C NMR (100 MHz, DMSO-d_6): δ (ppm):119.0, 121.3, 122.7, 125.3, 129.6, 132.5, 160.2; Analysis – Calcd. For $C_8H_5ClN_2O_2$: C 48.88, H 2.56, N 14.25%. Found: C 48.81, H 2.49, N 14.3%; MS (*m/z*): 196.5 (M^+).$^+$). m. p. 225-227^{0}C

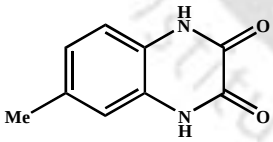

6-METHYL-1,4-DIHYDRO-QUINOXALINE-2,3-DIONE
^{1}H NMR (400 MHz, DMSO-d_6):δ (ppm): 2.21 (*s*, 3H), 6.78 (d, 1H, *J* = 7.8 Hz), 7.22 (*s*, 1H), 7.51 (*d*, 1H, *J* = 7.8 Hz), 10.11 (*m*, 2H); ^{13}C NMR (100 MHz, DMSO-d_6): δ (ppm): 21.2, 117.5,119.3, 123.7, 127.3, 131.2, 135.7, 156.5; Analysis –Calcd. for $C_9H_8N_2O_2$: C 61.36, H 4.58, N 15.90%. Found: C 61.22, H 4.51, N 16.15%; MS (*m/z*): 176.0 (M^+). m. p. 207-210^{0}C

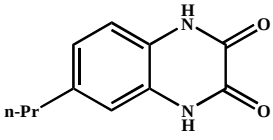

6-PROPYL-1,4-DIHYDRO-QUINOXALINE-2,3-DIONE
^{1}H NMR (400 MHz, DMSO-d_6): δ (ppm): 0.89 (*t*, 3H), 1.54 (*m*, 2H), 2.55 (*t*, 2H, *J* = 7.1 Hz), 6.71 (*d*, 1H, *J* = 8.9 Hz), 7.32 (*s*, 1H), 7.62 (*d*, 1H, *J* = 8.9 Hz), 9.53 (*s*, 2H); ^{13}C NMR (100 MHz, DMSO-d_6): δ (ppm): 13.5, 24.6, 37.9, 120.5, 122.3, 123.5, 126.7, 131.2, 135.1, 159.4; Analysis – Calcd. for $C_{11}H_{12}N_2O_2$: C 64.69, H 5.92, N 13.72%. Found: C 64.61, H 5.80, N 12.5%; MS (*m/z*): 204.0 (M^+). m. p. 229-233^{0}C

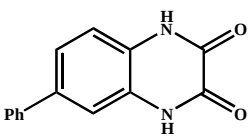

6-PHENYL-1,4-DIHYDRO-QUINOXALINE-2,3-DIONE
^{1}H NMR (400 MHz, DMSO-d_6): δ (ppm) 7.21–7.37 (*m*, 4H), 7.48 (*d*, 2H, *J* = 9.8 Hz), 7.68 (*d*, 1H, *J* = 9.8 Hz), 7.91 (*s*, 1H), 9.27 (*s*, 2H); ^{13}C NMR (100 MHz, DMSO-d_6): δ (ppm) 118.6, 121.4, 123.2, 127.3, 129.0, 131.2, 132.5, 136.4, 159.3; Analysis – Calcd. for $C_{14}H_{10}N_2O_2$: C 70.58, H 4.23,N 11.76%. Found: C 70.52, H 4.11, N 11.83%; MS (*m/z*): 238.0 (M^+). m. p. 289-293^{0}C

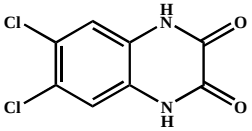

6,7-DICHLORO-1,4-DIHYDRO-QUINOXALINE-2,3-DIONE

^{1}H NMR (400 MHz, DMSO-d_6): δ (ppm): 7.62 (*s*, 2H), 9.79 (*s*, 2H); ^{13}C NMR (100 MHz, DMSO-d_6): δ (ppm): 121.6, 128.4, 131.3, 163.5; Analysis – Calcd. For $C_8H_4Cl_2N_2O_2$: C 41.59, H 1.75, N 12.13%. Found: C 41.53, H 1.78, N 12.15%; MS (*m/z*): 230.0 (M^+).

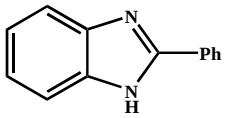

2-PHENYL-BENZIMIDAZOLE

A white solid; m.p.290–292°C. IR (KBr) ν 1640 cm^{-1} (C-N), 3250 cm^{-1} (N-H). ^{1}H NMR (400 MHz, DMSO-d_6): δ (ppm): 7.21–7.73 (7H, m, Ar), 8.16–8.22 (2H, m,Ar), MS (EI) m/z 194 (M^+).

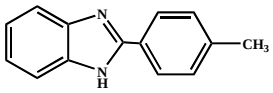

2-(4-METHYL-PHENYL)-BENZIMIDAZOLE

A white solid;m.p. 268–270°C. IR (KBr) ν 1641 cm^{-1} (C-N),3250 cm^{-1} (N-H). ^{1}H NMR (400 MHz, DMSO-d_6): δ (ppm): 2.60 (3H, m, CH_3),7.20–7.60 (6H, m, Ar), 8.00–8.08 (2H, m, Ar), MS (EI) m/z 208 (M^+).

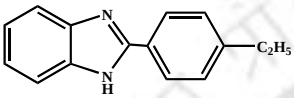

2-(4-ETHYL-PHENYL)-BENZIMIDAZOLE

A white solid; m.p. 175–176°C. IR (KBr) ν 1640 cm^{-1} (C-N), 3251 cm^{-1} (N-H). ^{1}H NMR (400 MHz, DMSO-d_6): δ (ppm): 2.30–2.50 (5H, m, C_2H_5), 7.20–7.43 (4H, m, Ar), MS (EI) m/z 222 (M^+).

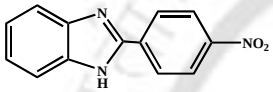

2-(4-NITRO-PHENYL)-BENZIMIDAZOLE

A yellow solid; m.p. 312–314°C. IR (KBr) ν 1641 cm^{-1} (C-N), 3253 cm^{-1}(N-H). ^{1}H NMR (400 MHz, DMSO-d_6): δ (ppm): 7.20–7.60 (6H, m, Ar), 8.00–8.08 (2H, m, Ar), MS (EI) m/z 239 (M^+).

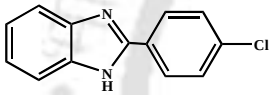

2-(4-CHLORO-PHENYL)-BENZIMIDAZOLE

A white solid; m.p. 291–293°C. m.p. 291–293°C. IR (KBr) ν 1642 cm^{-1} (C-N), 3252 cm^{-1}(N-H). ^{1}H NMR (400 MHz, DMSO-d_6): δ (ppm): 7.20–7.60 (6H, m, Ar), 8.00–8.08 (2H, m, Ar), MS (EI) m/z 230 (M^+).

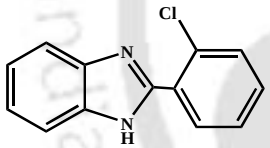

2-(2-CHLORO-PHENYL)-BENZIMIDAZOLE

A white solid;m.p. 232–234°C. IR (KBr) ν 1642 cm^{-1} (C-N), 3251 cm^{-1} (N-H). ^{1}H NMR (400 MHz, DMSO-d_6): δ (ppm): 7.20–7.60 (6H, m, Ar), 8.00–8.08 (2H, m, Ar), MS (EI) m/z 228 (M^+).

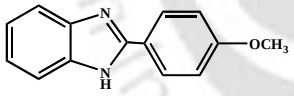

2-(4-METHOXY-PHENYL)-BENZIMIDAZOLE

A white solid; m.p. 225–226°C. IR (KBr) ν 1639 cm^{-1} (C-N),3249 cm^{-1} (N-H). ^{1}H NMR (400 MHz, DMSO-d_6): δ (ppm): 3.52 (3H, m, CH_3), 7.20–7.60 (6H, m, Ar), 8.00 – 8.08 (2H, m, Ar), MS (EI) m/z 224 (M^+).

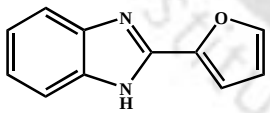

2-FURANYL-BENZIMIDAZOLE

A white solid; m.p.285–287°C. IR (KBr) ν 1641 cm^{-1} (C-N), 3252 cm^{-1} (N-H). ^{1}H NMR (400 MHz, DMSO-d_6): δ (ppm): 6.80–7.00 (3H, m, Furanyl), 7.21–7.43 (4H,m, Ar), MS (EI) m/z 184 (M^+).

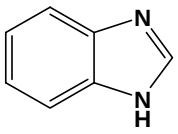

1H-BENZIMIDAZOLE

A white solid; IR (KBr) ν 1641 cm^{-1} (C-N), 3252 cm^{-1} (N-H). ^{1}H NMR (400 MHz, DMSO-d_6): δ (ppm): 7.26–7.70 (4H, m, Ar),8.08 (H, m, Ar) ^{13}C NMR (100 MHz, DMSO-d_6): δ (ppm): 115.4,122.9,137.9, 141.5,; MS (EI) m/z 118 (M^+).

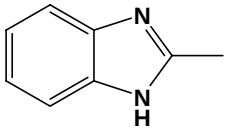

2-METHYL-1H-BENZIMIDAZOLE

A white solid; IR (KBr) ν 1639 cm^{-1} (C-N), 3250 cm^{-1} (N-H). ^{1}H NMR (400 MHz, DMSO-d_6): δ (ppm): 2.42 (3H, m, CH_3), 7.26–7.70 (4H,m, Ar), ^{13}C NMR (100 MHz, DMSO-d_6): δ (ppm): 18.8,115.3,123,138.9,152 (MS (EI) m/z 132 (M^+).

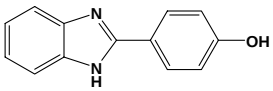

4-(-1H-BENZIMIDAZOLE-2-YL)PHENOL

A white solid; IR (KBr) ν 1640 cm^{-1} (C-N), 3254 cm^{-1} (N-H). ^1H NMR (400 MHz, DMSO-d_6): δ (ppm): 7.20–7.60 (6H, m, Ar), 8.00 – 8.08 (2H, m, Ar), ^{13}C NMR (100 MHz, DMSO-d_6): δ (ppm) 115.3, 116.4, 123, 128.9, 152.9 MS (EI) m/z 210 (M^+).

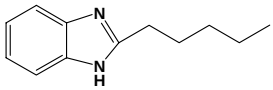

2-PENTYL-1H-BENZIMIDAZOLE

A white solid; IR (KBr) ν 1640 cm^{-1} (C-N), 3254 cm^{-1} (N-H). ^1H NMR (400 MHz, DMSO-d_6): δ (ppm): 7.20–7.60 (6H, m, Ar), 0.96-1.62 (8H, m, C_5H_{11}) ^{13}C NMR (100 MHz, DMSO-d_6): δ (ppm): 14.1, 22.8, 30.7, 31.5,33.2, 115.3, 123, 138.9, 151.4 ;MS (EI) m/z 189 (M^+).

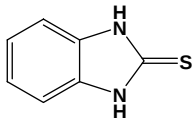

1H-BENZIMIDAZOLE-2(3H)-THIONE

^1H NMR (400 MHz, DMSO-d_6): δ (ppm): 6.21-6.37 (4H, m, Ar), ^{13}C NMR (100 MHz, DMSO-d_6): δ (ppm): 125.1, 126.8, 136, 168.4; MS (EI) m/z 150 (M^+).

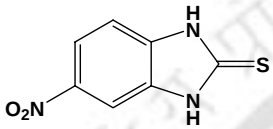

5-NITRO-1H-BENZIMIDAZOLE -2(3H)-THIONE

^1H NMR (400 MHz, DMSO-d_6): δ (ppm): 6.47-7.30 (3H, m, Ar), ^{13}C NMR (100 MHz, DMSO-d_6): δ (ppm): 117.4, 120.7, 127.7, 136.9, 142.1, 144.7, 168; MS (EI) m/z 195 (M^+).

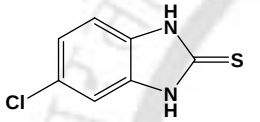

5-CHLORO-1H-BENZIMIDAZOLE-2(3H)-THIONE

^1H NMR (400 MHz, DMSO-d_6): δ (ppm): 6.15-6.38 (3H, m, Ar), ^{13}C NMR (100 MHz, DMSO-d_6): δ (ppm):120.2, 125.2, 127.2, 130.6, 134.1, 137.4, 168.4 ; MS (EI) m/z 184 (M^+).

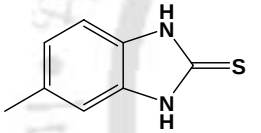

5-METHYL-1H-BENZIMIDAZOLE-2(3H)-THIONE

^1H NMR (400 MHz, DMSO-d_6): δ (ppm): 6.01-6.17 (3H, m, Ar), ^{13}C NMR (100 MHz, DMSO-d_6): δ (ppm): 24.3, 125.4, 126.5, 133, 135.9, 168 ; MS (EI) m/z 164 (M^+).

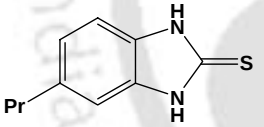

5-PROPYL-1H-BENZIMIDAZOLE-2(3H)-THIONE

^1H NMR (400 MHz, DMSO-d_6): δ (ppm): 6.07-6.23 (3H, m, Ar), 0.96-2.55 (3H, m, $CH_3CH_2CH_2$); ^{13}C NMR (100 MHz, DMSO-d_6): δ (ppm): 13.7, 24.2, 38.2, 124.5, 125.6, 133.3, 136.1, 168.4 ; MS (EI) m/z 192 (M^+).

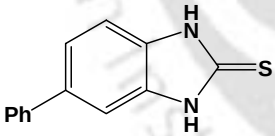

5-PHENYL-1H-BENZIMIDAZOLE-2(3H)-THIONE

^1H NMR (400 MHz, DMSO-d_6): δ (ppm): 6.27-6.59 (3H, m, Ar), 7.22-7.48 (5H, m, Ar); ^{13}C NMR (100 MHz, DMSO-d_6): δ (ppm):125.1, 127.3, 127.7, 127.9,129.3, 132.8, 134.9, 136.5, 136.4 ; MS (EI) m/z 226 (M^+).

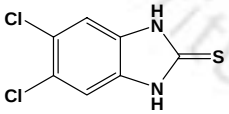

5,6-DICHLORO-1H-BENZIMIDAZOLE-2(3H)-THIONE

^1H NMR (400 MHz, DMSO-d_6): δ (ppm): 6.16 (2H, m, Ar), ^{13}C NMR (100 MHz, DMSO-d_6): δ (ppm): 128.6, 129.7, 135.5, 168.4; MS (EI) m/z 218 (M^+).

List of Publications

1. Thakuria, H.; Pramanik, A.; Borah, B. M.; Das, G. *Tetrahedron Lett.* **2006**, *47*, 3135.

2. Thakuria, H.; Das, G. *J. Chem. Sci.*, **2006**, *118*, 1.

3. Thakuria, H.; Borah, B. M.; Das, G. *Eur. J. Inorg. Chem.* **2007**, 524.

4. Thakuria, H.; Borah, B. M.; Das, G. *J. Mol. Cat. A*, **2007**, *274*, 1.

5. Thakuria, H.; Das, G. *Polyhedron* **2007**, *26*, 149.

6. Thakuria, H.; Borah, B. M.; Pramanik, A.; Das, G. *J. Chem. Cryst.* **2007**, *37*, 807.

7. Thakuria, H.; Das, G. *ARKIVOC*, **2008**, *XV*, 321.

8. "Polycarboxylate derivative of α-Amino acid as growth modifier of sulphide minerals" H. Thakuria, G. Das (under communication)

9. "Malachite Nanoparticle: An efficient heterogeneous catalyst for Beckmann, Knoevenagel, Aza-Michael reaction" H. Thakuria, G.Das, (under Communication).